2019

Holographic Models for Strongly Coupled Phases of Matter

Anthony Hoover
Lehigh University, arh314@lehigh.edu

Holographic Models for Strongly Coupled Phases of Matter

by

Anthony Hoover

Presented to the Graduate and Research Committee

of Lehigh University

in Candidacy for the Degree of

Doctor of Philosophy

in

Physics

Lehigh University

May 2019

Approved and recommended for acceptance as a dissertation in partial fulfillment of the requirements for the degree of Doctor of Philosophy.

_____
Date

_____
Dissertation Advisor

Committee Members:

_____
Sera Cremonini, Committee Chair

_____
Rosi Reed

_____
Michael Stavola

_____
Yong Kim

_____
Huai-Dong Cao

Acknowledgements

I would like to thank my advisor Dr. Sera Cremonini. I know you were not necessarily looking for a new graduate student as soon as you started your career at Lehigh (let alone three!) but my decision to ask about working with you was probably one of the best decisions I ever made. Your unwavering patience and calm knowledge has made me a much better physicist, writer, speaker, and person. You pushed me when I needed to be and complimented me when I was having doubts about my performance. I have often said that I would never have obtained my Ph.D without you and I still firmly believe that to this day.

Thank you to Dr. Rosi Reed, Dr. Yong Kim, Dr. Michael Stavola, Dr. Huai-Dong Cao, and Dr. Slava Rotkin all of whom have served as members of my committee and several of whom have shared their knowledge with me in classes while I was at Lehigh. I have appreciated all of your helpful comments, questions and suggestions as I have worked on my research. Though it hasn't always been easy to answer the more difficult questions, I can say that I am a better physicist and presenter as a result.

Thanks to several members of my research group who have made this research possible and have supported me in interests both accademic and non. Erin Blauvelt, Steven Waskie, Li Li. You have all helped me to improve my knowledge of string theory and it has been a true pleasure working with you.

I want to express the immense gratitude that I have for my wife and best friend Liz. You have put up with so much from me throughout our time together. You have always been a listening ear and the best support system regardless of whether or not you understood my research. We have gone through so much since I started graduate school. We got married, we started new hobbies, we explored, we laughed, we went on mini dates when neither of us had time to do anything else, we survived car accidents, mild and major sicknesses, and familial losses. There is truely nobody else that I would rather have those experiences with than you.

I'd like to thank my family who has always supported me in anything and everything I ever did from the moment I was born. Though you did not get to see me every day (and sometimes every month) while I was busy working on my research, you never gave up on me. I am forever grateful to have such a strong support system to fall back on when I am at my worst. Mom and Dad, I can never repay you for everything that you have done for me. From answering my panicked phone calls to not getting (too) mad at me when I don't respond to your emails. I know that I can always come to you for advice and guidance. Nick and Ashley, thank you for keeping me sane by making sure I always have puzzles or board games to look forward to.

Finally, thank you to my friends, many of whom have experienced the Ph.D. track as well, all of whom have listened to me talk way too much. Richard and Alyssa Hanes, Eric Kaiser, O.N.e O'Neill, Alex Arnold, Lauren Dallachiesa, Ian Crawley, Catherine Tomkiel, Alex Morrese, Dan and Dee Brown.

Contents

List of Figures

Abstract

This thesis examines magnetotransport in holographic models that describe gravity coupled to a non-linear gauge field sector and scalars. Momentum dissipation in the system is generated by including axionic terms which break translational invariance. Such theories can be used to describe systems with non-linear interactions between charge carriers, which are expected to play an important role in strongly correlated electron matter. The first model studied in the thesis is based on the Dirac-Born-Infeld D-brane action. We construct new fully backreacted black hole solutions to this theory and compute the associated conductivities, using holographic techniques. We show that some of these new geometries also support magnetic-field-induced metal-insulator transitions. We then extend the construction of holographic conductivities and the magnetotransport analysis to a more general class of models with a non-linear gauge sector. We study non-relativistic Lifshitz and hyperscaling violating geometries in this larger class of theories, which can be used to describe dual systems that are quantum critical. Working in a dilute charge limit, we identify clean scaling regimes in the transport properties of the dual system. In particular, we realize the temperature scalings of the entropy, resistivity, Hall angle and magnetoresistance seen in the strange metal phase of the cuprate high temperature superconductors. Our results rely crucially on the presence of nonlinear interactions among the charge carriers.

Chapter 1

Introduction

1.1 Why a Theory of Quantum Gravity?

Compared to the other fundamental forces in nature, gravity is the weakest. Einstein's theory of general relativity is an effective description for gravitational effects at large length scales. It describes the way in which the fabric of space-time bends around massive objects, and teaches us that what one typically perceives as gravity is really the curvature of space-time. General relativity has been tested to great accuracy, with the recent LIGO detection of gravity waves providing the last missing piece of evidence. Quantum theories, on the other hand, explain the behavior of elementary particles that make up matter at atomic and subatomic scales. Since the masses of these particles are very small, one typically does not need to consider gravitational forces when analyzing elementary particle interactions and working below atomic lengths (as long as we remain well above the Planck scale).

At first glance, these theories seem to be mutually exclusive. They are valid effective descriptions at either large (gravitational) or small (quantum) length scales. The difference between them is further exemplified when considering that general

relativity is deterministic while quantum mechanics is inherently probabilistic. In their respective realms, each theory is well developed and understood. However, to describe an extremely dense object (a large mass confined to a tiny distance) we need to understand both gravitational and quantum effects at once. This leads naturally to the question, which framework should be used in this case?

The answer is interestingly: neither. General relativity, being a classical theory, is not equipped to handle the small length scales at which quantum effects become crucial. Similarly, quantum mechanics does not come with a built in operator for gravitational forces and is not well suited to describe the large curvatures of space-time associated with a massive object. Thus, our usual tools fail to explain setups in which extreme energies are concentrated over small distances. In such cases, we need a new theory of *Quantum Gravity* which is capable of capturing the effect of both forces at once. Of course, we are already aware of a few cases where such a theory is needed. The most well known example is a black hole, an object so massive that it tears the fabric of space-time at the curvature singularity in its core. The small length scales near the singularity imply that quantum effects cannot be ignored, motivating the need for a quantum description of gravity.

Moreover, black holes behave like thermodynamic objects and emit black body radiation [1]. They carry an entropy, which was computed in the 1970's by Hawking and Bekenstein [2] using semi-classical arguments, and found to be

$$S = \frac{k}{4\sqrt{G\hbar/c^3}} A, \tag{1.1}$$

where k is the Boltzmann constant, A is the area of the black hole horizon, and $\sqrt{G\hbar/c^3}$ is the Planck length. Their calculation was based on considering particles pair-produced out of the vacuum near the horizon of the black hole. In empty space, particle pairs are constantly created out of the vacuum and immediately afterwards

annihilate each other, disappearing into the vacuum again. However, if this process occurs near the horizon of a black hole, one of the particles can be absorbed by the black hole while the other can escape. The latter carries energy away from the black hole, thus giving rise to radiation. Therefore, black hole radiation is a quantum mechanical effect and by extension so is its entropy. Since entropy is a measure of the number of microstates associated with the system (with a given macrostate), the Bekenstein-Hawking result led to a longstanding fundamental question about what may be the quantum microstates that make up a black hole (and how they may be encoded in its area). It is important to emphasize that this question can not be answered within the theory of general relativity, or using quantum mechanics alone. It requires the development of a quantum theory of gravity, and indeed, string theory has since then provided a detailed answer to some of these questions, identifying the microstates of large classes of black holes and reproducing precisely their Bekenstein-Hawking entropy[1] [3].

Another prime example demonstrating the need for a theory of quantum gravity is the evolution of the early universe. Immediately following the big bang, the universe started out very dense and hot. Explaining the Big Bang singularity and constructing well-motivated models of inflation (the early period of accelerated expansion of the universe) once again requires knowledge of quantum gravity.

1.2 String Theory as a Framework for Quantum Gravity

When the energy scale is much lower than the Planck scale, $E << M_p$, ordinary quantum field theory (QFT) methods can be applied to gravity, leading to an ef-

[1]The string theory result takes into account quantum effects not captured by the semi-classical approximation of Bekenstein and Hawking. It reduces to the latter in the appropriate semi-classical limit.

fective field theory (EFT) description of gravity. However, such an EFT breaks down at the Planck scale. To understand why this is so, consider the simplest Feynman diagram describing the interaction of elementary particles in QFT. Due to their point-like nature, two particles are drawn as meeting at a common point while interacting with a third particle. Such point-like interactions can often lead

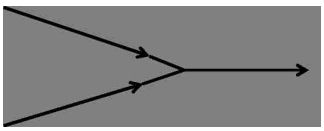

Figure 1.1: A point-like interaction in quantum field theory.

to the presence of divergences or *infinities* in the corresponding quantum field theory scattering amplitudes. However, in quantum field theory there is a well defined procedure for dealing with these divergences, known as renormalization. This is accomplished through the addition of *counterterms* which cancel the divergences and give rise to finite results which agree to a high degree of accuracy with experiments. It should be noted, however, that this process can only be carried out if a theory contains finitely many divergences. In such cases, the corresponding quantum field theory is called *renormalizable*.

First attempts to quantize gravity using standard QFT techniques introduced the graviton, a point-like massless spin-2 field that is responsible for the mediation of the gravitational force, much like the photon mediates the electromagnetic force. However, further study of scattering amplitudes between gravitons led to the discovery that once loops are accounted for in the corresponding Feynman diagram, the number of divergences that are present in the theory becomes infinite at the Planck scale. It is for this reason that gravity is described as not renormalizable. With infinitely many divergences, we cannot simply introduce counterterms to fix the problem (a theory which contains an infinite number of counterterms is not well

defined). This indicates that in the high energy limit, our EFT of gravity is itself not well defined.

It is then natural to ask if there may be another description for the basic constituents of nature beyond the standard point-like assumption. Instead of modeling the world as a collection of point particles, in string theory the basic constituents are one dimensional objects[2], open and closed strings. One key difference can be seen in the structure of the Feynman diagram describing, for instance, the interactions between closed strings, as shown in Figure 1.2. Notice that unlike its counterpart

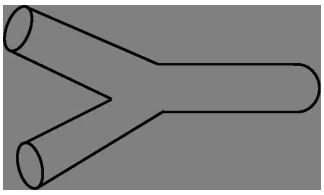

Figure 1.2: A closed string interaction in string theory with interaction strength g_s (the string coupling).

in Figure 1.1, the interaction does not occur at a single point, but rather in an extended region. As it turns out, the absence of a point-like interaction is crucial for avoiding the problem of infinite divergences, highlighting a major advantage of using strings as the basic constituents of our universe.

Strings are very small objects, whose typical size is set by the Planck length[3], and are thus governed by quantum mechanical effects. But why is string theory a theory of quantum gravity? It has been shown that strings can oscillate in a number of different modes much like tiny quantum mechanical harmonic oscillators. It is these modes that give rise to elementary particles. Interestingly, one such vibration mode can be shown to give rise to a particle with the required properties of a graviton.

[2]String theory also contains D-branes which are higher dimensional extended objects on which open strings can end.

[3]The Planck length describes the scale at which quantum gravitational effects become important, $l_p = \sqrt{\frac{\hbar G}{c^3}}$. The string length is $l_s = 10^{-34}m$.

Therefore, string theory is a quantum mechanical theory that includes gravity.

One of the remarkable successes of string theory as a model of quantum gravity came in 1996 when Strominger and Vafa successfully described the entropy of a black hole (1.1) via a counting of bound supersymmetric string states. Their counting was able to perfectly reproduce the fact that entropy is related to black hole area by a factor of $\frac{1}{4}$ as predicted by Hawking and Beckenstein [1], providing evidence for using string theory as a viable framework for a theory of quantum gravity [3]. Shortly afterwards, new powerful techniques were developed to connect theories of gravity to quantum field theories in one less dimension, which in turn offered a natural explanation for why the black hole entropy is proportional to area and not volume as one would naively expect. This is called the *holographic principle* and will be the subject of this research.

1.3 The Holographic AdS/CFT Correspondence

Our understanding of the quantum structure of space-time and the connection between theories of gravity and quantum field theories was greatly advanced with the development of the AdS/CFT correspondence, also known as *holography*. First formulated by Maldacena in 1997 [4], it was then made more precise by Edward Witten [5] and the group consisting of Igor Klebanov, Steven Gubser and Alexander Polyakov [6]. Since then the conjecture has passed countless tests, and has been shown to have wide reaching applications.

Holography states that certain theories of gravity (more precisely, certain string theories) have an equivalent, *dual* description in terms of theories that are purely quantum mechanical and which live in one less dimension – much like how an optical hologram is created by encoding information about how light scatters off a three

dimensional object onto a two dimensional surface. In its original incarnation, the correspondence related gravity on anti-de Sitter (AdS) space to a very special type of quantum field theory, a conformal field theory (CFT) living on the boundary of AdS space[4]. For this reason the conjecture was named the AdS/CFT correspondence. To appreciate its significance, we start by describing a few key facts about AdS space, and then briefly explain why it is related to a field theory that is conformal.

1.3.1 AdS Space

In order to get a feel for the structure of AdS, we first contrast it with the geometry that describes the surface of a ball, *i.e.* a sphere. A five dimensional sphere S^5 of radius R is described by

$$X_0^2 + X_1^2 + X_2^2 + X_3^2 + X_4^2 + X_5^2 = R^2, \tag{1.2}$$

and is a solution to Einstein's equations with constant *positive* curvature. The rotational symmetry group associated with the sphere(1.2) is SO(6), the group of orthogonal 6 x 6 matrices with a determinant of +1.

AdS, on the other hand, is a maximally symmetric solution to Einstein's equations characterized by a constant *negative* curvature. While this can be hard to visualize, it may be useful to note that AdS can be represented as a hyperboloid[5]. In particular, let's consider AdS_5, *i.e.* five-dimensional AdS space-time. A convenient way to write AdS_5 is

$$-X_0^2 - X_1^2 + X_2^2 + X_3^2 + X_4^2 + X_5^2 = R^2, \tag{1.3}$$

[4]The technical statement is that Type IIB String Theory compactified on $AdS_5 \times S^5$ is dual to $\mathcal{N} = 4$ SU(N) Supersymmetric Yang Mills (SYM) theory.

[5]Recall that an example of a surface with negative curvature is a hyperbolic plane.

where $X_0, X_1, \ldots, X_5$ are the so-called embedding coordinates and R is a constant which represents the overall size of AdS_5. Notice that although we are using six coordinates to characterize (1.3), the equation is a constraint, and therefore not all the coordinates are independent of each other. Thus, we are indeed dealing with a five-dimensional space-time whose metric is given by

$$ds^2 = -dX_0^2 - dX_1^2 + dX_2^2 + dX_3^2 + dX_4^2 + dX_5^2. \tag{1.4}$$

In these coordinates, X_0 is related in a non-trivial way to the time coordinate of the space-time, as we will see below. The embedding coordinates make it easy to see the hyperbolic structure of AdS and make the symmetry of the space-time apparent.

Indeed, AdS space-time has a symmetry group associated with it, much like the five-dimensional sphere above. The symmetry group of AdS_5 is SO(2,4), a label derived from the fact that two of the six coordinates in (1.4) come with a negative sign and the remaining four come with a positive sign. Specifically, SO(4) describes the rotational symmetry that leaves the four positive coordinates $\{X_2, X_3, X_4, X_5\}$ in (1.3) invariant while SO(2) acts on the two negative coordinates $\{X_0, X_1\}$. Crucially, SO(2,4) is also the symmetry group of the conformal group in four dimensions, and thus we see the first hint of the connection between the properties of AdS space and those of a conformal field theory.

The conformal group is the group of transformations on a space that preserves angles. It is also the group of transformations which preserve the form of the metric $g_{\mu\nu}$ up to a scale factor,

$$g_{\mu\nu} \to \Omega^2(x) g_{\mu\nu}. \tag{1.5}$$

Some simple examples of conformal transformations include translations, rotations and scaling transformations, while a more obscure example is known as the special

conformal transformation[6]. Indeed, the four-dimensional conformal group precisely describes $\mathcal{N} = 4$ SU(N) SYM Theory, which is to date the quantum theory that is best understood holographically.

A more useful representation of AdS_5 is obtained by making the following coordinate transformation,

$$\begin{aligned} X_0 &= R\cosh\rho\cos\tau\,, \quad X_1 = R\cosh\rho\sin\tau, \\ X_i &= R\sinh\rho\,\Omega_i\,, \quad (i = 2,3,4,5;\ \sum_i \Omega_i^2 = 1), \end{aligned} \tag{1.6}$$

where $\{\rho, \tau, \Omega_i\}$ are known as the *global* coordinates of AdS. By substituting into (1.4), the AdS_5 metric can be written in the form,

$$ds^2 = R^2(-\cosh^2\rho\, d\tau^2 + d\rho^2 + \sinh^2\rho\, d\Omega_3^2), \tag{1.7}$$

where τ denotes the (global) time coordinate, ρ is a radial coordinate and the Ω_i are the angular coordinates describing the three-dimensional sphere, S^3. In global coordinates, we can visualize AdS as the cylinder shown in figure 1.3. The global time coordinate τ runs along the vertical axis of the cylinder, and each fixed time slice of the cylinder gives the S^3, denoted in the metric by $d\Omega_3^2$. The radial coordinate ρ interpolates from the interior of AdS (the so-called "bulk") to its boundary located at $\rho \to \infty$ at which one is left only with the metric of the sphere. The meaning of the isometry group SO(2,4) now becomes more apparent. The SO(4) group describes the rotations of the S^3, while the SO(2) part corresponds to translations in the τ direction.

Another representation of AdS_5 which will be more useful for holography is found

[6]The infinitesimal form of the special conformal transformation is given by: $x^\mu \to x^\mu + b^\mu x^2 - 2x^\mu b\cdot x$.

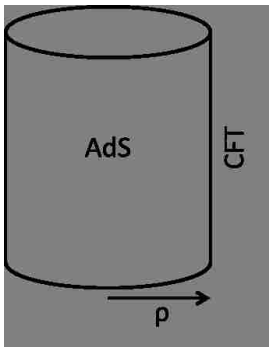

Figure 1.3: CFT exists on the boundary of AdS in the limit $r \to \infty$

by using the following coordinate transformation,

$$X_0 = \frac{1}{2r}\Big(1 + r^2(R^2 + \vec{x}^2 - t^2)\Big)\,, \quad X^i = Rrx^i\,, \quad i = 2,3,4$$
$$X_5 = Rrt\,, \qquad\qquad X^1 = \frac{1}{2r}\Big(1 - r^2(R^2 - \vec{x}^2 + t^2)\Big), \tag{1.8}$$

in terms of which the metric is of the form,

$$ds^2 = R^2\Big(\frac{dr^2}{r^2} + r^2(-dt^2 + d\vec{x}^2)\Big). \tag{1.9}$$

The coordinates $\{r, t, \vec{x}\}$ are known as the Poincare coordinates and cover a wedge of the global cylinder. Written in this way, we note that r has special significance. In the limit that r approaches infinity, the metric reduces to exactly the flat Minkowski metric in 4 dimensions on the boundary. The latter is appropriate for considering quantum field theories that live in flat space. In this case the Poincare coordinates are more useful than global coordinates, as the spatial boundary for global AdS is a sphere. On the other hand, as r gets smaller we approach the deep interior of AdS. For this reason, r is known as the *holographic coordinate* in the AdS/CFT correspondence.

The identification of a shared symmetry group between AdS and the conformal

group is a hint that the two are connected. However, there is an even deeper connection between AdS and CFT stemming from the equality of their partition functions, as we discuss next.

1.3.2 Partition Function and Correlation Functions

At the heart of the AdS/CFT correspondence is a certain "dictionary" that maps objects in one theory to objects in another. For example, a gravitational field ϕ on the AdS side of the duality will map to an operator O on the CFT side. This dictionary comes from the equivalence between the partition function Z_{AdS} of the gravitational theory and the partition function Z_{CFT} of the CFT,

$$Z_{\text{Gravity}}[\phi] = Z_{CFT}[J], \tag{1.10}$$

where J is the source of the operator θ dual to the bulk field ϕ. The identification of the partition function suggests that space-time in some sense *emerges* from the underlying quantum degrees of freedom. Even though the gravitational theory and the dual quantum field theory live in a different number of dimensions, they encode precisely the same amount of information, which is simply packaged differently on the two sides of the duality. In particular, one can compute correlation functions on both sides of the duality, and match them to each other. In highly (super)symmetric cases, this matching has been explicitly carried out. The results have always been found to be in perfect agreement and provide precise checks of the duality.

In quantum field theory, there is a well known procedure for computing correlation functions for an operator O starting from the partition function Z. Indeed the function $Z[J]$ acts as the generating functional for correlation functions, where J denotes the source for the operator O under consideration. An n-point correlation

function can be expressed using the path integral formalism as

$$G_n(x_1, \ldots, x_n) = \frac{\int D\phi\, \phi(x_1) \ldots \phi(x_n) \exp(iS(\phi)/\hbar)}{\int D\phi \exp(iS(\phi)/\hbar)}, \tag{1.11}$$

where $D\phi$ means that we are integrating over all possible configurations of the field and S is the classical action evaluated at that field configuration. We can obtain G_n from the generating functional given by

$$Z[J] = \int D\phi \exp[iS[\phi] + i \int d^4x J(x) O(x)], \tag{1.12}$$

where for concreteness we are assuming four dimensions. The source J is coupled to the dual operator O. This means that varying the partition function $Z(J)$ with respect to the source J will return the operator multiplied by the original partition function. This procedure allows us to generate correlation functions. The n-point correlation function is then given by

$$G_n(x_1, \ldots, x_n) = (-i)^n \frac{1}{Z[0]} \left. \frac{\partial^n Z}{\partial J[x_1] \ldots \partial J[x_n]} \right|_{J=0}. \tag{1.13}$$

This same procedure can be used on the gravity side of the correspondence to compute correlation functions of bulk fields. The way in which these results are then mapped to the CFT is by ensuring that the role of the CFT source J is played by the boundary value of the bulk gravitational field ϕ_0

$$J = \lim_{r \to \infty} \phi = \phi_0. \tag{1.14}$$

As an example, if the CFT operator we are interested in is a scalar operator, its dual field on the gravitational side of the correspondence is a (generically massive) scalar field moving through AdS. Ignoring for simplicity interactions, the equation

of motion for a free scalar field of mass m in AdS is

$$(\Box + m^2)\phi(r) = 0. \tag{1.15}$$

Near the boundary of AdS, the two linearly independent solutions to this equation are proportional to r^{Δ_+} and r^{Δ_-} where Δ_+ and Δ_- are constants related to m and the number of space-time dimensions[7]. We can then find the most general solution (again near the boundary) by taking the linear combination,

$$\phi(r) = \phi_0 r^{\Delta_+} + \phi_1 r^{\Delta_-}, \tag{1.16}$$

where we are working with Poincare coordinates, i.e. a flat AdS boundary. In our notation, $\phi_0 r^{\Delta_+}$ is the leading term in the asymptotic expansion (often it is non-normalizable) while $\phi_1 r^{\Delta_-}$ is subleading. The constants ϕ_0 and ϕ_1 (which do not depend on the radial coordinate r but will generically depend on the boundary coordinates) play an important role in the AdS/CFT correspondence. Specifically, the leading mode ϕ_0 is precisely the source J of the operator O that is dual to the field. On the other hand, the subleading mode ϕ_1 is the vacuum expectation value (VEV) of that same operator. We are thus seeing a deep and rich connection between the gravitational and quantum field theories. To extract, for example, the VEV of a certain operator, one must study the boundary behavior of the corresponding gravitational field. Additionally, the exponents $\Delta_\pm$ (which depend on the mass m of the field) are related to the scaling dimension of the CFT operator O [8]. This procedure is actually much more general and can be done for any operator or field (not just scalar fields). We will utilize this recipe for computing correlation functions

[7]The scaling exponents are given by $\Delta_\pm = \frac{d-1}{2} \pm \sqrt{m^2 + (\frac{d-1}{2})^2}$.

[8]The scaling dimension Δ for a field ϕ is defined by the transformation: $\phi(x) \to \lambda^\Delta \phi(x')$ under the coordinate transformation: $x \to x' = \lambda x$.

when we examine the conductivities of the high-temperature superconductors. As we will see, the conductivity is given by the current-current two point correlation function.

1.3.3 The Foundation of Holography

The original statement behind AdS/CFT is that a correspondence exists between $\mathcal{N} = 4$ SU(N) SYM theory and type IIB string theory on $AdS_5 \times S^5$ [4, 5, 6]. Here we briefly review the main argument for such a correspondence. In addition to strings, string theory is comprised of extended objects called Dp-branes, which have p spatial dimensions. Thus, a D0-brane is a point particle and a D1-brane is a string itself, while a D3-brane consists of three spatial dimensions. The AdS/CFT correspondence arises by considering a configuration of D-branes in type IIB string theory and taking a limit where the dynamics on the branes decouples from the bulk. In particular, consider N parallel D3-branes placed near each other within a $(9 + 1)$ dimensional flat space-time geometry. As we are about to see, there are two complimentary ways to examine this system. One is to consider the string excitations of the D-brane configuration, while the other is to describe geometrically the gravitational solutions generated by the D-branes.

In the former perspective, the action describing this setup can be written as the sum of three types of string excitations,

$$S = S_{bulk} + S_{brane} + S_{int}, \tag{1.17}$$

where S_{bulk} characterizes the fluctuations of the background geometry and consists of closed strings, while S_{brane} describes the excitations of the D-branes themselves. Since open strings can only exist with their endpoints attached to the D-branes, S_{brane} consists of the fluctuations of these open strings. Lastly, S_{int} describes the

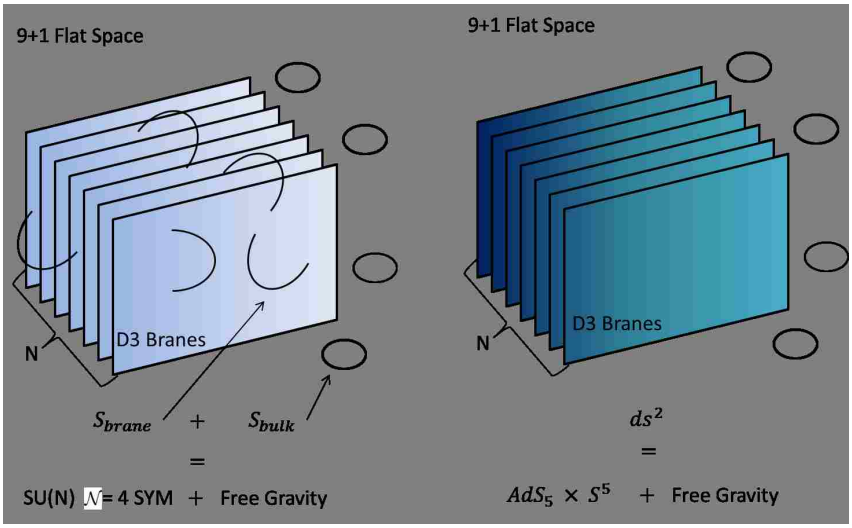

Figure 1.4: Two perspectives for viewing a stack of D3 branes leads to the two sides of the AdS/CFT correspondence.

interactions between the open and closed modes of the strings.

In the low energy limit of this system only the massless modes from the open and closed string sectors contribute to the overall action. This limit is realized by integrating out the massive degrees of freedom from the Lagrangian in (1.17). In this regime, S_{int} is negligible because the closed strings in the bulk decouple from the open strings on the D-branes, and one is left with the two independent systems S_{bulk} and S_{brane}. Let's focus on S_{bulk} first. The metric for the bulk geometry can be written perturbatively as

$$g_{\mu\nu} = \eta_{\mu\nu} + \kappa h_{\mu\nu}, \tag{1.18}$$

where $\eta_{\mu\nu}$ is the flat space metric, $h_{\mu\nu}$ is a perturbation about flat space and $\kappa = g_s l_s^4$ is magnitude of the string coupling. In the low energy limit consisting only of massless modes, $\kappa \to 0$. Thus, the bulk action becomes completely free gravity on a flat space background. Meanwhile, the massless contributions from S_{brane} are

defined only on the (3 + 1) dimensional surfaces of the branes and are described by SU(N) $\mathcal{N} = 4$ SYM theory. To summarize, from the point of view of the string excitations, in the low energy limit we have free gravity in the bulk and a four-dimensional gauge theory on the branes described by the SYM theory.

We now turn to a complimentary view of this setup by considering the gravitational solution describing the D-branes configuration in supergravity. In type IIB string theory, the geometry describing a stack of N D3-branes in a flat (9 + 1) dimensional space is given by,

$$\begin{aligned} ds^2 &= f^{-\frac{1}{2}}(-dt^2 + dx_1^2 + dx_2^2 + dx_3^2) + f^{\frac{1}{2}}(dr^2 + r^2 d\Omega_5^2), \\ f &= 1 + \frac{L^4}{r^4}, \qquad L^4 = 4\pi g_s l_s^4 N. \end{aligned} \tag{1.19}$$

The D3-branes can gravitate very strongly and collapse upon themselves, forming objects known as black branes, which get their name from the fact that light cannot escape from the large gravity of the branes. Their metric is a slight modification of (1.19) and is very similar to that of a black hole, except that for the black brane the geometry along $\{t, x_1, x_2, x_3\}$ is flat. In this geometry, the energy E of an observer at infinity ($r \to \infty$) can be related to the energy E_p of an observer at a finite value of r by,

$$E = f^{-\frac{1}{4}} E_p, \tag{1.20}$$

where the factor of $f^{-\frac{1}{4}}$ is known as a *redshift factor*. Due to the redshift factor, an object at $r \to 0$ appears to have lower energy to an observer at infinity, showing that $r \to 0$ identifies the low energy regime of the theory. In this low energy limit, there are two types of excitations. One set of these are localized close to $r \sim 0$ (these are near horizon excitations) while the other describe massless particles that

propagate through the bulk of the space-time. The bulk excitations decouple from those in the $r = 0$ limit[9] because their wavelength is larger than the gravitational radius of the branes. Therefore, the theory consists of free gravity in the bulk that is decoupled from the near horizon geometry. Moreover, applying the low energy limit to the blackening function (1.19), gives $f \to \frac{L^4}{r^4}$. This means that the brane solution in (1.19) can be described by the metric,

$$ds^2 = \frac{r^2}{L^2}(-dt^2 + dx_1^2 + dx_2^2 + dx_3^2) + L^2\frac{dr^2}{r^2} + L^2 d\Omega_5^2, \tag{1.21}$$

which is exactly the geometry of $AdS_5 \times S^5$. Note that L, which is now the radius of AdS_5, also controls the size of the sphere and is related to the number of D3-branes in the stack. Thus, we see that from the supergravity perspective we also end up with two decoupled sectors, free gravity in the bulk and near horizon modes living in $AdS_5 \times S^5$.

In both of these complementary descriptions we have a decoupled free gravity sector in the bulk. From the point of view of the strings, the dynamics of the D-branes is then described by N=4 SYM. On the other hand, from a geometrical perspective, the near horizon region of the D-branes is described by $AdS_5 \times S^5$. Since the two descriptions are complementary, we conclude that there is a correspondence between $N = 4$ SYM theory in $3+1$ dimensions and type IIB superstring theory on $AdS_5 \times S^5$.

It is important to note that pure AdS is dual to a CFT at zero temperature. Finite temperature configurations in the decoupled field theory correspond to brane configurations in AdS. Thus, if we wish to describe a CFT at nonzero temperature, we need to introduce a black hole inside of AdS. One such example is the

[9]From now on, we will refer to these as near horizon modes since this argument also applies to a black brane.

Schwarzschild AdS black hole given by,

$$ds^2 = -f(r)dt^2 + \frac{dr^2}{f(r)} + r^2 d\Omega^2, \tag{1.22}$$

where the so-called *blackening function*[10] $f(r)$ is given by

$$f(r) = 1 - \frac{2M}{r} + \frac{r^2}{L^2}. \tag{1.23}$$

The Schwarzschild black hole has a horizon temperature of

$$T = \frac{L^2 + 3r_h^2}{4\pi r_h L^2}, \tag{1.24}$$

where r_h is the black hole horizon found by solving $f(r) = 0$. While this discussion has been focused on CFTs, holography has been shown to be much broader and can be used to describe a large class of quantum field theories (QFT). As we will see, through holography we will also be able to realize a variety of renormalization group flows from certain field theories in the UV (which could be a CFT) to a number of QFTs in the IR. For example, one can describe IR nonrelativistic phases using the so-called Lifshitz geometry,

$$ds^2 = \left(-\frac{dt^2}{r^{2z}} + \frac{L^2 dr^2}{r^2} + \frac{dx^2 + dy^2}{r^2} \right). \tag{1.25}$$

This solution is parameterized by a dynamical critical exponent, z, and is invariant under the nonrelativistic scaling,

$$t \to \lambda^z t \quad , \quad x_i \to \lambda x_i \quad , \quad r \to \lambda r. \tag{1.26}$$

[10]The location of a black hole horizon is determined by the vanishing of the blackening function. The black hole temperature is then fixed by the horizon radius.

Geometries of this form can be used to model nonrelativistic phases as described by Lifshitz field theories, as we will see in later chapters. In addition, one could consider larger classes of gravitational solutions exhibiting an additional scaling exponent θ. These so-called hyperscaling violating solutions modify the Lifshitz metric (1.25) by an overall conformal factor and take the form,

$$ds^2 = r^\theta \left(-\frac{dt^2}{r^{2z}} + \frac{L^2 dr^2}{r^2} + \frac{dx^2 + dy^2}{r^2} \right). \tag{1.27}$$

Introducing a nonzero hyperscaling violating exponent, θ, modifies the scaling of the entropy density,

$$s \sim T^{\frac{d-\theta}{z}}, \tag{1.28}$$

and indicates that the free energy in these systems is anomalous[11]. Finally, black hole solutions of this form can be obtained by introducing the appropriate blackening function $f(r)$, leading to geometries of the form,

$$\begin{aligned} ds^2 &= r^\theta \left(-f(r)\frac{dt^2}{r^{2z}} + \frac{L^2 dr^2}{r^2 f(r)} + \frac{dx^2 + dy^2}{r^2} \right), \\ f(r) &= 1 - \left(\frac{r}{r_h} \right)^{2+z-\theta}. \end{aligned} \tag{1.29}$$

The holographic dictionary has been extended to include these geometries. We will return to these gravitational solutions in future chapters where they will be relevant to probe a variety of strongly correlated phases of matter.

1.3.4 Holography as a Strong/Weak Coupling Duality

One of the most useful properties of the AdS/CFT correspondence is that it is a weak/strong coupling duality. This means that problems involving quantum me-

[11]The effective degrees of freedom controlling the behavior of such systems live in $d_{eff} = d - \theta$ dimensions, and not in the naive number of dimensions.

chanical systems which are strongly coupled can be described in terms of tractable weakly coupled gravitational theories and vice-versa.

In order to gain insight for why AdS/CFT is a strong/weak coupling duality, we will first explain how the fundamental constants of each theory are mapped to each other. On the string theory side of the duality, we have three fundamental length scales, the length of the string l_s, the radius L of the AdS_5 space-time, and l_p, the Planck length. The gauge theory side of the duality, described by SU(N) $\mathcal{N} = 4$ SYM also has several fundamental constants. Unlike the string theory side, however, these are dimensionless quantities. Among these is the coupling strength of the SYM theory given by g_{YM} and the number of colors (the size of the SU(N) matrices) given by N. It is useful to define the 't Hooft coupling λ as a function of these parameters,

$$\lambda = g_{YM}^2 N, \tag{1.30}$$

as the theory at large N is most naturally optimized as an expansion in λ and $\frac{1}{N}$ (rather than g_{YM}^2 and $\frac{1}{N}$)[12].

Through the AdS/CFT dictionary we can express the 't Hooft coupling as a function of string theory parameters,

$$\lambda = \frac{L^4}{l_s^4} \sim N. \tag{1.31}$$

Additionally, N can be related to Newton's gravitational constant through the correspondence,

$$\left(\frac{L}{l_p}\right)^3 \sim \left(\frac{L}{G_N}\right)^3 \sim N^2. \tag{1.32}$$

In order to have a reliable semi-classical gravity description, both loops and

[12]There are N fields running in loops, which changes the expansion parameter from g_{YM}^2 to λ.

$\lambda << 1$	$\lambda >> 1$
• QFT is weakly coupled • Non-perturbative quantum gravity	• QFT is strongly coupled • Perturbative gravity regime

Figure 1.5: Summary of features associated with large or small 't Hooft coupling λ.

higher curvature terms must be suppressed on the string theory side. This means $L >> l_p$ and $L >> l_s$, or $\lambda >> 1$ and $N >> 1$. In this regime, the CFT is strongly coupled. On the other hand, if the CFT is weakly coupled, $\lambda << 1$, we have $L << l_s$. In this case, string and higher curvature corrections are not suppressed and the resulting string theory is strongly coupled. Thus, we see that by working in the perturbative gravity regime, one can probe the strong coupling sector of the dual field theory.

Chapter 2

Strongly Correlated Electron Matter

2.1 Conventional BCS Superconductors

A superconductor is a material which possesses zero resistance and expels a magnetic field from its interior when cooled below a characteristic critical temperature T_C. These two properties are completely independent of one another, meaning they each have a different fundamental origin [7]. A phenomenological description of superconductivity was put forth by Landau and Ginzburg in 1950 [8]. This is accomplished by introducing a complex scalar field $\psi = |\psi|e^{i\phi}$ which is related to the density n_s of superconducting electrons by $n_s = |\psi|^2$. This scalar field will act as an order parameter for the superconducting phase transition in the material, which was shown to be of second order. In particular, this phase transition can be seen from the behavior of the free energy F near the critical temperature T_C, where $|\psi|$ is small. For small values of $|\psi|$ the free energy can be expanded as in,

$$F = \alpha(T - T_c)|\psi|^2 + \frac{\beta}{2}|\psi|^4 + \frac{1}{2m}|(-i\hbar\nabla - 2qA)\psi|^2 \tag{2.1}$$

where α and β are positive constants, A is the electromagnetic vector potential and higher order terms have been omitted[1]. We will examine for simplicity the case of a homogeneous superfluid with no superconducting current. To minimize the free energy, we look for solutions where $F = 0$. In this case, we find

$$|\psi|^2 = -\frac{\alpha(T - T_c)}{\beta}. \tag{2.2}$$

In the regime of $T > T_c$, the free energy can only be minimized by $|\psi|^2 = 0$ and $\alpha = 0$ since the norm of the scalar field must be positive or zero. On the other hand, for $T < T_c$, we find that the free action can be minimized for $\psi \neq 0$. Thus below T_c, a phase transition occurs as the scalar field ψ condenses, with $|\psi|^2$ indicating the fraction of electrons that have condensed into a superfluid.

The microscopic mechanisms underlying conventional superconductors were discovered in 1957 by Bardeen, Cooper, and Schrieffer and are described in a framework referred to as BCS theory and its extensions [9]. BCS theory explains the presence of an attractive interaction between pairs of electrons, mediated by phonons, which describe the vibrations of the lattice. This provides a coupling mechanism which leads to the formation of electron pairs known as Cooper pairs below the critical temperature T_c. Cooper pairs can be separated by hundreds of nanometers, thus placing their coupling distance above the lattice spacing of the metal itself. Classically, this coupling can be thought of as a distortion within the positive ion lattice of the metal. An electron distorts the grid by pulling the positive ions that makeup

[1]Note that the free energy is independent of the phase ϕ of the order parameter, $\psi = |\psi|e^{i\phi}$ and thus above T_c the theory is invariant under a U(1) symmetry. The U(1) symmetry is broken spontaneously when the scalar condenses and the system chooses one of the ground states.

the lattice towards itself, creating a cloud of positive charge in the surrounding area (known as a *dressed electron*). A dressed electron is then able to couple to an additional electron thus forming a Cooper pair. However the effect is best described quantum mechanically as it can be shown that a bound electron pair is energetically favorable.

The Schrödinger equation for the two electron system is given by,

$$\left[-\frac{\hbar^2 \nabla^2_{\boldsymbol{r}_1}}{2m} - \frac{\hbar^2 \nabla^2_{\boldsymbol{r}_2}}{2m} + V(\boldsymbol{r}_1 - \boldsymbol{r}_2) \right] \Psi(\boldsymbol{r}_1, \boldsymbol{r}_2) = E\Psi(\boldsymbol{r}_1, \boldsymbol{r}_2), \tag{2.3}$$

where $\Psi(\boldsymbol{r}_1, \boldsymbol{r}_2)$ is the wave-function and E is the energy of the pair. Switching to the center of mass coordinate $\boldsymbol{R} = \frac{1}{2}(\boldsymbol{r}_1 + \boldsymbol{r}_2)$ and the relative displacement coordinate $\boldsymbol{r} = \boldsymbol{r}_1 - \boldsymbol{r}_2$ allows us to assume a wave-function of the form

$$\Psi(\boldsymbol{R}, \boldsymbol{r}) = \psi(\boldsymbol{r}) e^{i\boldsymbol{K}\cdot\boldsymbol{R}}, \tag{2.4}$$

due to the fact that the potential is independent of $\boldsymbol{R}$. Here $\boldsymbol{K}$ is the momentum conjugate to the center of mass. With this assumption, the Schrödinger equation simplifies to

$$\left[-\frac{\hbar^2 \nabla^2_{\boldsymbol{r}}}{m} + V(\boldsymbol{r}) \right] \psi(\boldsymbol{r}) = (E - \frac{\hbar^2 K^2}{4m}) \psi(\boldsymbol{r}). \tag{2.5}$$

The lowest energy can be identified by setting the center of mass momentum to zero. It is then useful to take the Fourier transform of the wave equation and rewrite (2.5) as

$$\int \frac{d^3k'}{(2\pi)^3} V(\boldsymbol{k} - \boldsymbol{k'}) \psi(\boldsymbol{k'}) = (E - 2\epsilon_{\boldsymbol{k}})\, \psi(\boldsymbol{k}), \tag{2.6}$$

$$\psi(\boldsymbol{k}) = \int d^3r\, \psi(\boldsymbol{r}) e^{-i\boldsymbol{k}\cdot\boldsymbol{r}}, \tag{2.7}$$

where $\epsilon_{\boldsymbol{k}} = \frac{\hbar k^2}{2m}$ is the free energy of an electron. It turns out to be convenient to define the modified wave-function $\Delta(\boldsymbol{k})$,

$$\Delta(\boldsymbol{k}) = (E - 2\epsilon_{\boldsymbol{k}})\psi(\boldsymbol{k}), \tag{2.8}$$

in terms of which equation (2.6) becomes

$$\Delta(\boldsymbol{k}) = -\int \frac{d^3k'}{(2\pi)^3} \frac{V(\boldsymbol{k} - \boldsymbol{k'})}{2\epsilon_{\boldsymbol{k'}} - E} \Delta(\boldsymbol{k'}). \tag{2.9}$$

For simplicity we assume a constant attractive potential $V(\boldsymbol{k} - \boldsymbol{k'}) = -V$ for $\epsilon_{\boldsymbol{k}} < \hbar\omega_D$ and zero otherwise. This potential will serve as a toy model for the interactions between the electrons and the phonons. Here ω_D is the Debye frequency, the maximum allowed frequency for which electrons can still interact with the lattice. Since electronic excitations with frequencies above the Debye cutoff are decoupled from the lattice of the material, they are unable to utilize the positive ions in the coupling process. Thus the Debye frequency acts as a useful cutoff for this model. With this assumption in place, we look for solutions to (2.9) where $\Delta(\boldsymbol{k}) = \Delta$, again for simplicity. This gives

$$\frac{2}{\rho(\hbar\omega_D)V} = \ln(1 + \frac{2\hbar\omega_D}{2\epsilon_{\boldsymbol{k}} - E}), \tag{2.10}$$

where the density of states per spin $\rho(\epsilon)$ is defined as

$$\rho(\epsilon) = \frac{m^{3/2}}{\sqrt{2}\hbar^3\pi^2}\sqrt{\epsilon}. \tag{2.11}$$

If it can be shown that Cooper pairs form even in the presence of a small attractive potential, $V << 1$, than it follows that Cooper pairs can also form for larger potentials. Therefore, we assume the limit $\rho(\hbar\omega_D)V << 1$, which leads to the expression

$$E = 2\epsilon_{\boldsymbol{k}} - 2\hbar\omega_D e^{-2/\rho(\hbar\omega_D)V}, \tag{2.12}$$

showing that the energy of the paired electrons is less than the free energy of the two electrons alone. The electron pair is therefore bound, since splitting the pair would require additional energy. Thus, we have shown quantum mechanically that Cooper pairs will form under appropriate conditions. The formation of Cooper pairs below the critical temperature is precisely the second order phase transition described by Landau and Ginzburg. Once Cooper pairs have condensed, the material becomes superconducting as the DC resistivity drops to zero. Most of our present knowledge for how interacting electrons behave in conventional metals relies on Landau Fermi liquid theory. This also includes a description of conventional BCS superconductors, as we will discuss next.

2.2 Landau Fermi Liquid Theory and its Breakdown

Landau proposed that conventional superconducting behavior may be modeled in the following way. Firstly, introduce a non-interacting particle with a desired momentum into the ground state of the Fermi sea. If interactions with the surrounding electrons are then turned on gradually, the particle behaves in the same way as a fermion in an excited state. The momentum and spin of the particle are unchanged, but the count is incremented. This type of object is known as a *quasiparticle*. Landau suggested describing the excited states of interacting fermion systems as being in a one-to-one correspondence with noninteracting systems of fermionic quasiparticles.

Landau Fermi Liquid theory fundamentally relies on three basic assumptions, all of which revolves around Landau's model of independently moving fermionic

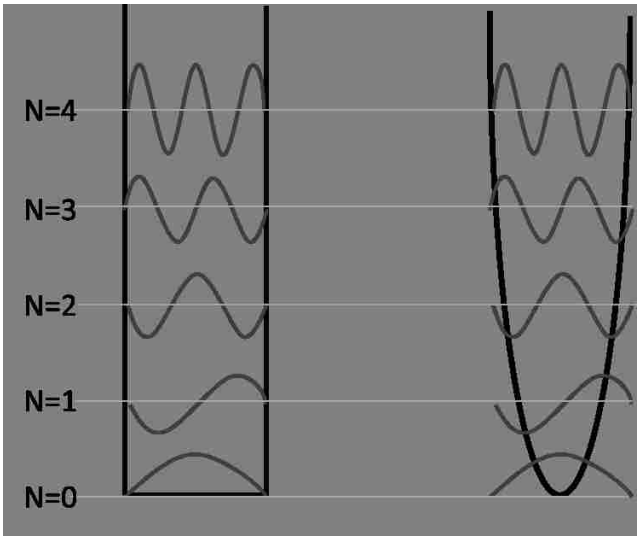

Figure 2.1: Illustration of bound states being described by their number of nodes in an infinite well and in a weakly interacting quadratic potential.

quasiparticles as an equivalent description for interacting fermions in condensed matter. The first of these assumptions is that the momentum and spin remain valid quantum numbers for the quasiparticle. The second assumption is that the interactions between the quasiparticle and the rest of the Fermi sea can be turned on adiabatically. These two assumptions can be thought of as a continuity of the labels used to describe quantum states across a smooth transformation. Consider for example a free particle in an infinite well as in figure 2.1. The fundamental quantum mechanical states are trivially sinusoidal waves with a specified number of nodes N. If we then introduce a weak quadratic potential as in figure 2.1, so that the particle is no longer free, solutions are found to be more complicated sine-like waves, but the number of nodes can still be used to identify energy states. An adiabatic transformation is thus defined as a change to the system which preserves the fundamental quantum numbers of the system. The third and final assumption of Landau Fermi liquid theory is that the produced quasiparticle state has an extended lifetime. This allows for the decay of the quasiparticle into more complicated states

at a later time.

Recall that in order for Cooper pairs to form, we had to assume that the energy of the free electrons was less than the energy associated with the Debye frequency. This limits the temperature range in which BCS theory is applicable. In particular, we can find the maximum applicable temperature as a function of the Debye temperature $T_{Debye} = \frac{\hbar}{k}\omega_D$. The energy of a free electron is related to the temperature T by the standard relationship

$$E = \frac{3}{2}kT. \tag{2.13}$$

Therefore in order to satisfy $E < \hbar\omega_D$, we require

$$T < \frac{2}{3}T_{Debye}. \tag{2.14}$$

Most superconducting materials achieve the formation of Cooper pairs at a critical temperature below $30K$ at standard elevation and pressure. In fact it is believed that the limit for the formation of Cooper pairs is somewhere between $30K$ and $40K$. However, there are some classes of superconducting materials which exhibit zero DC resistance with critical temperatures well above this limit. These materials are referred to as high-temperature (high-T_c) superconductors and are not described by BCS theory. Indeed, they fall outside the realm of Landau Fermi liquid theory.

In such unconventional superconductors, the pairing mechanism is not known. For instance, the attractive interaction between the dressed electrons may not be due to phonons, but instead to spin-spin interactions. Moreover, high T_c superconductors are believed to be inherently strongly interacting and thus may not admit any weakly interacting quasiparticle description. Finally, a quantum critical phase transition can result in the breakdown of Landau Fermi liquid theory. As was stated

previously, a quasiparticle state must maintain the system's fundamental quantum numbers. However, the quantum critical phase transition fundamentally changes these quantum numbers. Thus, in such regeims quasiparticles are unable to exist and as a result these materials do not behave like normal Fermi liquids. Next we will discuss these issues in more detail.

2.3 The Phase Diagram of High-Temperature Superconductors

The most famous high-temperature superconductor is yttrium barium copper oxide (YBCO), which is an example of the cuprate class of superconductor. Cuprate superconductors are characterized by layers of copper oxide separated by nontrivial spacer layers as shown in figure 2.2. With a critical temperature of $95K$, YBCO remains superconducting well above the limit of standard BCS theory. Due to the strongly coupled nature of the electrons in the superconducting materials, it is particularly challenging to model their behavior and in particular their dynamics. The typical phase diagram for high-T_c cuprate superconductors is shown in figure 2.3. Notice that as we vary the temperature and hole doping (a reduction in the number of conducting electrons per copper atom by chemical substitution) we find a rich structure of phases with different properties and symmetries. Thus, to better understand the mechanisms behind their unconventional behavior it is crucial to understand properties of this phase diagram.

Next we discuss the various corners of the phase diagram. At large doping levels, one finds a phase well described by standard Fermi liquid theory, in which the electrons in the metal behave as a cloud of ideal gas particles. In this regime the resistivity is quadratic in the temperature, $R(T) \sim T^2$. With the lowest amount

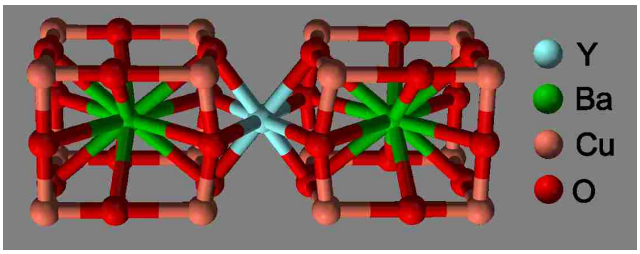

Figure 2.2: Schematic diagram of a YBCO superconducting material. Note the layered copper oxide edges in the diagram with internal yttrium and barium components.

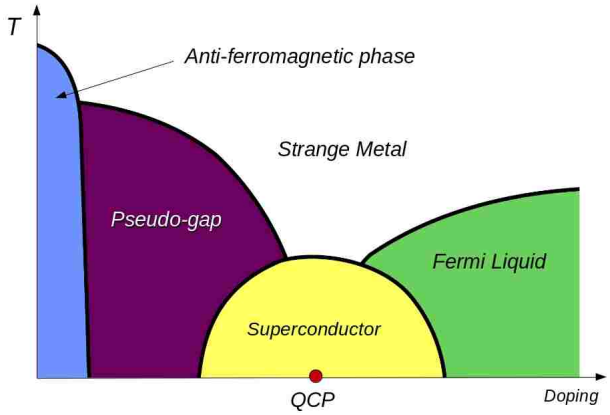

Figure 2.3: Typical phase diagram for high temperature superconductors (image from [10]).

of doping, the material enters the anti-ferromagnetic phase. In this phase all of the charges in the system are regularly distributed with nearest neighbor charges having opposite spin. This shows that materials like YBCO are not metals in their natural (undoped) state. In order to obtain metal-like conductivity, we must dope the system by removing electrons in order to break the anti-ferromagnetic properties of the material. While the anti-ferromagnetic phase can exist at temperatures higher than many of the other phases of the superconducting diagram, it is still limited by the Néel temperature of the material, the temperature above which the metal enters a standard paramagnetic phase.

In conventional superconductors, there is a nontrivial amount of energy required to excite a single electron. This is because one needs some additional energy to first break the Cooper pair once it formed. As no electrons can be excited with an amount of energy below this threshold, there is said to be an *energy gap* within the superconductor below the critical temperature. In these conventional systems, the gap dissapears above the critical temperature since Cooper pairs can no longer form and an electron can be excited for much less energy. A similar gap of states occurs in the phase diagram for the high temperature superconductor. However, the gap can occur at temperatures above T_C and is therefore referred to as a *pseudo-gap*. While there are some similarities to the behavior of the pseudo-gap and the conventional energy gap, the two are actually not correlated in any way. In fact, the question of why the pseudo-gap forms is thought to be a very important problem in understanding high T_C superconductors.

At the center of the phase diagram is the superconducting dome. This is the phase of matter in which the material becomes superconducting and electrons are free to move with no resistance. It is known that in heavy fermion metals[2], the existence of a *quantum critical point*[3] in the phase diagram leads to a pseudogap and to other anomalous behavior in nearby phases of matter [11]. Due to the similarities between the heavy fermion phase diagram and that of the cuprates, it is believed that there should also be a quantum critical point at the center of the superconducting dome. Since quantum critical points can dominate regions of the phase diagram well above zero temperature (such regions are then described by a finite temperature quantum critical theory), the quantum critical point is thought to determine the behavior not only within the superconducting dome, but also in

[2]A heavy fermion metal is an intermetallic compound with electrons in the 4f or 5f band.

[3]A quantum critical point(QCP) is a point in the phase diagram where a phase transition occurs at zero temperature, driven by quantum fluctuations. In particular, at the QCP quantum fluctuations diverge and become scale invariant.

other nearby phases of the diagram such as the so-called strange metal phase.

The anomalous strange metallic state in the high-temperature superconducting cuprates is one of the most remarkable puzzles in condensed matter physics [12]. In the strange metal phase common to various types of high Tc superconductors (cuprates and iron-based superconductors to name a few), the resistivity is linearly proportional to the temperature

$$R \sim T. \tag{2.15}$$

This behavior is robust and can not be explained using weakly interacting electrons. In the same temperature regime, weakly interacting electrons would have $R \sim T^2$ instead, as in the Fermi liquid corner of the phase diagram. Additionally, there is a strange scaling of the optical conductivity $\sigma(\omega) \sim \omega^{-2/3}$ for the cuprate high Tc superconductors at intermediate frequencies, which is again robust across different temperatures [13]. This strange metal behavior has been argued to be due to the fact that the temperature is the dominant energy scale in the system, and therefore sets the scattering rate near a QCP, resulting in the T-linear resistivity [14].

To summarize, the unconventional behavior of the high T_c superconductors appears to be linked to the complexity of their phase diagram and the co-existence of a number of phases. In particular, the possible competition or cooperation between the various orders seems to play a crucial role in their dynamics. Also of interest is the consequences of different symmetry breaking mechanisms (breaking translations, rotations or Lorentz invariance) on the generic behavior of strongly interacting quantum field theories (QFTs). The goal of this thesis is to examine some of these outstanding questions of high T_C superconductivity by using holography as a tool for probing the strongly correlated physics.

2.4 Holography for Strongly Correlated Matter

As previously discussed, holography provides new analytic tools for computing correlation functions in strongly coupled quantum field theories. Thus, it can be used to study properties of strongly correlated quantum phases of matter, and in particular their dynamics. For example, AdS/CFT techniques have led to the identification of a simple ratio for the shear viscosity η over entropy density s of strongly coupled fluids. In particular, in a large class of field theories[4], one expects to find the universal ratio $\frac{\eta}{s} = \frac{1}{4\pi}$. This simple result has been adopted in simulations of the QCD quark gluon plasma. This result is a concrete example of the fact that these techniques can give reliable, quantitative insights into strongly correlated systems.

Many of the strongly coupled systems described earlier in this chapter have unconventional conductive properties. High temperature superconductors are a prime example. As we have already stressed, accurately describing high temperature superconductivity is challenging because of the strongly interacting nature of the electrons in the material. Holography provides a new set of analytical tools to model their behavior.

As a first step to model superfluids and high temperature superconductors in a way reminiscent of the Landau Ginzburg model of section 2.1, the spontaneous symmetry breaking of a U(1) symmetry was realized in a gravitational model in [16] and [17], where it was shown that there is a critical temperature below which a charged condensate forms via a second order phase transition and the (DC) conductivity becomes infinite.

More specifically, in [16] it was shown for the first time that coupling gravity to a matter Lagrangian consisting of a charged scalar field in AdS would result in the

[4]This ratio is universal in the limit of strong coupling and infinite number of colors. Corrections to this universal behavior are also understood [15].

spontaneous breaking of a U(1) symmetry near the horizon of a black hole. This symmetry breaking causes the scalar field to condense near the black hole horizon in a similar way to how the Higgs Mechanism generates mass below a certain critical temperature. Specifically, the model used has the Lagrangian:

$$16\pi G_N \mathcal{L} = R - \frac{6}{L^2} - \frac{1}{4}F_{\mu\nu}^2 - |\partial_\mu \psi - iqA_\mu \psi|^2 - m^2|\psi|^2, \tag{2.16}$$

which involves the Ricci scalar R, a cosmological constant term $\frac{6}{L^2}$, kinetic terms for the complex charged scalar field ψ and the gauge field A_μ as well as a quadratic potential for the scalar field (assumed to have a mass m). The important part of this Lagrangian for observing spontaneous symmetry breaking is the term which couples the gauge field to the scalar field of charge q, of the form $q^2A^2|\phi|^2$. As we will see below, this term will contribute to the effective mass of the scalar field ψ.

In the unbroken phase (which describes the theory above the critical temperature, $T > T_C$), the solution to this theory is the Reissner-Nordstrom black hole in AdS_4 given by:

$$\begin{aligned} ds^2 = -f dt^2 + \frac{dr^2}{f} + r^2 d\Omega_{2,k}^2\,, \qquad & f = 1 - \frac{2M}{r} + \frac{Q^2}{4r^2} + \frac{r^2}{L^2} \\ A_\mu dx^\mu = \Phi(r) dt\,, \qquad & \Phi(r) = \frac{Q}{r} - \frac{Q}{r_H}, \end{aligned} \tag{2.17}$$

where M and Q denote the mass and charge respectively and L the radius of AdS_4. In this high temperature regime, the theory does not allow for a scalar field ($\psi = 0$) – when the temperature is sufficiently high, a non-zero scalar field is simply not a solution to the equations of motion in this theory. As we lower the temperature, however, we will notice that the scalar field condenses to a non-zero value. Indeed,

it can be shown that in the Lagrangian (2.16) the scalar field has an effective mass:

$$m_{eff}^2 = m^2 + g^{tt}q^2\Phi^2. \tag{2.18}$$

Notice that since g^{tt} is negative, a sufficiently large gauge field Φ will cause the effective mass squared to be negative. This signals an instability to a new phase, in particular, the condensation of the scalar field. When this happens, the scalar field $\psi(r)$ can develop a VEV, breaking the U(1) symmetry (it gives the gauge field an effective mass $\sim \psi^2 A^2$). This symmetry-breaking process corresponds to the black hole developing so-called scalar hair. When solving the equations of motion for ψ near the AdS boundary, we obtain a solution of the form of (1.16):

$$\psi(r) = \frac{A_\psi}{r^{3-\Delta}} + \frac{B_\psi}{r^\Delta} + \dots, \tag{2.19}$$

where we are omitting subleading terms. As explained in section 1.3.2, the constants A_ϕ and B_ϕ play a crucial role on the quantum side of the duality. In particular, one describes the source and the other the VEV of the quantum operator O dual to ϕ, which in this setup describes a scalar condensate. Numerical studies [18] of the behavior of the VEV $\langle O \rangle$ have shown that the condensate has the following dependence on temperature,

$$\langle O \rangle \approx 144 T_c^2 (1 - \frac{T}{T_c})^{\frac{1}{2}}, \tag{2.20}$$

which can clearly be seen in the graph of figure 2.4 and has a behavior typical of *mean field theory*.

In [17], the previous results were then expanded to include the computation of the conductivity using techniques in holography. Conductivities are extracted from

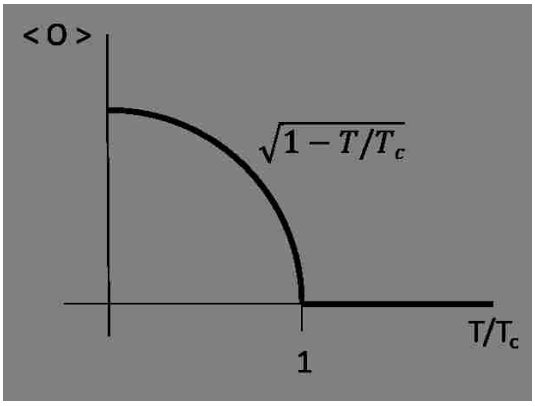

Figure 2.4: The condensation of the VEV below a critical temperature.

current-current correlations, and in the holographic dictionary a current in the QFT is dual to a gauge field in the bulk. It turns out to be convenient to consider the x component of the gauge field A_x. Finding the asymptotic solution to its equation of motion as was done for the scalar field in (2.19) gives,

$$A_x = A_x^{(0)} + \frac{A_x^{(1)}}{r} + \ldots, \tag{2.21}$$

where $A_x^{(0)}$ and $A_x^{(1)}$ are the source and VEV of the dual quantum operator to the gauge field, which is the current J_μ. Here the gauge field is simply a vector potential for the electric field in AdS. The limit of the electric field can be obtained from:

$$(E_x)_{AdS} = -\frac{\partial A_x^{(0)}}{\partial t} = i\omega A_x^{(0)}, \tag{2.22}$$

where we have assumed a time dependence of $e^{-i\omega t}$. We can then use the holographic dictionary to obtain expressions for the conductivities. Specifically, the electric field on the boundary is exactly the limit of the electric field in the bulk: $(E_x)_{AdS} = (E_x)_{CFT}$ and the VEV of the boundary current is given by: $J_x = A_x^{(1)}$. We can then

use Ohm's law to find the conductivity of the holographic system,

$$\sigma(\omega) = \frac{J_x}{E_x} = -\frac{iA_x^{(1)}}{\omega A_x^{(0)}}. \tag{2.23}$$

Thus, we can determine the behavior of this conductivity at low temperatures by solving Maxwell's equation of motion for the gauge field, A_x. For a Lagrangian of the form in (2.16), Maxwell's equation is given by,

$$A_x'' + \frac{f'}{f}A_x' + (\frac{2}{f^2} - \frac{2\psi^2}{f})A_x = 0, \tag{2.24}$$

which can be solved numerically.

The plot in figure 2.5 shows that at $T > T_c$ the conductivity is constant. Below the critical temperature, the real part of the conductivity depends on the magnitude of ω. At large ω, the conductivity converges. However, at $\omega = 0$, we see a delta function in the conductivity, confirming that there is zero DC resistance for this material when $T < T_c$.

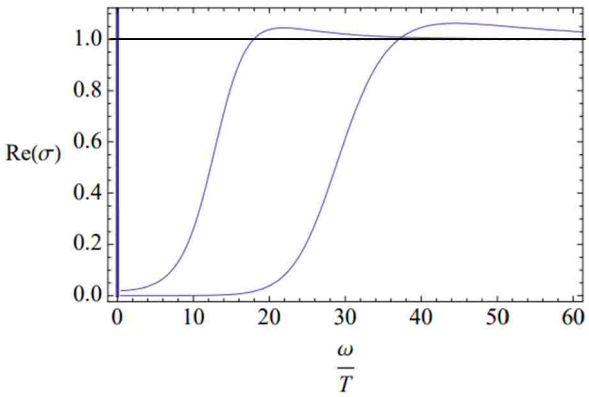

Figure 2.5: The real part of the conductivity as a function of ω/T. Here the black horizontal line gives the conductivity at $T > T_c$ while the blue lines give the conductivity for two values of $T < T_c$. Note the delta function at $\omega = 0$ demonstrating infinite DC conductivity.

The somewhat simple analysis outlined here opened the door for many detailed investigations of quantum phases of matter using holography. Since the work of [8,9] this research program has developed substantially and has been extended in a variety of ways, with an increasing level of sophistication. The outline for the rest of this thesis is the following.

Thesis Outline - In chapter 3, we will adopt these techniques to examine transport properties of a class of holographic theories which can support some of the scalings seen in cuprate high temperature superconductors [19]. We will examine in particular the string theory motivated non-linear Dirac-Born-Infeld model. In chapter 4, we present a breakdown of the fundamental ingredients necessary in order for a class of solutions to admit anomalous scaling behavior [20]. Finally, in chapter 5 we will apply these findings to a model with generic non-linear interactions between the charge carriers in order to generalize our previous results [21].

Chapter 3

Backreacted DBI Magnetotransport

As we have seen, holographic techniques have provided new avenues for exploring the behavior of strongly coupled quantum phases of matter. In recent years much of the focus has been on understanding the transport properties of models that may be in the same universality class as strongly correlated electron systems, whose unconventional behavior is believed to be tied to the richness and complexity of their phase diagram (see e.g. [22] for a recent review). A particularly puzzling behavior is that of the linear temperature dependence of the electrical resistivity $R \sim T$ displayed by the strange metal phase of many correlated systems in condensed matter, which is often associated with the existence of an underlying quantum critical point. This strange metal behavior has been argued to be due to the fact that the temperature is the dominant energy scale in the system, and therefore sets the scattering rate near a quantum critical point, resulting in the T-linear resistivity[23].

A natural question is then whether the same argument applies to magnetotransport phenomena in quantum critical systems, with the magnetic field behaving

much like temperature. Indeed, it has been shown recently [24] that in the pnictide superconductor $BaFe_2(As_{1-x}P_x)_2$ near its quantum critical point the magnetic field h plays the same role as the temperature T, with the in-plane resistance described well by

$$R_{DC} = \sqrt{\hat{\alpha}\, T^2 + \hat{\eta}\, h^2}\,, \tag{3.1}$$

where $\hat{\alpha}, \hat{\eta}$ are constants which relate the scattering rate to the temperature and magnetic field scales (see [24] for more details). It is believed that in quantum critical metals h and T compete with each other to set the scale of the scattering rate, and thus magnetic fields provide yet another way to probe the unconventional linear resistivity of the strange metal phase.

It was shown in [25] that the behavior (3.1) can be generated holographically by working with a string-inspired Dirac-Born-Infeld (DBI) model, which can be thought of as a non-linear realization of electrodynamics which encodes the low-energy dynamics of D-branes. In particular, the result (3.1) is a special case of a broader class of allowed scaling behaviors, which are realized by considering finite temperature backgrounds exhibiting hyperscaling violation $\theta \neq 0$ and a non-trivial dynamical exponent $z \neq 1$. A specific choice of exponents z and θ then yields precisely (3.1).

However, the analysis of [25] was done in the probe approximation, building on the work of [26, 27], in which the backreaction of the charge density and magnetic field on the geometry is neglected. Indeed, in the probe DBI limit the charge degrees of freedom are subleading as compared to the uncharged ones (the D-branes leave the background unchanged since their backreaction is not taken into account). As a result, the coefficient of the momentum conserving δ-function is hierarchically suppressed and the DC conductivity is finite even though the system has transla-

tional invariance[1]. However, once the full backreaction of the DBI action is taken into account, the above probe description breaks down and one recovers the usual infinite DC conductivity due to the presence of translational symmetry.

In this chapter we are going to extend the results of [25, 26, 27] by going beyond the probe limit and examining the effect of backreaction of the DBI action on the geometry. In order to introduce momentum dissipation and ensure that the theory can lead to a finite DC conductivity, we add axionic scalars [28], thus breaking translational invariance. The axions are taken to depend on the spatial directions linearly, making the analysis tractable. We will find new classes of solutions, including geometries that exhibit Lifshitz scaling and hyperscaling violation, which can be associated with new quantum critical regimes. Armed with these backgrounds, we will examine the implications on the transport properties of the dual system. The question we are interested in is that of the role of the fully non-linear effects encoded by the DBI interactions on the conductive properties – are there any features inherent to the backreacted analysis that would be absent in the probe approximation? Our focus will be on the interplay between temperature and magnetic field, in the presence of momentum relaxation. We will find a very rich structure for the resistivity that arises in this class of models.

The outline of this chapter is as follows. Section 3.1 introduces our holographic DBI model while Section 3.2 contains the computation of the DC conductivity matrix and a discussion of simple limiting cases. In Section 3.3 we present exact black brane solutions for the case of a trivial dilatonic scalar, and discuss the associated magnetic-field-induced metal-insulator transition. Section 3.4 contains new exact hyperscaling violating and Lifshitz-like scaling geometries and discusses the asso-

[1]In systems with translational symmetry, the conductivity is typically infinite, because charges can propagate indefinitely without dissipating momentum. This leads to a δ function in the DC conductivity.

ciated transport behavior. Finally, in Section 3.5 we include for complenetss the magnetotransport analysis for the simpler Born-Infeld theory.

3.1 The Holographic Setup

We consider a four-dimensional model describing gravity coupled to a neutral scalar field ϕ, two axions ψ^I and an abelian gauge field A_μ, whose dynamics is described by the DBI action,

$$S = \int d^4x\sqrt{-g}\left[\mathcal{R} - \frac{1}{2}(\partial\phi)^2 - V(\phi) - \frac{Y(\phi)}{2}\sum_{I=1}^{2}(\partial\psi^I)^2\right] + S_{DBI}\,, \tag{3.2}$$

with[2] the DBI term

$$S_{DBI} = -\int d^4x Z_1(\phi)\left[\sqrt{-\det(g_{\mu\nu} + Z_2(\phi)F_{\mu\nu})} - \sqrt{-\det(g_{\mu\nu})}\right]. \tag{3.3}$$

The couplings $Z_1(\phi), Z_2(\phi), Y(\phi)$ are introduced to lead to non-trivial interactions between the scalar sector and the gauge field. It is well known that dimensional reductions usually involve several matter fields and non-trivial potentials for the lower-dimensional scalars. It would be interesting to find an actual top-down construction in which the couplings of the D-brane action are fixed uniquely (see, for example, [25]). However in this chapter we focus on a bottom-up approach and view (3.3) as an effective theory, without worrying about its detailed string theory origin. In particular, we would like to see whether this effective theory can lead to interesting behaviors for the magnetotransport of the putative dual quantum system.

[2]The second term in S_{DBI}, which could have been incorporated into $V(\phi)$, is chosen to make it apparent that in the weak flux limit $F \to 0$ one recovers the standard gauge field kinetic term.

The equations of motion associated with the action (3.2) take the form

$$\begin{aligned}\nabla_\mu\nabla^\mu\phi - V'(\phi) - \frac{Y'(\phi)}{2}\sum_{I=1}^{2}(\partial\psi^I)^2 - Z_1'(\phi)\left[\sqrt{\frac{-\det(g+Z_2(\phi)F)}{-\det g}}-1\right]\\ +\frac{Z_1(\phi)Z_2'(\phi)}{2}\sqrt{\frac{-\det(g+Z_2(\phi)F)}{-\det g}}(g+Z_2(\phi)F)^{-1[\mu\nu]}F_{\mu\nu}=0\,,\end{aligned} \tag{3.4}$$

$$\nabla_\mu\left[Z_1(\phi)Z_2(\phi)\sqrt{\frac{-\det(g+Z_2(\phi)F)}{-\det g}}(g+Z_2(\phi)F)^{-1[\mu\nu]}\right]=0\,, \tag{3.5}$$

$$\nabla_\mu\left(Y(\phi)\nabla^\mu\psi^I\right)=0\,, \tag{3.6}$$

$$\begin{aligned}\mathcal{R}_{\mu\nu}-\frac{1}{2}\mathcal{R}g_{\mu\nu}=\frac{1}{2}\left(\partial_\mu\phi\partial_\nu\phi-\frac{1}{2}g_{\mu\nu}(\partial\phi)^2\right)+\frac{Y(\phi)}{2}\sum_{I=1}^{2}\left(\partial_\mu\psi^I\partial_\nu\psi^I-\frac{1}{2}g_{\mu\nu}(\partial\psi^I)^2\right)\\ -\frac{1}{2}g_{\mu\nu}V(\phi)+T^{DBI}_{\mu\nu}\,,\end{aligned} \tag{3.7}$$

with the DBI stress energy tensor $T^{DBI}_{\mu\nu}=-\frac{1}{\sqrt{-g}}\frac{\delta S_{DBI}}{\delta g^{\mu\nu}}$ given by

$$T^{DBI}_{\mu\nu}=-\frac{Z_1(\phi)}{2}\sqrt{\frac{-\det(g+Z_2(\phi)F)}{-\det g}}g_{\mu\alpha}(g+Z_2(\phi)F)^{-1(\alpha\beta)}g_{\beta\nu}+\frac{Z_1(\phi)}{2}g_{\mu\nu}\,. \tag{3.8}$$

Here $(g+Z_2(\phi)F)^{-1\mu\nu}$ is the inverse of $(g+Z_2(\phi)F)_{\mu\nu}$, with the subscript $^{(\,)}$ denoting the symmetric part (and $^{[\,]}$ the antisymmetric part). The current in the dual field theory, evaluated at the boundary, reads

$$\begin{aligned}J^\mu&=\sqrt{-\gamma}\,n_\nu\,Z_1(\phi)Z_2(\phi)\sqrt{\frac{-\det(g+Z_2(\phi)F)}{-\det g}}\,(g+Z_2(\phi)F)^{-1[\nu\mu]}\Big|_\partial\\ &=Z_1(\phi)Z_2(\phi)\sqrt{-\det(g+Z_2(\phi)F)}\,(g+Z_2(\phi)F)^{-1[r\mu]}\Big|_\partial\,,\end{aligned} \tag{3.9}$$

The quantities γ and n^μ in this expression are, respectively, the induced metric and outward pointing normal vector at the asymptotically AdS boundary. Here we have

used r to denote the holographic radial direction.

Assuming homogeneity and isotropy, the bulk metric and the matter fields take the generic form,

$$\begin{aligned} ds^2 &= -D(r)dt^2 + B(r)dr^2 + C(r)(dx^2+dy^2), \quad \phi = \phi(r), \\ \psi^1 &= k\,x, \quad \psi^2 = k\,y, \quad A = A_t(r)\,dt + \frac{h}{2}(xdy - ydx)\,, \end{aligned} \tag{3.10}$$

with h denoting the magnitude of the magnetic field. The axions depend on the spatial coordinates linearly, which breaks translational invariance and gives rise to momentum relaxation. The parameter k controls the strength of the momentum dissipation in the system. Substituting the ansatz into (3.4)-(3.7), we obtain the following equations:

$$\begin{aligned} &\frac{1}{\sqrt{BD}C}\left(\sqrt{\frac{D}{B}}C\phi'\right)' + \frac{\Omega}{C\sqrt{BD}}\frac{Z_2'(\phi)}{Z_2(\phi)}\left((C^2+2h^2Z_2(\phi)^2)A_t'^2 - h^2BD\right) \\ &\qquad -Z_1'(\phi)\left(\frac{Z_1(\phi)Z_2(\phi)^2}{\Omega C\sqrt{BD}} - 1\right) - \frac{k^2}{C}Y'(\phi) - V'(\phi) = 0\,, \end{aligned} \tag{3.11}$$

$$\frac{D'C'}{DC} + \frac{1}{2}\frac{C'^2}{C^2} - \frac{1}{2}\phi'^2 + BZ_1(\phi)\left(\frac{\Omega C\sqrt{BD}}{Z_1(\phi)Z_2(\phi)^2} - 1\right) + \frac{\Omega B\sqrt{BD}h^2}{C} + \frac{k^2B}{C}Y(\phi) + BV(\phi) = 0\,, \tag{3.12}$$

$$\frac{2C''}{C} - \left(\frac{B'}{B} + \frac{C'}{C} + \frac{D'}{D}\right)\frac{C'}{C} + \phi'^2 = 0\,, \tag{3.13}$$

$$\frac{2D''}{D} - \frac{2C''}{C} - \left(\frac{B'}{B} - \frac{C'}{C} + \frac{D'}{D}\right)\frac{D'}{D} + \frac{B'C'}{BC} - 2\Omega\sqrt{BD}\left(\frac{CA_t'^2}{D} + \frac{Bh^2}{C}\right) - \frac{2k^2B}{C}Y(\phi) = 0\,, \tag{3.14}$$

$$(\Omega(C^2 + h^2Z_2(\phi)^2)A_t')' = 0\,, \tag{3.15}$$

where for convenience we have introduced the function

$$\Omega(r) = \frac{Z_1(\phi)Z_2(\phi)^2}{\sqrt{(C^2+h^2Z_2(\phi)^2)(BD - Z_2(\phi)^2A_t'^2)}}\,. \tag{3.16}$$

3.2 DC Conductivities with a Finite Magnetic Field

Next, we calculate the DC conductivities for our DBI model using the method developed in [18, 29] [3], which generalizes the techniques to extract correlation functions outlined in chapter 1 and in section 2.4. We consider the following set of perturbations,

$$\begin{aligned} \delta g_{ti} = C(r) h_{ti}(r)\,, \quad \delta g_{ri} = C(r) h_{ri}(r)\,, \\ \delta A_i = -E_i\, t + a_i(r), \quad \delta\psi_1 = \chi_1(x), \quad \delta\psi_2 = \chi_2(x)\,, \end{aligned} \tag{3.17}$$

with $i = x, y$, and further simplify our analysis by using diffeomorphisms to set

$$D(r) = \frac{1}{B(r)}\,. \tag{3.18}$$

The vector equation (3.15) can be immediately integrated, leading to the radially independent quantity

$$\rho = \Omega(C^2 + h^2 Z_2(\phi)^2) A_t'\,, \tag{3.19}$$

which is nothing but the charge density J^t in the dual field theory as defined in (3.9). There are two constant fluxes that are provided by the perturbed vector equations,

$$\partial_r J^x(r) = \partial_r J^y(r) = 0\,, \tag{3.20}$$

where

$$J^x(r) = -\Omega C D(a_x' + h\, h_{ry}) - \frac{C^2 h_{tx} - h E_y Z_2^2}{C^2 + h^2 Z_2^2}\,\rho\,, \tag{3.21}$$

$$J^y(r) = -\Omega C D(a_y' - h\, h_{rx}) - \frac{C^2 h_{ty} + h E_x Z_2^2}{C^2 + h^2 Z_2^2}\,\rho\,, \tag{3.22}$$

[3] Other studies on the transport coefficients based on Einstein-Maxwell-like theories in the presence of a magnetic field can be found *e.g.* in [30, 31, 32, 33, 34, 35, 36, 37].

are both currents in the dual field theory. Since they are conserved along the radial direction, they can be calculated anywhere in the bulk, with a particularly convenient choice being the horizon.

The perturbation equations coming from Einstein's equations (3.7) are

$$h''_{tx} + \frac{2C'}{C} h'_{tx} + \Omega A'_t (a'_x + h\, h_{ry}) - \frac{1}{CD}\left(k^2 Y + h^2 \Omega\right) h_{tx} - \frac{h\Omega}{CD} E_y = 0\,, \tag{3.23}$$

$$h''_{ty} + \frac{2C'}{C} h'_{ty} + \Omega A'_t (a'_y - h\, h_{rx}) - \frac{1}{CD}\left(k^2 Y + h^2 \Omega\right) h_{ty} + \frac{h\Omega}{CD} E_x = 0\,, \tag{3.24}$$

$$kY\chi'_1 + \Omega h\, a'_y - \frac{\Omega C A'_t}{D}(E_x - h\, h_{ty}) - \left(k^2 Y + \Omega h^2\right) h_{rx} = 0\,, \tag{3.25}$$

$$kY\chi'_2 - \Omega h\, a'_x - \frac{\Omega C A'_t}{D}(E_y + h\, h_{tx}) - \left(k^2 Y + \Omega h^2\right) h_{ry} = 0\,, \tag{3.26}$$

while the axion equations (3.6) yield

$$\chi''_1 + \left(\frac{C'}{C} + \frac{D'}{D} + \frac{Y'\phi'}{Y}\right)(\chi'_1 - k\, h_{rx}) - k\, h'_{rx} = 0\,, \tag{3.27}$$

$$\chi''_2 + \left(\frac{C'}{C} + \frac{D'}{D} + \frac{Y'\phi'}{Y}\right)(\chi'_2 - k\, h_{ry}) - k\, h'_{ry} = 0\,. \tag{3.28}$$

Notice that (3.27) and (3.28) are implied by the other equations.

Since we are interested in a background geometry with a regular horizon at $r = r_h$, we have

$$\begin{aligned} A_t &= A'_t(r_h)(r - r_h) + \ldots\,, \\ D &= D'(r_h)(r - r_h) + \cdots = 4\pi T (r - r_h) + \ldots\,, \end{aligned} \tag{3.29}$$

while the constraint of regularity on the perturbation equations near r_h demands

the following expansions,

$$\begin{aligned} a_i &= -\frac{E_i}{4\pi T}\log(r-r_h)+\ldots, \quad h_{ti} = Dh_{ri}+\ldots, \\ \chi_1 &= \chi_1(r_h)+\ldots, \quad \chi_2 = \chi_2(r_h)+\ldots\ . \end{aligned} \tag{3.30}$$

The latter can be obtained by switching to the Eddington-Finklestein coordinate

$$v = t - \int^r \frac{1}{D(z)}dz = t - \frac{1}{4\pi T}\log(r-r_h)+\ldots, \tag{3.31}$$

where we have demanded that $v \to -\infty$ as $r \to r_h$. Using the above regularity conditions, we extract the horizon data for h_{tx} and h_{ty} from (3.25) and (3.26),

$$h_{tx}(r_h) = -\frac{\rho\, E_x + h\, J^y}{k^2 C(r_h) Y(\phi(r_h))}, \quad h_{ty}(r_h) = -\frac{\rho\, E_y - h\, J^x}{k^2 C(r_h) Y(\phi(r_h))}\,. \tag{3.32}$$

Substituting the relations above into (3.21) and (3.22) and using (3.30), we find

$$\begin{pmatrix} 1+\frac{h^2\Omega}{k^2 Y} & -\frac{Ch\rho}{k^2 Y(C^2+h^2Z_2^2)} \\ \frac{Ch\rho}{k^2 Y(C^2+h^2Z_2^2)} & 1+\frac{h^2\Omega}{k^2 Y} \end{pmatrix} \begin{pmatrix} J^x \\ J^y \end{pmatrix} = \\ \begin{pmatrix} C\left(\Omega+\frac{\rho^2}{k^2Y(C^2+h^2Z_2^2)}\right) & h\rho\left(\frac{\Omega}{k^2Y}+\frac{Z_2^2}{C^2+h^2Z_2^2}\right) \\ -h\rho\left(\frac{\Omega}{k^2Y}+\frac{Z_2^2}{C^2+h^2Z_2^2}\right) & C\left(\Omega+\frac{\rho^2}{k^2Y(C^2+h^2Z_2^2)}\right) \end{pmatrix} \begin{pmatrix} E_x \\ E_y \end{pmatrix}, \tag{3.33}$$

evaluated at the horizon $r = r_h$. In these expressions the function Ω introduced in (3.16) takes the form

$$\Omega = \frac{Z_2}{C^2+h^2Z_2^2}\sqrt{\rho^2 + Z_1^2 Z_2^2 (C^2+h^2Z_2^2)}\,. \tag{3.34}$$

Finally, relating the two currents J^x and J^y in the matrix equation (3.33) to the

electric fields E_x and E_y via

$$J^x = \sigma_{xx}\, E_x + \sigma_{xy}\, E_y\,, \quad J^y = \sigma_{yx}\, E_x + \sigma_{yy}\, E_y\,, \tag{3.35}$$

the DC conductivities can be easily extracted and are given by

$$\begin{aligned}
\sigma_{xx} &= \sigma_{yy} = \frac{k^2 CY\left[\Omega(h^2\Omega + k^2 Y)(C^2 + h^2 Z_2^2)^2 + C^2\rho^2\right]}{(h^2\Omega + k^2 Y)^2(C^2 + h^2 Z_2^2)^2 + h^2 C^2\rho^2}\,, \\
\sigma_{xy} &= -\sigma_{yx} \\
&= \frac{h\rho[(h^2\Omega + k^2 Y)^2(h^2 Z_2^4 + 2C^2 Z_2^2) + (h^2\Omega + k^2 Y)C^4\Omega + C^2\rho^2 - C^2 k^2 Y(C^2\Omega + k^2 Y Z_2^2)]}{(h^2\Omega + k^2 Y)^2(C^2 + h^2 Z_2^2)^2 + h^2 C^2\rho^2}\,.
\end{aligned} \tag{3.36}$$

The conductivity matrix is controlled by four functions, the three scalar couplings Z_1, Z_2, Y and the component C of the bulk metric. All four are functions of the holographic radial coordinate r and in (3.36) are evaluated at the horizon $r = r_h$. Moreover, since r_h is in general a function of temperature T, the matrix (3.36) is implicitly temperature-dependent, while the dependence on the remaining scales in the system – the magnetic field h, the strength of momentum dissipation k and the charge density ρ – is explicitly visible. We should note that our results for σ_{xx} overlap with those obtained recently in [38].

From the expressions (3.36) we can then extract the inverse Hall angle,

$$\cot\Theta_H = \frac{\sigma_{xx}}{\sigma_{xy}}, \tag{3.37}$$

and the resistivity matrix by inverting the conductivity matrix,

$$R_{xx} = R_{yy} = \frac{\sigma_{xx}}{\sigma_{xx}^2 + \sigma_{xy}^2}\,, \quad R_{xy} = -R_{yx} = -\frac{\sigma_{xy}}{\sigma_{xx}^2 + \sigma_{xy}^2}\,. \tag{3.38}$$

From now on all functions will be understood to be evaluated at the horizon, but for convenience we will omit the explicit dependence on r_h. Since the general formulae for σ_{ij} and R_{ij} are quite cumbersome, we consider first some simple limiting cases.

3.2.1 Weak momentum dissipation

A simple case to consider is that of slow momentum relaxation, *i.e.* small k. As a consistency check, we first look at the limit $k \to 0$, which corresponds to no momentum dissipation at all. The conductivity tensor then reduces to

$$\sigma_{xx} = \sigma_{yy} = 0, \quad \sigma_{xy} = -\sigma_{yx} = \frac{\rho}{h}\,, \tag{3.39}$$

and is independent of the temperature as well as the details of the theory we are working with. This can be understood as a generic consequence of Lorentz invariance when $k \to 0$, and agrees with the Hall conductivity result of [39]. Including the leading and subleading corrections coming from momentum dissipation, we find

$$\begin{aligned}
\sigma_{xx} = \sigma_{yy} &= \frac{C}{h^2}k^2 Y - \frac{C\Omega(C^2+h^2Z_2^2)^2}{h^4\Omega^2(C^2+h^2Z_2^2)^2+h^2C^2\rho^2}(k^2Y)^2 + \dots\,, \\
\sigma_{xy} = -\sigma_{yx} &= \frac{\rho}{h} - \frac{\rho}{h}\frac{C^2(C^2+h^2Z_2^2)}{h^4\Omega^2(C^2+h^2Z_2^2)^2+h^2C^2\rho^2}(k^2Y)^2 + \dots\,.
\end{aligned} \tag{3.40}$$

As expected, the matrix components are now sensitive to the detailed structure of the model, and are temperature dependent through the implicit dependence on r_h.

3.2.2 Vanishing magnetic field

In the absence of magnetic field, $\sigma_{xy} = 0$, and the DC conductivity reduces to the simple expression

$$\sigma_{DC} = \sigma_{xx} = Z_2\sqrt{Z_1^2Z_2^2 + \frac{\rho^2}{C^2}} + \frac{\rho^2}{k^2YC} = Z_2\sqrt{Z_1^2Z_2^2 + \frac{16\pi^2\rho^2}{s^2}} + \frac{4\pi\rho^2}{k^2Ys}\,, \tag{3.41}$$

where $s = 4\pi\, C(r_h)$ is the entropy density [4]. As seen in a number of cases in the literature, the DC conductivity can be interpreted [40] as being composed of two physically distinct and independent pieces: a coherent contribution σ_{DC}^{diss} due to momentum relaxation for the charge carriers in the system, and an incoherent contribution, known as the charge conjugation symmetric term σ_{DC}^{ccs}, which is independent of the charge density ρ. In the absence of magnetic field, there are examples showing that the DC conductivity consists of such two distinct terms, simply added together. However, more generally the contributions can combine to form the DC conductivity in a rather non-trivial fashion. Indeed, notice that in (3.41) we do not have a clean separation between σ_{DC}^{ccs} and terms dissipating momentum for charge carriers. The first contribution in the square root persists at zero charge density, *i.e.* the charge conjugation symmetric term is given by $\sigma_{DC}^{ccs} = Z_1 Z_2^2$. The other two terms are associated with the charge density ρ and are due to momentum dissipation effects. Thus, here we have given an explicit realization of a setup in which there is no simple separation between σ_{DC}^{ccs} and σ_{DC}^{diss}.

3.2.3 Vanishing charge density

The DC resistivity in the absence of charge density reads

$$R_{DC} = R_{xx} = \frac{1}{Z_1 Z_2^2}\sqrt{1+\frac{Z_2^2}{C^2}h^2}+\frac{h^2}{k^2 Y C} = \frac{1}{Z_1 Z_2^2}\sqrt{1+\frac{16\pi^2 Z_2^2}{s^2}h^2}+\frac{4\pi h^2}{k^2 Y s}\,, \quad (3.42)$$

which falls into the charge conjugation regime, since the charge density is vanishing. It should be pointed out that charge fluctuations still exist at zero charge density, and it would seem the incoherent conductivity should be identified as being due to diffusion of charge fluctuations. Notice the similarity of the structure of this result

[4] In the action (3.2) we have used units with $\frac{1}{16\pi G_N} = 1$, where G_N is Newton's constant. So the entropy density by definition is $s = \frac{C(r_h)}{4G_N} = 4\pi C(r_h)$.

with that of (3.41). In particular, we have $\sigma_{xy} = R_{xy} = 0$ because $\rho = 0$. In contrast, in the case with vanishing magnetic field the theory is parity symmetric, which requires the Hall conductivity to vanish for any value of charge densityρ.

3.2.4 Strong momentum dissipation limit

Next, we consider the case in which the momentum dissipation $\sim k$ is dominant compared to the other scales in the system. Working to leading order in the strong momentum dissipation limit, we obtain the conductivities

$$\begin{aligned}\sigma_{xx} &= \sigma_{yy} = \Omega C - \frac{C(\Omega^2 h^2 (C^2 + h^2 Z_2^2)^2 - C^2\rho^2)}{(C^2 + h^2 Z_2^2)^2}\frac{1}{k^2 Y} + \dots\,, \\ \sigma_{xy} &= -\sigma_{yx} = \frac{h\rho Z_2^2}{C^2 + h^2 Z_2^2} + \frac{2C^2 h\rho\Omega}{C^2 + h^2 Z_2^2}\frac{1}{k^2 Y} + \dots\,,\end{aligned} \tag{3.43}$$

and the corresponding resistivities

$$\begin{aligned}R_{xx} =& R_{yy} = \frac{C}{Z_2}\frac{\sqrt{\rho^2 + Z_1^2 Z_2^2 (C^2 + h^2 Z_2^2)}}{\rho^2 + C^2 Z_1^2 Z_2^2} - \\ & \frac{C[\rho^2(\rho^2 + C^2 Z_1^2 Z_2^2) + h^2 Z_1^2 Z_2^4 (\rho^2 - C^2 Z_1^2 Z_2^2)]}{Z_2^2 (\rho^2 + C^2 Z_1^2 Z_2^2)^2}\frac{1}{k^2 Y} + \dots\,, \\ R_{xy} =& -R_{yx} = -\frac{h\rho}{\rho^2 + C^2 Z_1^2 Z_2^2} - \\ & \frac{2h\rho C^2 Z_1^2 Z_2 \sqrt{\rho^2 + Z_1^2 Z_2^2 (C^2 + h^2 Z_2^2)}}{Z_2^2 (\rho^2 + C^2 Z_1^2 Z_2^2)^2}\frac{1}{k^2 Y} + \dots\,.\end{aligned} \tag{3.44}$$

We focus on the conductivities at leading order, which are given by

$$\begin{aligned}\sigma_{xx} &= \sigma_{yy} = \Omega C = \frac{Z_2 C}{C^2 + h^2 Z_2^2}\sqrt{\rho^2 + Z_1^2 Z_2^2 (C^2 + h^2 Z_2^2)}\,, \\ \sigma_{xy} &= -\sigma_{yx} = \frac{h\rho Z_2^2}{C^2 + h^2 Z_2^2}\,.\end{aligned} \tag{3.45}$$

The inverse Hall angle reads

$$\cot\Theta_H = \frac{\sigma_{xx}}{\sigma_{xy}} = \frac{C}{h\rho Z_2}\sqrt{\rho^2 + Z_1^2 Z_2^2 (C^2 + h^2 Z_2^2)}\,, \tag{3.46}$$

and the in-plane resistivity

$$R_{DC} = R_{xx} = \frac{C}{Z_2}\frac{\sqrt{\rho^2 + Z_1^2 Z_2^2 (C^2 + h^2 Z_2^2)}}{\rho^2 + C^2 Z_1^2 Z_2^2}\,. \tag{3.47}$$

Interestingly, we find that these expressions are precisely the same as the ones which were obtained in the probe DBI case [25], using a different approach.

This can be understood as follows. When the momentum dissipation is strong enough, the contribution to the geometry coming from the DBI sector is negligible compared to that of the axionic sector. Thus, in this case the background geometry is seeded by the axions, and the dynamics of the U(1) gauge field can be captured by treating it as a probe around the resulting geometry. This can be easily seen from the background equations (3.11)-(3.14). When the terms coming from the DBI action are negligible compared to the axionic terms, we obtain a closed system which only involves the axions as well as ϕ coupled to gravity,

$$\frac{1}{\sqrt{BDC}}\left(\sqrt{\frac{D}{B}}C\phi'\right)' - \frac{k^2}{C}Y'(\phi) - V'(\phi) = 0\,, \tag{3.48}$$

$$\frac{D'C'}{DC} + \frac{1}{2}\frac{C'^2}{C^2} - \frac{1}{2}\phi'^2 + \frac{k^2 B}{C}Y(\phi) + BV(\phi) = 0\,, \tag{3.49}$$

$$\frac{2C''}{C} - \left(\frac{B'}{B} + \frac{C'}{C} + \frac{D'}{D}\right)\frac{C'}{C} + \phi'^2 = 0\,, \tag{3.50}$$

$$\frac{2D''}{D} - \frac{2C''}{C} - \left(\frac{B'}{B} - \frac{C'}{C} + \frac{D'}{D}\right)\frac{D'}{D} + \frac{B'C'}{BC} - \frac{2k^2 B}{C}Y(\phi) = 0\,. \tag{3.51}$$

The gauge field A_t can then be determined from (3.15).

As was shown in [25, 41], the coupled equations of motion (3.48)-(3.51) admit IR hyperscaling scaling violating geometries,

$$\begin{aligned} ds^2 &= r^\theta \left(-f(r)\frac{dt^2}{r^{2z}} + \frac{L^2 dr^2}{r^2 f(r)} + \frac{dx^2+dy^2}{r^2} \right) , \\ \phi &= \kappa \, \ln(r), \quad \psi^1 = k\, x, \quad \psi_2 = k\, y \, , \end{aligned} \tag{3.52}$$

with

$$\begin{aligned} & f(r) = 1 - \left(\frac{r}{r_h}\right)^{2+z-\theta} , \; z = \frac{\alpha^2-\eta^2+1}{\alpha(\alpha+\eta)} \; , \; \theta = \frac{2\eta}{\alpha}, \quad \kappa = -\frac{2}{\alpha} \, , \\ & L^2 = \frac{(z+2-\theta)(\theta-2z)}{V_0} \; , \; k^2 L^2 = 2(z-1)(z+2-\theta) \, , \\ & \eta = \pm \frac{\theta}{\sqrt{(\theta-2)(\theta+2-2z)}} \; , \; \alpha = \pm \frac{2}{\sqrt{(\theta-2)(\theta+2-2z)}} \, , \end{aligned} \tag{3.53}$$

when the dilaton couplings V and Y are approximated by exponentials in the IR,

$$V(\phi) \sim -V_0 \, e^{\eta \, \phi}, \quad Y(\phi) \sim e^{\alpha \, \phi} \, , \tag{3.54}$$

with η, α constants. In order to have a well defined geometry and a resolvable singularity one should take into account the Gubser's physicality criterion [42, 103], which restricts the range of the scaling exponents $\{z, \theta\}$ appearing in (4.12). In particular, the allowed parameter range is given by

$$\begin{aligned} & \text{IR} \quad r \to 0 : \quad [z \leqslant 0, \theta > 2], \quad [0 < z < 1, \theta > z+2] \, , \\ & \text{IR} \quad r \to \infty : \; [1 < z \leqslant 2, \theta < 2z-2], \quad [z > 2, \theta < 2] \, , \end{aligned} \tag{3.55}$$

depending on the location of the IR. It was also shown in [25] that by setting

$$\frac{C(r_h)}{Z_2(\phi(r_h))} \sim T, \quad Z_1(\phi(r_h)) Z_2(\phi(r_h))^2 \sim \frac{1}{T} \, , \tag{3.56}$$

where T is the temperature, one can obtain the scaling behavior

$$R_{DC} \sim \sqrt{aT^2 + h^2}\,, \tag{3.57}$$

with a a constant which depends on the details of the action. The main point to note for this case is that for appropriate choices of parameters it is possible to reproduce the in-plane resistance (3.1). The anomalous temperature dependence of the resistivity and Hall angle of the cuprate strange metals has recently been realized in this setup [20]. The backreacted DBI case, however, leads to a much richer transport behavior, as we will see next.

3.3 Magnetic-Field-Induced Metal-Insulator Transition

If we choose the dilaton field ϕ to be trivial, the background black brane geometry can be solved exactly. Even in this simple case the physics is still quite rich, and we find a finite-temperature transition – or crossover – from metallic to insulating behavior, induced by the magnetic field.

We take the couplings to be of the form [5]

$$Z_1 = z_1\,, \quad Z_2 = Y = 1\,, \quad V = -V_0, \quad \phi = 0\,, \tag{3.58}$$

where z_1 and V_0 are positive constants. Once again we set $D(r) = 1/B(r)$. The metric function $C(r)$ is then found by solving (3.13), and is given by

$$C(r) = r^2. \tag{3.59}$$

Here we have chosen the AdS boundary to be at $r \to \infty$. The remaining (non-trivial)

[5] A class of exact solutions for the DBI theory without axions have been studied in [44].

equations of motion are then

$$A_t' - \frac{\rho}{z_1\sqrt{r^4 + \frac{\rho^2+h^2z_1^2}{z_1^2}}} = 0\,, \tag{3.60}$$

$$rD' + D - \frac{r^2}{2}(V_0 + z_1) + \frac{1}{2}k^2 + \frac{z_1}{2}\sqrt{r^4 + \frac{\rho^2 + h^2z_1^2}{z_1^2}} = 0\,, \tag{3.61}$$

$$D'' - \frac{2}{r^2}D - \frac{1}{r^2}k^2 - \frac{\rho^2 + h^2z_1^2}{r^2z_1\sqrt{r^4 + \frac{\rho^2+h^2z_1^2}{z_1^2}}} = 0\,. \tag{3.62}$$

We find that the last equation is implied by the second one. Solving (3.61), we obtain

$$\begin{aligned} D(r) = \frac{r^2}{6}(V_0 + z_1) - \frac{z_1}{6}\sqrt{r^4 + \frac{h^2z_1^2 + \rho^2}{z_1^2}} - \frac{1}{2}k^2 - \frac{M}{r} \\ -\frac{1}{3}\sqrt{h^2z_1^2 + \rho^2}\;{}_2F_1\left(\frac{1}{4}, \frac{1}{2}; \frac{5}{4}; -\frac{r^4z_1^2}{\rho^2 + h^2z_1^2}\right), \end{aligned} \tag{3.63}$$

where M corresponds to the mass of the black brane and is determined by the location of the horizon r_h via $D(r_h) = 0$. The U(1) gauge field is given by

$$\begin{aligned} A_t(r) &= \int_{r_h}^{r} \frac{\rho}{\alpha\sqrt{u^4 + \frac{\rho^2+h^2z_1^2}{z_1^2}}}\,du \\ &= c_1 + \rho\, r\sqrt{\frac{1}{h^2z_1^2 + \rho^2}}\;{}_2F_1\left(\frac{1}{4}, \frac{1}{2}; \frac{5}{4}; -\frac{r^4z_1^2}{\rho^2 + h^2z_1^2}\right), \end{aligned} \tag{3.64}$$

with the constant c_1 given by requiring as usual that the gauge field vanishes at the horizon, $A_t(r_h) = 0$. Finally, the temperature associated with the black brane geometry takes the form

$$T = \frac{D'(r_h)}{4\pi} = \frac{V_0 + z_1}{8\pi}r_h - \frac{1}{8\pi r_h}k^2 - \frac{z_1}{8\pi r_h}\sqrt{r_h^4 + \frac{\rho^2 + h^2z_1^2}{z_1^2}}\,, \tag{3.65}$$

and the entropy density reads

$$s = 4\pi r_h^2 \,. \tag{3.66}$$

By making use of (3.65) to express the location of the horizon in terms of T, one can find the temperature dependence of the conductivity matrix (3.36) as well as the resistivity matrix (3.38), which of course also depends on the magnetic field h, the charge density ρ and the momentum dissipation parameter k.

It is interesting to ask whether the black brane solution we just presented leads to metallic or insulating behavior. To this end, we are going to adopt the following working definition of a metal versus an insulator,

$$\text{Metal}: \quad \frac{dR_{xx}}{dT} > 0 \,, \qquad \text{Insulator}: \quad \frac{dR_{xx}}{dT} < 0 \,, \tag{3.67}$$

and inspect the temperature dependence of the conductivities. We will focus on cases with finite momentum dissipation, since in the limit $k \to 0$ shown in (3.39) the conductivity is quite simple, due to Lorentz invariance. For simplicity and without loss of generality, from now on we fix our theory parameters to be

$$z_1 = 1, \quad V_0 = 6 \,. \tag{3.68}$$

We start by considering two simple cases which correspond to, respectively, vanishing magnetic field and charge density. The former turns out to be associated with metallic behavior, while the latter with insulating. We then look at the more generic situation, in which both h and ρ are non-zero, and find a finite temperature crossover between the two types of behavior.

3.3.1 Vanishing magnetic field

We examine first the case in which the magnetic field is absent. The Hall part of the conductivity is zero, and the resistivity can be obtained from (3.41),

$$R_{DC} = R_{xx} = 1/\sigma_{xx} = \frac{k^2 r_h^2}{\rho^2 + k^2\sqrt{r_h^4 + \rho^2}}\,, \tag{3.69}$$

For a fixed value of $k/\sqrt{\rho}$,[6] the resistivity R_{DC} increases monotonically with increas-

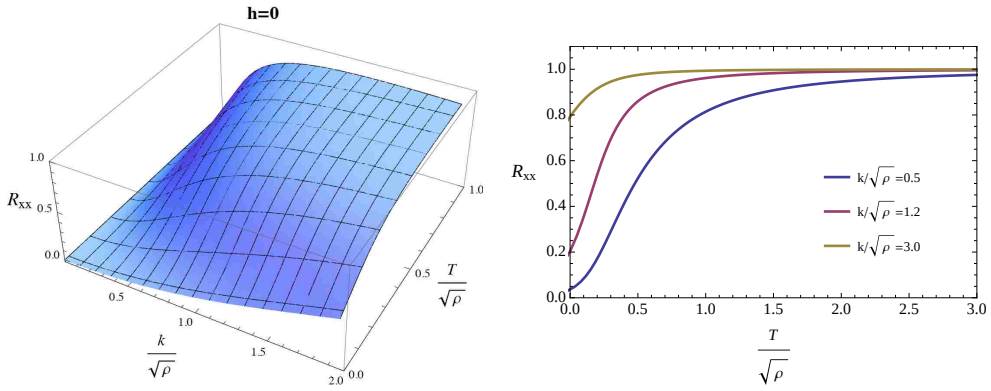

Figure 3.1: The DC resistivity R_{xx} when $h = 0$ as a function of $T/\sqrt{\rho}$ and $k/\sqrt{\rho}$. Moving from top to bottom, the curves in the right panel correspond to decreasing values of $k/\sqrt{\rho}$.

ing temperature, as shown in Figure 3.1. Thus, according to the criterion (3.67), the resulting behavior is metallic. The curves displayed in the right panel of Figure 3.1 correspond to, from top to bottom, decreasing values of $k/\sqrt{\rho}$. We therefore see that by lowering the amount k of momentum dissipation one also decreases the resistivity, with the effect being especially pronounced at low T. What this indicates is that as $k \to 0$ we should recover a divergent conductivity, which is expected from the fact that we would be approaching the regime of no momentum dissipation.

[6] Without loss of generality, we will assume $\rho \geqslant 0$ from now on.

3.3.2 Vanishing charge density

In the case with vanishing charge density, the component σ_{xy} is also zero. The resistivity can now be obtained from (3.42),

$$R_{DC} = R_{xx} = \frac{h^2 + k^2\sqrt{r_h^4 + h^2}}{k^2 r_h^2}\,. \tag{3.70}$$

For a fixed value of $k/\sqrt{h}$, the quantity R_{DC} decreases monotonically as the tem-

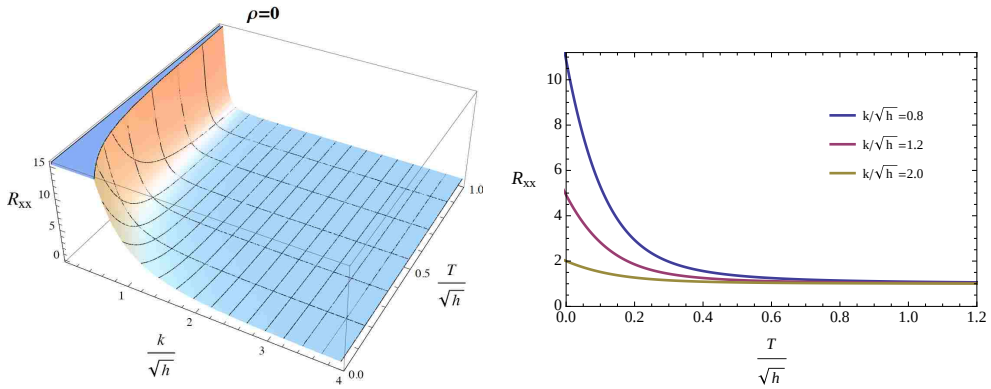

Figure 3.2: The DC resistivity R_{xx} at vanishing charge density as a function of $T/\sqrt{h}$ and $k/\sqrt{h}$. In the right panel, from top to bottom the ratio $k/\sqrt{h}$ increases.

perature increases, as can be seen from Figure 3.2. According to (3.67), this corresponds to an insulating like behavior. Moreover, the curves in the right panel of Figure 3.2 show that the smaller the ratio $k/\sqrt{h}$, the larger the resistivity, with the enhancement more pronounced at low temperatures. We wonder whether this effect is entirely model dependent, or whether it could be a feature of the role of disorder or momentum dissipation on insulating phases.

3.3.3 Magnetotransport at finite magnetic field and charge density

We move on to the more generic case in which both h and ρ are non-zero, which is significantly more complex. There is now a non-trivial Hall component to the conductivities, and the general resistivity components are given by

$$\begin{aligned} R_{xx} &= k^2 r_h^2 \frac{\rho^2 Q^2 \left(Q^2-k^4\right)+k^2\sqrt{Q^2+r_h^4}\left(\rho^2\left(k^4-Q^2\right)+k^4 r_h^4\right)+k^4 r_h^4(h^2-\rho^2)}{\rho^4\left(Q^2-k^4\right)^2+2k^4\rho^2 r_h^4\left(h^2+k^4-\rho^2\right)+k^8 r_h^8}, \\ R_{yx} &= h\,\rho\,\frac{2k^6 r_h^4\sqrt{Q^2+r_h^4}+\rho^2\left(Q^2-k^4\right)^2+k^4 r_h^4\left(h^2+k^4-3\rho^2\right)}{\rho^4\left(Q^2-k^4\right)^2+2k^4\rho^2 r_h^4\left(h^2+k^4-\rho^2\right)+k^8 r_h^8}, \end{aligned} \tag{3.71}$$

where we have introduced $Q^2=\rho^2+h^2$. The inverse Hall angle reads

$$\begin{aligned} \cot\Theta_H &= \frac{\sigma_{xx}}{\sigma_{xy}}=\frac{R_{xx}}{R_{yx}} \\ &= \frac{k^2 r_h^2}{h\rho}\frac{\rho^2 Q^2\left(Q^2-k^4\right)+k^2\sqrt{Q^2+r_h^4}\left(\rho^2\left(k^4-Q^2\right)+k^4 r_h^4\right)+k^4 r_h^4(h^2-\rho^2)}{2k^6 r_h^4\sqrt{Q^2+r_h^4}+\rho^2\left(Q^2-k^4\right)^2+k^4 r_h^4\left(h^2+k^4-3\rho^2\right)}. \end{aligned} \tag{3.72}$$

We display the behavior of the in-plane resistance R_{xx} in Figure 3.3 at the momentum dissipation parameter $k/\sqrt{\rho}=1$. We find the following features:

- $h<\rho$: R_{xx} increases monotonically as one increases the temperature, corresponding to metallic behavior.
- $h>\rho$: As the temperature increases, R_{xx} first rises, then reaches a maximum at a certain ratio $T_0/\sqrt{\rho}$, and then decreases monotonically. The value of $T_0/\sqrt{\rho}$ depends on $k/\sqrt{\rho}$ and h/ρ. We have metallic behavior at low temperatures and insulating at high temperatures. Thus, this can be thought of as a metal-insulator transition – or crossover – induced by the magnetic field.

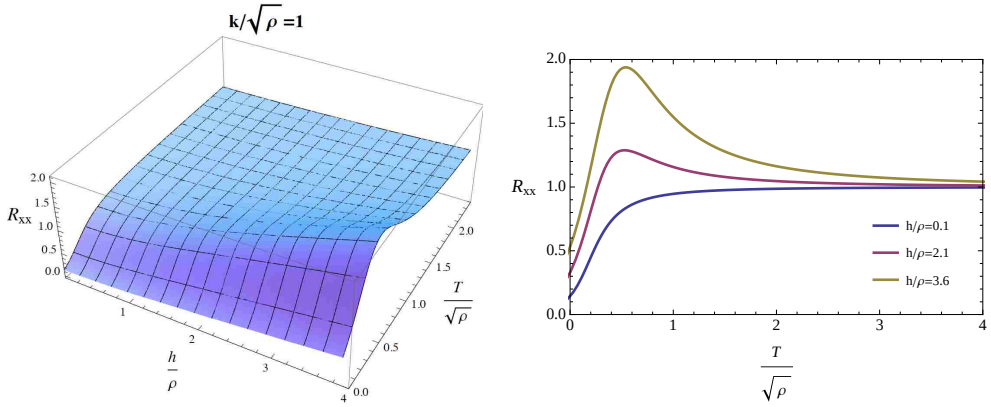

Figure 3.3: The resistance R_{xx} at finite charge density as a function of h/ρ and $T/\sqrt{\rho}$. We choose the momentum dissipation parameter $k/\sqrt{\rho} = 1$. In the right panel, the curves from top to bottom correspond to decreasing values of h/ρ.

We also display the resistance R_{xx} for a larger value of the momentum dissipation parameter, $k/\sqrt{\rho} = 3$, in Figure 3.4. The temperature dependence of R_{xx} is similar to that in the previous case when $h < \rho$. However, the non-monotonic behavior at large values of the magnetic field disappears and R_{xx} decreases monotonically as one increases the temperature, which is reminiscent of an insulating behavior. Note that the change in the behavior of the resistivity is once again induced by the magnetic field. Metal-insulator transitions or crossovers have been studied using other gravity setups, see, *e.g.* [45, 46, 47, 48, 49, 50].

The threshold value for the magnetic field, $h/\rho = 1$, can be understood in the following way. Consider the high temperature limit $T \gg (k, \sqrt{\rho}, \sqrt{h})$ in which T is the dominant scale in the problem. In this limit at leading order the temperature (3.65) is given by the simple expression

$$T = \frac{V_0}{8\pi} r_h = \frac{3}{4\pi} r_h \,, \tag{3.73}$$

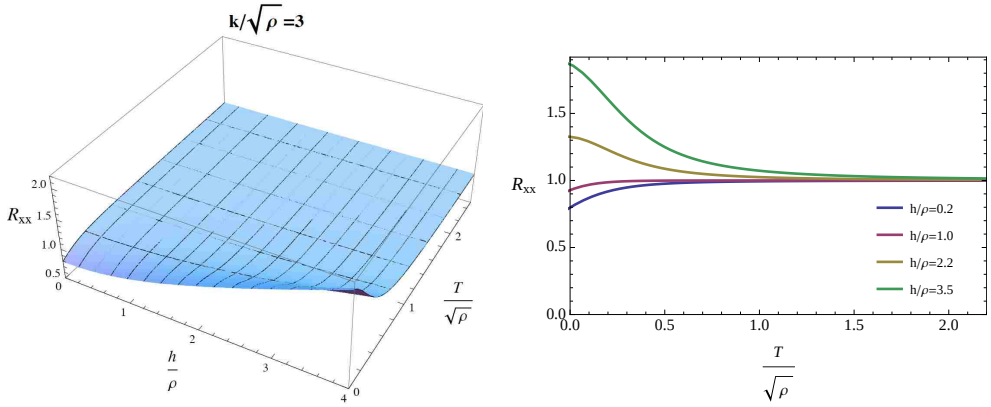

Figure 3.4: The resistance R_{xx} at finite charge density versus h/ρ and $T/\sqrt{\rho}$. We choose the momentum dissipation parameter $k/\sqrt{\rho} = 3$. In the right panel, the curves from top to bottom correspond to decreasing values of h/ρ.

and the corresponding resistance R_{xx} reads

$$R_{xx} = 1 + \frac{h^2 - \rho^2}{k^2 r_h^2} + \mathcal{O}(r_h^{-3}) = 1 + \frac{9}{16\pi^2}\frac{h^2 - \rho^2}{k^2}\, T^{-2} + \mathcal{O}(T^{-3})\,. \tag{3.74}$$

It is clear that when $h < \rho$, R_{xx} increases monotonically with T (working under the assumption above that the temperature is the largest scale in the problem), displaying metallic behavior. On the other hand, it decreases with increasing T when $h > \rho$, displaying insulating behavior. In this regime, the Hall component and the inverse Hall angle become

$$R_{yx} = \frac{9}{8\pi^2}\frac{h\rho}{k^2}\, T^{-2} + \mathcal{O}(T^{-3})\,, \quad \cot\Theta = \frac{8\pi^2}{9}\frac{k^2}{h\rho}\, T^2 + \mathcal{O}(T^0)\,. \tag{3.75}$$

At this point one would like to restore all theory parameters (3.58). The general results in the high temperature regime are given by

$$\begin{aligned} R_{xx} &= \frac{1}{z_1} + \frac{V_0^2}{64\pi^2}\frac{h^2 z_1^2 - \rho^2}{k^2 z_1^2}\, T^{-2} + \mathcal{O}(T^{-3})\,, \\ R_{yx} &= \frac{V_0^2}{32\pi^2}\frac{h\rho}{k^2 z_1}\, T^{-2} + \mathcal{O}(T^{-3})\,, \qquad\qquad T \gg (k, \sqrt{\rho}, \sqrt{h})\,, \\ \cot\Theta &= \frac{32\pi^2}{V_0^2}\frac{k^2}{h\rho}\, T^2 + \mathcal{O}(T^0)\,. \end{aligned} \tag{3.76}$$

The threshold value for the magnetic field is therefore given by $h/\rho = 1/z_1$. Finally, note that in order to generate more arbitrary scalings, one needs to allow for more complicated background geometries, in which the neutral scalar ϕ should be dynamical. We turn to this question next.

3.4 Non-relativistic Scaling Geometries

We are now going to examine the behavior of the resistivities for geometries supported by a non-trivial scalar field profile, and which exhibit non-relativistic scalings. We choose the couplings to have the simple exponential form

$$Z_1(\phi) = z_1 e^{\gamma\,\phi}\,, \quad Z_2(\phi) = e^{\delta\,\phi}\,, \quad V(\phi) = -V_0\, e^{\eta\,\phi}\,, \quad Y(\phi) = e^{\alpha\,\phi}\,, \tag{3.77}$$

in order to look for *exact* scaling solutions, loosely motivated by top-down realizations [25, 103]. However, one should keep in mind that we will assume that such non-relativistic solutions describe the IR of the geometry, and approach AdS in the UV, so that one can adopt the standard AdS/CFT dictionary. To this end, the scalar potential of (3.77) should be appropriately modified, to ensure that the scalar ϕ can indeed settle to a constant at the boundary. That this can be done is by now well known, and has been shown explicitly in a variety of cases in the literature.

Thus, here we will simply adopt 3.77 and focus on obtaining exact scaling backgrounds. We focus mostly on cases with no magnetic field, but also include a simple background solution for which h is non-zero. Scaling solutions for the Einstein-DBI-dilaton system were also studied first in [51] and later in [52]. However the models studied in those papers did not include axions, and therefore did not incorporate any mechanism for dissipating momentum, resulting in an infinite DC conductivity.

3.4.1 Hyperscaling-violating solutions without magnetic field

We are going to parametrize the geometry as in (3.10), and look for black brane solutions of the form

$$B(r) = \frac{L^2 r^{\theta-2}}{f(r)}\,, \quad C(r) = r^{\theta-2}\,, \quad D(r) = r^{\theta-2z} f(r)\,, \tag{3.78}$$

$$A = A_t(r)\,dt\,, \quad \phi(r) = \kappa \ln r\,, \quad \psi^1 = k\,x\,, \quad \psi^2 = k\,y\,, \tag{3.79}$$

where the parameters z and θ are, respectively, the Lifshitz and hyperscaling violating exponents. In this ansatz we have turned off the magnetic field, $h = 0$, for simplicity. Note that when the blackening function is trivial, $f(r) = 1$, one recovers the standard hyperscaling-violating geometries

$$ds^2 = r^\theta \left(-\frac{dt^2}{r^{2z}} + \frac{L^2 dr^2}{r^2} + \frac{dx^2 + dy^2}{r^2} \right), \tag{3.80}$$

which represent the extremal limit of (3.78) and can be thought of as generalized quantum critical geometries. Examining Einstein's equations, we immediately find from (3.13) that κ must obey

$$\kappa^2 = (\theta - 2)(\theta - 2z + 2)\,, \tag{3.81}$$

while from the gauge field equation (3.15) we find the derivative of A_t,

$$A_t' = \frac{\rho L\, r^{\theta-z-\delta\kappa-1}}{\sqrt{\rho^2 + z_1^2 r^{2[\theta-2+(\gamma+\delta)\kappa]}}}\,. \tag{3.82}$$

In order to obtain exact solutions for this system we will make some assumptions on the parameters of the model. First, notice that the gauge field expression (3.82) simplifies drastically when we set

$$\theta = 2 - \kappa(\gamma+\delta)\,, \tag{3.83}$$

in which case the gauge field obeys the much simpler condition

$$A_t' = \frac{\rho L\, r^{\theta-z-\delta\kappa-1}}{\sqrt{\rho^2 + z_1^2}}\,. \tag{3.84}$$

Combining (3.81) and (3.83) in this case yields the following relation between z and θ,

$$z = 1 + \frac{\theta}{2} + \frac{2-\theta}{2(\gamma+\delta)^2}\,. \tag{3.85}$$

We are most interested in the case in which the stress tensor terms in the field equations originating from the axions appear at the same order in powers of the radial coordinate as terms coming from the metric, neutral scalar and U(1) gauge fields. This motivates us to take

$$\delta = -\alpha = \frac{2}{\kappa}\,, \quad \eta = \gamma\,. \tag{3.86}$$

Finally, using (3.11), (3.12) and (3.14), we find an analytic solution for $f(r)$

$$f(r) = 1 - \left(\frac{r}{r_h}\right)^{2+z-\theta}\,, \tag{3.87}$$

where r_h is the location of the horizon, and

$$L^2 = \frac{2}{\delta^2}\frac{(\gamma+3\delta)(\gamma+\delta)+1}{V_0+z_1-k^2-\sqrt{\rho^2+z_1^2}}\,, \tag{3.88}$$

$$k^2 = \frac{\gamma^2+\gamma\delta-1}{\delta^2+\gamma\delta+1}\left(\frac{z_1^2}{\sqrt{\rho^2+z_1^2}}-z_1-V_0\right)-\frac{\rho^2}{\sqrt{\rho^2+z_1^2}}\,. \tag{3.89}$$

We have demanded that the extremal limit is given by (3.80).

Summarizing our results, in the case of vanishing magnetic field we have obtained the following quantum critical geometry, supported by a running scalar,

$$\begin{aligned} ds^2 &= r^\theta\left[-\frac{f(r)}{r^{2z}}dt^2+\frac{L^2}{r^2 f(r)}dr^2+\frac{dx^2+dy^2}{r^2}\right]\,,\\ \phi &= \kappa\ln(r),\quad \psi^1 = k\,x,\quad \psi^2 = k\,y\,, \end{aligned} \tag{3.90}$$

with

$$\begin{aligned} f(r) &= 1-\left(\frac{r}{r_h}\right)^{2+z-\theta},\quad z=\frac{1-\gamma^2+\delta^2}{\delta(\gamma+\delta)},\quad \theta=-\frac{2\gamma}{\delta},\quad \kappa=\frac{2}{\delta}\,,\\ L^2 &= \frac{2}{\delta^2}\frac{(\gamma+3\delta)(\gamma+\delta)+1}{V_0+z_1-k^2-\sqrt{\rho^2+z_1^2}} = \frac{(\theta-2)(\theta-z-2)}{V_0+z_1-k^2-\sqrt{\rho^2+z_1^2}}\,,\\ k^2 &= \frac{\gamma^2+\gamma\delta-1}{\delta^2+\gamma\delta+1}\left(\frac{z_1^2}{\sqrt{\rho^2+z_1^2}}-z_1-V_0\right)-\frac{\rho^2}{\sqrt{\rho^2+z_1^2}}\,,\\ &= \frac{2(z-1)}{(2z-\theta)}\left(V_0+z_1-\frac{z_1^2}{\sqrt{\rho^2+z_1^2}}\right)-\frac{\rho^2}{\sqrt{\rho^2+z_1^2}}\,,\\ \alpha &= -\delta,\quad \eta=\gamma,\quad A_t=\frac{L\rho}{(\theta-z-2)\sqrt{\rho^2+z_1^2}}\,r^{\theta-z-2}\,. \end{aligned} \tag{3.91}$$

We can also invert the expressions for z and θ to obtain

$$\gamma = \pm\frac{\theta}{\sqrt{(\theta-2)(\theta-2z+2)}}\,,\quad \delta = \mp\frac{2}{\sqrt{(\theta-2)(\theta-2z+2)}}\,. \tag{3.92}$$

The temperature associated with these solutions has the simple expression

$$T = \frac{|z+2-\theta|}{4\pi L}\, r_h^{-z}\,, \tag{3.93}$$

and the thermal entropy is therefore

$$s \sim r_h^{\theta-2} \sim T^{\frac{2-\theta}{z}}\,. \tag{3.94}$$

There are a number of conditions one should impose on these solutions to ensure that they are well-defined and supported by a matter sector that is physical. Such conditions will lead to constraints on the allowed range of $\{z, \theta\}$, and therefore on the range of theory parameters γ and δ. First, in order for the solution to be real one should demand [7]

$$k^2 > 0, \quad L^2 > 0, \quad (\theta-2)(\theta-2z+2) > 0\,. \tag{3.95}$$

Next, the Null Energy Condition (NEC) should be satisfied, *i.e.*

$$T_{\mu\nu}N^\mu N^\nu \geqslant 0\,, \tag{3.96}$$

for any null vector $N^\mu N_\mu = 0$. For the geometry (3.90), the two independent null vectors can be chosen as

$$N^t = \frac{1}{\sqrt{f}} r^{z-\theta/2}, \quad N^r = \frac{\sqrt{f}}{L} r^{1-\theta/2}\sin\tau, \quad N^x = r^{1-\theta/2}\cos\tau\,, \tag{3.97}$$

[7] Notice that when $z = 1$ we have $k^2 < 0$. Thus, the relativistic case $z = 1$ is not allowed when the axions are present in the theory, as it leads to unphysical conditions on the parameters. Moreover, in order to have $k^2 > 0$ the quantity $V_0 + z_1$ should be positive and sufficiently large.

with $\tau = 0$ or $\pi/2$. The NEC constraints on the scaling exponents are then

$$(\theta - 2)(\theta - 2z + 2) \geqslant 0, \quad (z - 1)(2 + z - \theta) \geqslant 0\,. \tag{3.98}$$

We also note that, in order for the IR region to be defined unambiguously, we want the (t, x, y) components of the (extremal) metric to scale in the same way with r. From the form of the metric in (3.90), this condition can be seen to give

$$(\theta - 2)(\theta - 2z) > 0\,. \tag{3.99}$$

The IR is then located where the (t, x, y) metric components vanish:

$$\begin{aligned} &\theta - 2 > 0 \quad \text{and} \quad \theta - 2z > 0 \quad \Rightarrow \quad \text{IR at } r = 0\,, \\ &\theta - 2 > 0 \quad \text{and} \quad \theta - 2z > 0 \quad \Rightarrow \quad \text{IR at } r = \infty\,. \end{aligned} \tag{3.100}$$

Finally, to ensure thermodynamic stability we would like the geometry to have positive specific heat[8]. From (3.94) we see that this implies

$$z\,(2 - \theta) > 0\,. \tag{3.101}$$

Figures 3.5 and 3.6 show the allowed ranges of z and θ which satisfy all of the constraints above, for two different choices of Lagrangian parameters V_0 and z_1. The charge density has been scaled to $\rho = 1$ in both plots. Notice that as $V_0 + z_1$ becomes smaller, the allowed parameter space decreases (disappearing completely when $V_0 + z_1$ is negative). The figures also indicate whether the UV is located at $r = 0$ or $r = \infty$, for a particular region of parameter space.

[8]This condition is not quite necessary and will not change our results by much. For the case with negative specific heat, the extremal geometry still takes the form (3.80), but is obtained by taking $T \to \infty$. One could obtain a gapped spectrum for the AC conductivity, for example, by incorporating the linear perturbation analysis [103, 53].

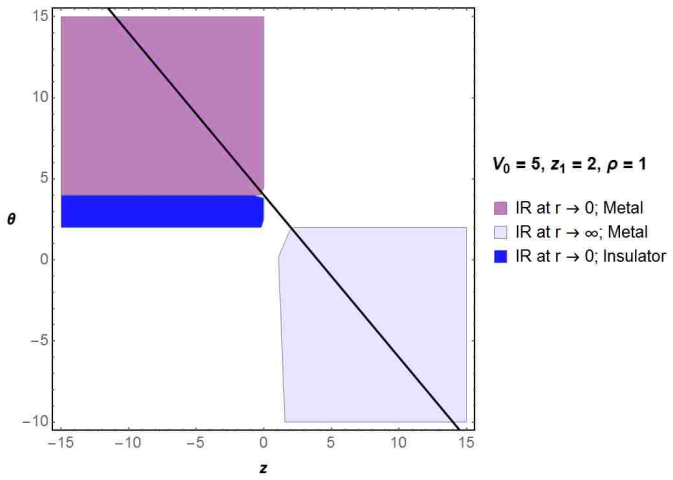

Figure 3.5: The shaded areas denote the allowed ranges of z and θ after taking into account all constraints on the theory parameter space. This case corresponds to $V_0 = 5, z_1 = 2, \rho = 1$. The straight line $\theta = 4 - z$ corresponds to a resistivity linear in temperature, which for these parameters is allowed in much of the phase space.

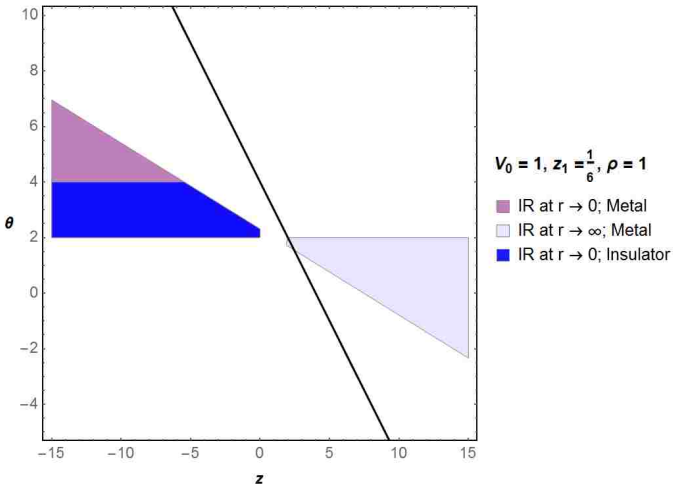

Figure 3.6: The shaded areas denote the allowed ranges of z and θ after taking into account all constraints on the theory parameter space. This case corresponds to $V_0 = 1, z_1 = 1/6, \rho = 1$. The straight line $\theta = 4 - z$ corresponds to a resistivity linear in temperature.

Armed with these geometries, we can now inspect the behavior of the conductivity. Substituting the solution into (3.41), the expression for σ_{DC} in the absence of magnetic field, we find that all the terms scale in the same way with temperature, yielding the simple expression

$$\sigma_{DC} \sim r_h^{4-\theta} \sim T^{\frac{\theta-4}{z}}. \tag{3.102}$$

Here we see clearly the system behaving as a metal or as an insulator, according to (3.67), depending on the sign of z and the range of θ. Figures 3.5 and 3.6 also display the parameter ranges associated with metallic or insulating behavior. Note that in this model there is no obstruction to obtaining a linear resistivity[9]. Indeed, requiring the latter singles out a line in parameter space,

$$\theta + z = 4 \quad \Rightarrow \quad R_{DC} = \frac{1}{\sigma_{DC}} \sim T\,, \tag{3.103}$$

which corresponds to taking $\delta = -\gamma \pm \frac{1}{\sqrt{3}}$. The linear resistivity case is indicated by the solid line in the figures. Notice that it is allowed in most of the parameter space, provided that $V_0 + z_1$ is sufficiently large and positive.

3.4.2 Dyonic solutions and negative magnetoresistance

For the solutions we have just examined the background magnetic field vanishes. It is much more difficult to obtain analytic dyonic solutions, for which both the electric charge density and the magnetic charge are non-trivial. Here we show a

[9]See *e.g.* [54, 55, 56, 57, 58] for the study of holographic strange metals in the probe DBI approximation.

simple family of exact solutions we obtained after turning on h:

$$\begin{aligned}
f(r) &= 1-\left(\frac{r}{r_h}\right)^{z-2}, \quad z=3-\frac{4}{\gamma^2}, \quad \theta=4, \quad \kappa=-\frac{4}{\gamma}, \\
L^2 &= \frac{2}{\gamma^2}\frac{4-\gamma^2}{V_0+z_1-k^2-\sqrt{\rho^2+z_1^2(1+h^2)}}=\frac{2(2-z)}{V_0+z_1-k^2-\sqrt{\rho^2+z_1^2(1+h^2)}}, \\
k^2 &= \frac{(z-1)}{(z-2)}\left[V_0+z_1-\frac{z_1^2}{(z-1)}\frac{(z-1)+h^2(z-2)}{\sqrt{\rho^2+z_1^2(1+h^2)}}\right]-\frac{\rho^2}{\sqrt{\rho^2+z_1^2(1+h^2)}}, \\
\alpha &= -\delta=\frac{\gamma}{2}, \quad \eta=\gamma, \quad A_t=\frac{L\rho}{(2-z)\sqrt{\rho^2+z_1^2(1+h^2)}}\,r^{2-z}.
\end{aligned} \tag{3.104}$$

Note that the hyperscaling violating exponent is fixed in these geometries, *i.e.* $\theta=4$ (and as a result, the IR is always located at $r=0$). In addition to the NEC, the parameters must be chosen in such a way to ensure that both k^2 and L^2 are positive. Moreover, condition (3.99) must hold. The parameter space for the Lifshitz exponent z and the magnetic field h allowed by these constraints is shown in Figure 3.7, for different choices of V_0 and z_1 (we did not require the specific heat to be positive, which in this case would only change the plots slightly). As in the previous solution, the phase space becomes smaller as the quantity V_0+z_1 decreases.

Substituting the solution (3.104) into (3.36) we obtain the conductivity matrix, which now depends only on the magnetic field, and not on the temperature. R_{xx} is an even function as a function of h, while the Hall part R_{xy} is an odd function. The resistance R_{xx} as a function of h for different values of z is presented in Figure 3.8. We find that the physical constraint shown in Figure 3.7 ensures that R_{xx} is not negative, as required for a well defined theory. The dual system falls into a particular quantum critical regime where the transport property is determined solely by the magnetic field, independent of the temperature. Depending on the choice of theory parameters V_0 and z_1, R_{xx} versus $|h|$ can have a non-monotonic (left panel) or monotonic (right panel) behavior.

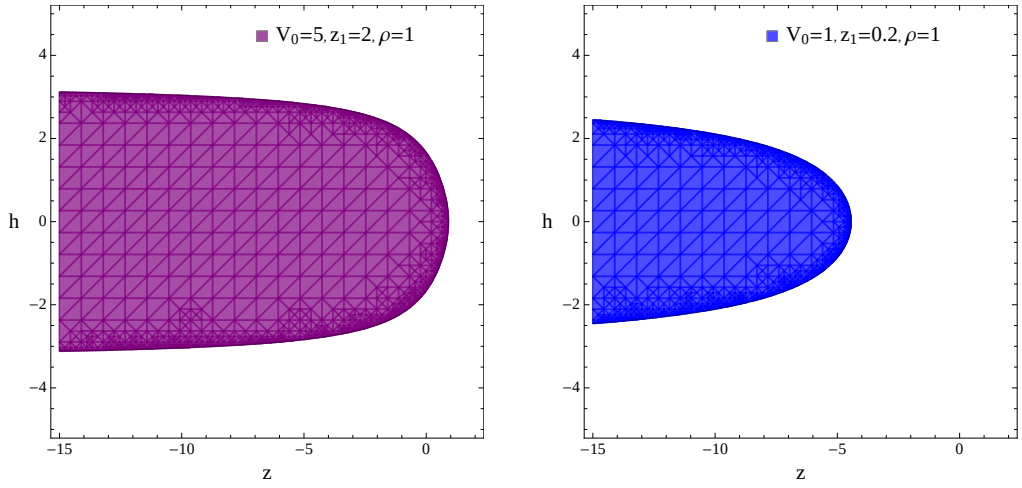

Figure 3.7: The shaded area denotes the allowed ranges of z and h after taking into account the NEC and requiring all theory parameters to be real.

Next, let's consider the behavior of the magnetoresistance supported by these solutions. Recall that the standard definition of magnetoresistance is given by

$$MR = \frac{R_{xx}(h) - R_{xx}(h=0)}{R_{xx}(h=0)}\,, \tag{3.105}$$

describing the tendency of a material to change the value of its electrical resistance in an externally-applied magnetic field. In particular, a negative magnetoresistance has been observed in many materials, see *e.g.* [59, 60, 61, 62, 63, 64, 65, 66]. Interestingly, one finds from Figure 3.8 that our system also exhibits negative magnetoresistance[10]. The left panel of Figure 3.8 shows a positive value of MR in the regime of small magnetic field. However, it is easy to see that in the right panel the magnetoresistance is negative, in all of the allowed parameter range. We emphasize that such negative MR would not be seen in the probe DBI limit. Indeed, as one can

[10]It would be interesting to generalize our discussion to higher-dimensional theories, in which we would have a longitudinal channel along the magnetic field and a transverse channel perpendicular to it. In certain cases one can obtain a negative longitudinal magnetoresistance (see *e.g.* [67, 68]).

see from (3.47), which is the probe approximation result, $R_{xx}(h)$ increases monotonically with the magnetic field, resulting in a positive MR value. As a side note, the case with a trivial dilatonic scalar ϕ examined in Section 3.3 also has positive magnetoresistance, as can be seen in Figures 3.3 and 3.4. A negative MR is obtained in the quantum critical region characterized by $(\theta = 4, z)$. However, notice that for these solutions k is not independent of h. In particular, this means the requirement that the system remains in a given quantum critical regime (described by a fixed θ, z) imposes a non-trivial relation between k and h.

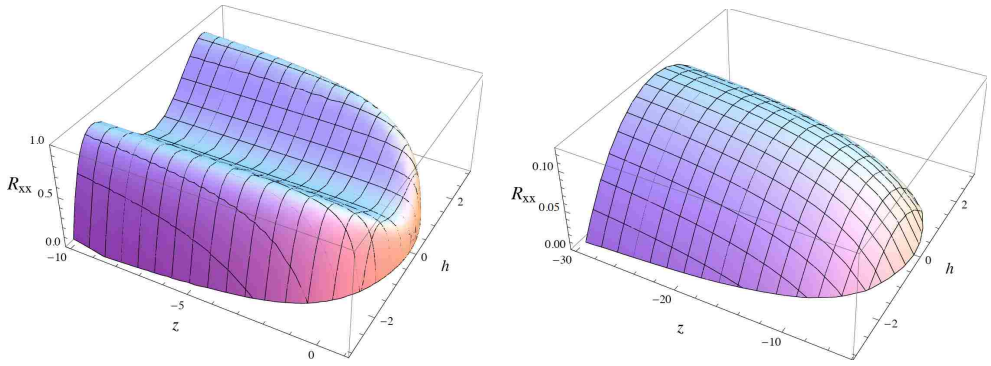

Figure 3.8: The in-plane resistance R_{xx} versus h for various values of z. It is an even function of h. Left panel: $V_0 = 5, z_1 = 2$. Right panel: $V_0 = 1, z_1 = 0.2$. The charge density has been fixed to $\rho = 1$.

In closing this discussion, it is worth noting that we have identified interesting features even in this very simple dyonic setup, using the geometry (3.104). More generic solutions with $h \neq 0$ and broader ranges of z and θ can, in principle, be obtained, but are significantly more complicated and have therefore been omitted. We expect them to have non-trivial magnetotransport properties and to lead to the same kinds of metal-insulator transitions we discussed in Section 3.3. Since h is an adjustable parameter, it is also interesting to see if one could obtain a quantum phase transition by tuning the magnetic field. We leave the analysis of these cases

to future work.

3.4.3 Solutions with AdS_2 geometry

In the discussion above we have focused on scaling solutions driven by a runaway scalar deep inside the bulk, $\phi_{IR} \to \infty$. These kinds of solutions emerge when we allow the coupling functions to have the simple exponential form (3.77), loosely motivated by top-down string theory realizations. As we already mentioned, even though these scaling solutions are exact, we are interested in the case in which they describe only the near horizon region of the space-time at low temperatures.

However, our theory with the simple couplings (3.77) allows for much richer solutions, including some for which in the IR the scalar approaches a constant at extremality. A simple example is given by the following $h = 0$ geometry.

$$\begin{aligned}
f(r) =& 1 - \left(\frac{r}{r_h}\right)^{2+z-\theta} + \frac{V_0 L^2}{(\theta-2)(\theta+z-4)} r^{2z-2} \left[1 - \left(\frac{r}{r_h}\right)^{4-z-\theta}\right] , \\
z =& \frac{1-\gamma^2+\delta^2}{\delta(\gamma+\delta)} , \quad \theta = -\frac{2\gamma}{\delta} , \quad \kappa = \frac{2}{\delta} , \\
k^2 =& \frac{2(z-1)}{(2z-\theta)} \left(z_1 - \frac{z_1^2}{\sqrt{\rho^2+z_1^2}}\right) - \frac{\rho^2}{\sqrt{\rho^2+z_1^2}} , \\
L^2 =& (\theta-2z)(\theta-z-2) \frac{\sqrt{\rho^2+z_1^2}(z_1+\sqrt{\rho^2+z_1^2})}{z_1\rho^2} , \\
\alpha =& -\delta , \quad \eta = \frac{1}{\gamma+\delta} , \quad A_t(r) = \frac{L\rho}{(\theta-z-2)\sqrt{\rho^2+z_1^2}} r^{\theta-z-2} , \\
\gamma =& \pm \frac{\theta}{\sqrt{(\theta-2)(\theta-2z+2)}}, \quad \delta = \mp \frac{2}{\sqrt{(\theta-2)(\theta-2z+2)}} .
\end{aligned} \tag{3.106}$$

whose blackening factor is much more involved than that (3.87) appearing in the solutions we discussed above. As a consequence, the temperature associated with

these geometries has a more complicated dependence on r_h, and is given by

$$T = \frac{r_h^{1-z}}{4\pi L}|f'(r_h)| = \frac{1}{4\pi L}\left|(z+2-\theta)r_h^{-z} - \frac{V_0 L^2}{(\theta-2)}r_h^{z-2}\right| . \tag{3.107}$$

Substituting this background into (3.41), the expression for σ_{DC} in the absence of magnetic field, we obtain

$$\sigma_{DC} \sim r_h^{4-\theta}. \tag{3.108}$$

Using (3.107) one can then convert r_h to temperature, obtaining the DC conductivity as a function of T.

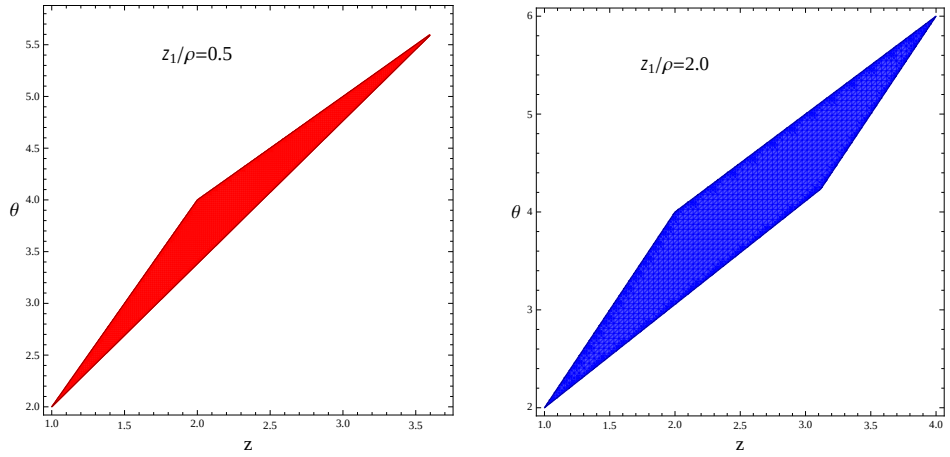

Figure 3.9: The shaded areas denote the allowed ranges of $\{\theta, z\}$ after considering the constraint (3.109). The range of the parameter space depends on the ratio z_1/ρ.

Note that by letting $V_0 = 0$ one could naively recover the standard hyperscaling-violating geometry with the blackening factor given by (3.87). The choice $V_0 = 0$, however, is not consistent with the various constraints on the parameter space (NEC and the requirement that L and k are real), as can be checked. Thus, V_0 must be taken to be non-vanishing, and the resulting solution is intrinsically different from the usual one (3.80) with (3.87). As a result, some of the constraints, such as (3.100),

no longer apply. The two restrictions one can impose are the NEC (3.96) and the reality of all metric/scalar/gauge field coefficients. The latter demands

$$L^2 \sim (\theta - 2z)(\theta - z - 2) > 0, \quad k^2 > 0, \quad (\theta - 2)(\theta - 2z + 2) > 0\,. \tag{3.109}$$

The NEC gives the same condition as (3.98). Moreover, one can show that (3.98) is already implied by the requirement that the solution be real. The resulting parameter range for the exponents $\{\theta, z\}$ depends on the ratio z_1/ρ. Toy examples are shown in Figure 3.9. In particular, one finds from Figure 3.9 that $(\theta - 2) > 0$ and $(z + 2 - \theta) > 0$, conditions which can be shown to be valid in general by considering (3.109).

Therefore, according to (3.107), the extremal limit $T \to 0$ is obtained at a finite value of the horizon radius,

$$\hat{r}_h = \left(\frac{(\theta - 2)(z + 2 - \theta)}{V_0 L^2}\right)^{1/(2z-2)}\,. \tag{3.110}$$

Indeed, the extremal near-horizon geometry for these solutions contains an AdS_2 factor, supported by a constant scalar $\phi_{IR} = \phi(\hat{r}_h)$, and is therefore associated with a finite entropy density. The DC conductivity σ_{DC} is also finite as $T \to 0$, unlike the hyperscaling-violating solution (3.90). At finite temperature, for certain choices of $\{\theta, z\}$ – or equivalently $\{\gamma, \delta\}$ – the resistivity will decrease as T is lowered, showing metallic behavior according to the criterion (3.67). However, it can also increase as the temperature decreases, which is reminiscent of an insulator. We are going to postpone a more thorough study of the transport properties associated with these solutions to future work. For now it suffices to say that they provide a concrete example of the richness of the near horizon backgrounds allowed in these constructions, even assuming the simple choice of scalar couplings (3.77).

3.5 Born-Infeld Theory

Another well-known non-linear generalization of Maxwell's electromagnetism is Born-Infeld theory, whose structure is similar to that of DBI theory, but somewhat simpler. From a phenomenological point of view, it might also be interesting to consider magnetotransport in this case. In particular, although the conductive behavior shares the same overall features as that of DBI, its dependence on the couplings of the theory is simpler. As a consequence, the identification of scaling regimes might be easier in the context of Born-Infeld interactions. With future applications in mind, here we present the general formula for magnetotransport for Born-Infeld theory.

The action we consider reads

$$S=\int d^4x\sqrt{-g}\left[\mathcal{R}-\frac{1}{2}(\partial\phi)^2-V(\phi)-\frac{Y(\phi)}{2}\sum_{I=1}^{2}(\partial\psi^I)^2-\frac{Z_a(\phi)}{2}(\sqrt{1+Z_b(\phi)\,F^2}-1)\right], \tag{3.111}$$

with the three couplings (Z_a, Z_b, Y) chosen to be functions of the neutral scalar ϕ. The last term in (3.111) is precisely the non-linear interaction known as the Born-Infeld term. We consider the same homogeneous and isotropic background as in (3.10), and obtain the charge density

$$\rho=\frac{\sqrt{-g}Z_a(\phi)Z_b(\phi)F^{tr}}{\sqrt{1+Z_b(\phi)\,F^2}}=\frac{CZ_aZ_bA_t'}{\sqrt{1+Z_b\left(\frac{2h^2}{C^2}-2A_t'^2\right)}}\,. \tag{3.112}$$

To calculate the transport coefficients we adopt the same method of Section 3, and find that the conductivity matrix is given by

$$\begin{aligned}\sigma_{xx}=\sigma_{yy}&=\frac{k^2\rho^2CY+k^2CY\Sigma(k^2CY+h^2\Sigma)}{h^2\rho^2+(k^2CY+h^2\Sigma)^2}\Big|_{r=r_h}\,,\\ \sigma_{xy}=-\sigma_{yx}&=\frac{2k^2h\rho CY\Sigma+h\rho(\rho^2+h^2\Sigma^2)}{h^2\rho^2+(k^2CY+h^2\Sigma)^2}\Big|_{r=r_h}\,,\end{aligned} \tag{3.113}$$

with the function $\Sigma(r)$ defined to be given by

$$\Sigma(r) = \sqrt{\frac{2Z_b(\phi)\rho^2 + C(r)^2 Z_a(\phi)^2 Z_b(\phi)^2}{C(r)^2 + 2h^2 Z_b(\phi)}}\,. \tag{3.114}$$

We see that the conductivity matrix is controlled by the three scalar couplings Z_a, Z_b, Y and by the spatial metric component C, all evaluated at the horizon $r = r_h$. They will depend on temperature T (through their dependence on r_h), magnetic field h as well as the amount of momentum dispassion k and charge density ρ.

The inverse Hall angle is then given by

$$\cot\Theta_H = \frac{\sigma_{xx}}{\sigma_{xy}} = \frac{k^2\rho^2 CY + k^2 CY\Sigma(k^2 CY + h^2\Sigma)}{2k^2 h\rho CY\Sigma + h\rho(\rho^2 + h^2\Sigma^2)}\,, \tag{3.115}$$

and the resistivity matrix, obtained by inversting (3.113), reads

$$\begin{aligned} R_{xx} = R_{yy} &= \frac{\sigma_{xx}}{\sigma_{xx}^2 + \sigma_{xy}^2} = \frac{k^2 CY(\rho^2 + k^2 CY\Sigma + h^2\Sigma^2)}{h^2\rho^2\Sigma^2 + (\rho^2 + k^2 CY\Sigma)^2}\,, \\ R_{xy} = -R_{yx} &= -\frac{\sigma_{xy}}{\sigma_{xx}^2 + \sigma_{xy}^2} = \frac{h\rho(\rho^2 + 2k^2 CY\Sigma + h^2\Sigma^2)}{h^2\rho^2\Sigma^2 + (\rho^2 + k^2 CY\Sigma)^2}\,. \end{aligned} \tag{3.116}$$

Since these expressions are quite involved, we would like to restrict our attention to three simple cases:

- No momentum dissipation: in the limit $k \to 0$, the momentum dissipation disappears and the conductivity tensor becomes

$$\sigma_{xx} = \sigma_{yy} = 0, \quad \sigma_{xy} = -\sigma_{yx} = \frac{\rho}{h}\,, \tag{3.117}$$

  the same result we obtained for the DBI case studied earlier in this chapter. As before, in this limit the conductivities are independent of the temperature and the details of the theory.

- No magnetic field: after turning off the background magnetic field, we obtain

$$\sigma_{DC} = \sigma_{xx} = \sqrt{Z_a^2 Z_b^2 + \frac{2Z_b\rho^2}{C^2}} + \frac{\rho^2}{k^2 CY} = \sqrt{Z_a^2 Z_b^2 + \frac{32\pi^2 Z_b\rho^2}{s^2}} + \frac{4\pi\rho^2}{k^2 Y s}, \tag{3.118}$$

  where $s = 4\pi\, C(r_h)$ is the entropy density. The dependence on the couplings of the theory is now slightly different from that of the DBI case, as expected from the different structure of the action. Note that $\sigma_{xy} = 0$ when $h = 0$. A particular simple case with $Z_{a,b}$ and Y constants and without the neutral scalar ϕ was discussed in [69], where some features of Mott-like states were identified.

- No charge density: The DC resistivity when $\rho = 0$ reads

$$R_{DC} = R_{xx} = \frac{1}{Z_a Z_b}\sqrt{1 + \frac{2Z_b}{C^2}h^2} + \frac{h^2}{k^2 CY} = \frac{1}{Z_a Z_b}\sqrt{1 + \frac{32\pi^2 Z_b}{s^2}h^2} + \frac{4\pi h^2}{k^2 Y s}, \tag{3.119}$$

  and the Hall part vanishes, $R_{xy} = 0$.

The explicit dependence on the two scales T and h can be determined after substituting specific background geometries into the general resistivity expressions. However, finding black hole solutions for the Born-Infeld-Axion theory (3.111) is beyond the scope of this thesis, and is delegated to future work.

3.6 Summary of Results

We have examined the behavior of the DC conductivity/resistivity matrix as a function of the physical scales in the problem – temperature, charge density, magnetic field and momentum dissipation [11] – taking into account the full backreaction of the D-brane action on the geometry. Axionic fields were used to break translational

[11] Due to a scaling symmetry, only three of these four scales are actually physical.

invariance and ensure momentum relaxation. A dilatonic scalar appropriately coupled to the DBI interaction term was introduced to generate scaling solutions. We have found a highly complex and rich structure for the magnetotrasport, given in expressions (3.36) (3.38), which simplifies somewhat in a number of limiting cases. In full generality, the dependence of the conductivity matrix on the physical scales in the system and the couplings of the theory is significantly more complicated than that of the probe DBI limit, which is summarized in (3.45).

In general the various contributions to the DC conductivity combine in a non-trivial fashion – the terms associated with momentum relaxation of the charge carriers in the system and those independent of the charge degrees of freedom are not added together in a simple way. Thus, this provides an explicit example in which there is no clean separation between coherent and incoherent contributions. The results of the probe DBI approximation are recovered in the limit of strong momentum dissipation, for which the contribution of the DBI action to the geometry is negligible as compared to that of the axionic sector. In the opposite limit of weak momentum relaxation, the conductivity tensor to leading order is independent of temperature and of the details of the theory, as a consequence of Lorentz invariance [39]. Only at next-to-leading order one finds non-trivial dependence on T and the specific parameters of the model.

We have identified several classes of new, exact solutions to the theory and discussed the physical constraints on the parameter space needed to have a well-defined holographic ground-state. Depending on the theory parameters, these solutions can describe either metallic or insulating phases. While they are valid everywhere in the geometry (they are exact), when their UV asymptotics are not AdS we will interpret them as describing only the IR of the geometry, in order to adopt the standard holographic AdS/CFT dictionary. That they can be embedded in AdS (by making

minor modifications to the scalar potential) is by now well known.

When the dilatonic scalar is trivial, the exact black-brane geometries are associated with a metal-insulator crossover, induced by varying the magnitude of the magnetic field. On the other hand, a running dilatonic scalar leads to exact hyperscaling violating, Lifshitz-like black brane solutions, which also exhibit either metallic or insulating behavior, depending on the range of parameters. For some of the simpler classes of scaling solutions we have obtained, we find that the DC conductivity in the absence of magnetic field scales with temperature as

$$\sigma_{DC} \sim T^{\frac{\theta-4}{z}} , \tag{3.120}$$

yielding a linear resistivity $R_{DC} = 1/\sigma_{DC} \sim T$ along the line $\theta + z = 4$ which is allowed in much of the physical parameter space of the theory. Interestingly, we have also identified a somewhat simple hyperscaling violating solution with non-vanishing magnetic field, and with $\theta = 4$. For this solution the result (3.120) still applies and σ_{DC} is constant. Thus, this special $\theta = 4$ geometry sits at the edge of the insulating and metallic behavior seen in (3.120). Moreover, for this dyonic case we observe a negative magnetoresistance, a feature which is absent in the probe DBI limit. Exact solutions with non-zero magnetic field and more arbitrary values of θ can also be identified, but are significantly more complicated. We expect them to lead to a similarly rich structure for the magnetotransport, and leave their analysis to future work.

The key message to take away from our analysis is that by taking into account backreaction, the transport behavior which can be realized in this theory is rich and highly complex. Non-trivial classes of IR geometries can be easily constructed, which allow for a wide range of scalings. They give rise to not only metallic or insulating behavior, but also new magnetic field driven metal-insulator crossovers as well as

a negative magnetoresistance. In this chapter we have only begun to explore the properties of these solutions, and their implications for transport. We anticipate that disorder driven transitions (driven by changing the magnitude k of the axionic scalars) may also be possible to realize in these models, perhaps using new classes of black brane solutions. It would also be interesting to construct the full geometries that interpolate between the IR solutions we have identified and the AdS_4 fixed point in the UV, and study their AC transport properties. Before closing, we note that while we were in the last stages of the project [19], the paper [38] appeared, whose conductivity analysis for DBI Q-lattice models partially overlaps with our results.

Chapter 4

Modeling Cuprate Scalings Holographically

Our goal in this chapter is to explore the origin of the anomalous scalings seen in chapter 3 and clarify the conditions needed to realize them. We work with the same string theory motivated gravitational model [19] studied in chapter 3 which takes into account non-linear interactions between the charged degrees of freedom, encoded by the DBI action. We focus on a limit in which the backreaction of the DBI interactions on the geometry can be safely neglected, the so-called probe limit. As a consequence, gravitational solutions to the theory are of a simple form, and the resulting conductivities are easy to study analytically. Meanwhile, the non-linear nature of the interactions between the charged degrees of freedom is retained in this regime. In this limit we are able to identify clean scaling regimes in a straightforward manner. Indeed, we will be able to realize $R \sim T$ and $\cot\Theta_H \sim T^2$, and more generically a wider range of scalings, precisely thanks to the non-linear dynamics of the gauge field sector.

We emphasize that our construction is the first consistent holographic realization

of the strange metal scalings of the resistivity and Hall angle – in particular, the latter two can be obtained simultaneously without violating the NEC. In our setup the behavior of the resistivity differs generically from that of the Hall angle because distinct couplings control different temperature scales in the system. Moreover, the theory admits non-relativistic, hyperscaling-violating black brane solutions whose scaling exponents can be chosen to reproduce the scalings of R and Θ_H observed in the cuprates.

Realizing the same scaling laws away from the probe limit should not pose any conceptual challenges, but rather only technical ones. Finding exact analytical solutions to the theory in the presence of backreaction is harder, and to do so one must rely on simplifications and restrictions on the parameters of the model. Such simplifications often lead to a situation where only one coupling sets the temperature scale in the system, and controls the behavior of all the conductivities. For these particular background solutions, then, the conductivity and Hall angle would both scale as the same power of T and would not math those of the cuprates. We illustrate this point at the end of this chapter. However, we emphasize that this is only a limitation of the analytical solutions, and numerically one can construct a much larger class of geometries, describing systems with different relaxation scales. There should be no conceptual obstacle to reproducing the phenomenology of the cuprates in these more general settings.

4.1 The holographic setup

We consider the same holographic model we studied in chapter 3 which we include here for completeness,

$$S = \int d^4x\sqrt{-g}\left[\mathcal{R} - \frac{1}{2}(\partial\phi)^2 - V(\phi) - \frac{Y(\phi)}{2}\sum_{I=1}^{2}(\partial\psi^I)^2\right] + \int d^4x Z_1(\phi)\left[\sqrt{-\det(g_{\mu\nu}+Z_2(\phi)F_{\mu\nu})} - \sqrt{-\det(g_{\mu\nu})}\right], \quad (4.1)$$

where the second term in the DBI part is chosen such that in the weak flux limit $F \to 0$ one recovers the standard gauge field kinetic term, F^2. Recall that the scalar couplings $Z_1(\phi), Z_2(\phi)$ and $Y(\phi)$ yield interactions between the scalar sector and the gauge field. Moreover, the axionic scalars, ψ^I are introduced to break translational symmetry and ensure that the system dissipates momentum and exhibits a finite DC conductivity. Magnetotransport in this model was studied first by [25] and later by [19] taking into account backreaction effects as we already mentioned in chapter 3. Early work on the conductivity in probe DBI setups can be found *e.g.* in [26, 27, 54, 55, 56, 57, 58].

As in [19] and also (3.10), here we work with geometries of the form

$$ds^2 = -D(r)dt^2 + B(r)dr^2 + C(r)(dx^2+dy^2),\ \phi = \phi(r),$$
$$\psi^1 = k\,x,\ \ \psi^2 = k\,y,\ \ A = A_t(r)\,dt + \frac{h}{2}(xdy - ydx)\,, \quad (4.2)$$

with h denoting the magnitude of the magnetic field and k the strength of momentum relaxation [28]. The general equations of motion are presented in chapter 3. Our focus below will be on solutions which exhibit hyperscaling violation ($\theta \neq 0$) and non-relativistic scalings ($z \neq 1$) in the IR of the geometry, and approach AdS in the UV.

The DC conductivities σ_{ij} for the theory (4.1) and the background geometry (3.10) were computed in [19] using the horizon method developed in [29, 18]. We refer the reader to [19] and the discussion in chapter 3 for the analysis. The key observation is that σ_{ij} is controlled by the three scalar couplings Z_1, Z_2, Y and the bulk metric component C, all evaluated at the horizon. Since the horizon radius is related to T, these are generically temperature dependent terms. Moreover, to the extent that they are independent of each other, they in principle provide different temperature scales in the system. The inverse Hall angle and resistivity are then extracted as in (3.37) and (3.38) by using

$$\cot\Theta_H = \frac{\sigma_{xx}}{\sigma_{xy}}\,, \quad R = R_{xx} = \frac{\sigma_{xx}}{\sigma_{xx}^2 + \sigma_{xy}^2}\,. \tag{4.3}$$

The conductivity associated with the DBI model is extremely rich and complex. Also, it provides yet another example in which one does *not* have the simple additive form $\sigma_{DC} = \sigma_{ccs} + \sigma_{diss}$. Indeed, the dissipative σ_{diss} and charge conjugation symmetric σ_{ccs} contributions in this model are intertwined in a non-trivial way, thanks here to the non-linear nature of the DBI interactions. The complexity of this DBI theory is both a challenge and an opportunity – while it is difficult to extract specific scaling properties without focusing on particularly simple sectors, one also expects to find a wide range of possible behaviors. In particular, the transport coefficients simplify significantly in a number of limiting cases, as discussed in [19]. The one that is most relevant to us here is the probe limit.

4.2 Probe DBI limit

The expressions for the conductivities of the DBI theory are much more tractable when the contribution to the geometry coming from the DBI sector is negligible

compared to that of other matter content. In this case the background geometry is seeded by the the scalar and axions, and the dynamics of the U(1) gauge field can be captured by treating it as a probe around the resulting geometry – this is the so-called probe DBI limit. Interestingly, we find that the same expression for $\cot\Theta_H$ and R_{xx} can be obtained from the fully-backreacted case when the momentum dissipation scale k dominates over the other physical scales in the system [19].

In the probe DBI limit the inverse Hall angle can be seen to take the simple form seen in (3.46)

$$\cot\Theta_H = \frac{C}{h\rho Z_2}\sqrt{\rho^2 + Z_1^2 Z_2^2 (C^2 + h^2 Z_2^2)}\,, \tag{4.4}$$

and the in-plane resistivity is given by (3.47)

$$R_{xx} = \frac{C}{Z_2}\frac{\sqrt{\rho^2 + Z_1^2 Z_2^2 (C^2 + h^2 Z_2^2)}}{\rho^2 + C^2 Z_1^2 Z_2^2}\,, \tag{4.5}$$

evaluated at the horizon. Moreover, in the probe regime the charge density ρ and the magnetic field h should be small compared to the other scales in the system. In particular, working in the limits $\rho^2 << Z_1^2 Z_2^2 C^2$ and $h^2 Z_2^2 << C^2$, the resistivity and the Hall angle reduce to the very simple expressions

$$\cot\Theta_H = \frac{C^2 Z_1}{h\rho}\,, \qquad R_{xx} = \frac{1}{Z_1 Z_2^2}\,, \tag{4.6}$$

where we have only kept leading order terms. The small ρ, h limits are entirely natural in the probe approximation, and will be shown below to be valid in appropriate temperature windows.

The key feature to appreciate in the expressions (4.6) for R_{xx} and $\cot\Theta_H$ is that they generically scale differently with temperature, precisely because they are

controlled by different quantities. The functions C, Z_1 and Z_2 *provide different temperature scales in the system* – as long as at least two of them are independent from each other. The technical advantage of the probe limit, as we will see shortly, is that it allows us to keep the scalar couplings Z_1 and Z_2 much more arbitrary than would be possible when working with specific backreacted solutions. This will give us more freedom to choose the scalings we are after.

In order to obtain the cuprates' scalings $R_{xx} \sim T$ and $\cot\Theta_H \sim T^2$ from (4.6), one then needs to have a system for which

$$\frac{C}{Z_2} = \frac{T^{3/2}}{\ell_0^{1/2}} \quad \text{and} \quad Z_1 Z_2^2 = \frac{z_0}{T}\,, \tag{4.7}$$

with ℓ_0 and z_0 two positive constants that depend on the specific theory one is considering. Moreover, the small ρ, h approximations we adopted to obtain (4.6) become, assuming a temperature dependence as in (4.7), $T >> \ell_0\rho^2/z_0^2$ and $T^3 >> \ell_0 h^2$.

At this stage it is convenient to introduce dimensionless expressions for the temperature and magnetic field, $\mathbf{T} = \frac{z_0^2}{\ell_0\rho^2}T$ and $\mathbf{h} = \frac{z_0^3}{\ell_0\rho^3}h$ respectively, as well as a constant $\zeta = \ell_0\rho^2/z_0^3$. When the condition (4.7) is satisfied, the expressions (3.46) and (3.47) then become

$$\begin{aligned} R_{xx} &= \zeta\frac{\mathbf{T}^{3/2}}{1+\mathbf{T}}\sqrt{1+\mathbf{T}+\mathbf{h}^2/\mathbf{T}^2}, \\ \cot\Theta_H &= \frac{\mathbf{T}^{3/2}}{\mathbf{h}}\sqrt{1+\mathbf{T}+\mathbf{h}^2/\mathbf{T}^2}\,. \end{aligned} \tag{4.8}$$

It is clear that one obtains

$$R_{xx} = \zeta\,\mathbf{T}, \qquad \cot\Theta_H = \frac{\mathbf{T}^2}{\mathbf{h}}\,, \tag{4.9}$$

in the "high temperature" limit $\mathbf{T} \gg 1 + \mathbf{h}^2/\mathbf{T}^2$. Note that this condition is given in terms of $\mathbf{T}$, defined by using the particular scale $\ell_0\rho^2/z_0^2$ that characterizes the theory one is considering. Thus, this is not necessarily a high–T limit, and it would indeed describe low temperatures provided that such scale is sufficiently higher than the temperature the experiment is probing.

So far our analysis was based on the assumption that condition (4.7) could be satisfied. We are now ready to show how it can be realized explicitly. To proceed further we need to extract the temperature dependence of $C(r), Z_1(\phi)$ and $Z_2(\phi)$. Thus, we need to focus on a particular background solution and specify a choice of couplings. In order to allow for the freedom to have scaling exponents, we are interested in geometries that are non-relativistic and hyperscaling-violating in the IR, and approach AdS in the UV.

As was shown in [25], when the dilaton couplings V and Y are approximated by exponentials in the IR, $V(\phi) \sim -V_0\, e^{\eta\,\phi}$ and $Y(\phi) \sim e^{\alpha\,\phi}$, the geometry in the probe limit is of the simple hyperscaling-violating form given in (3.52) as

$$ds^2 = r^\theta \left(-f(r)\frac{dt^2}{r^{2z}} + \frac{L^2 dr^2}{r^2 f(r)} + \frac{dx^2+dy^2}{r^2} \right), \tag{4.10}$$

$$\phi = \kappa\, \ln(r), \quad \psi^1 = k\, x, \quad \psi_2 = k\, y\,, \tag{4.11}$$

with

$$f(r) = 1 - \left(\frac{r}{r_h}\right)^{2+z-\theta},\ z = \frac{\alpha^2-\eta^2+1}{\alpha(\alpha-\eta)},\ \theta = \frac{2\eta}{\alpha}\,,$$
$$\kappa = -\frac{2}{\alpha}\,,\ L^2 = \frac{(z+2-\theta)(2z-\theta)}{V_0}\,,\ k^2 = \frac{2V_0(z-1)}{2z-\theta}.$$

Recall that in this limit the gauge field is a probe around this background solution, and its expression can be obtained by solving the U(1) equation of motion. Finally,

from the form of the blackening function we read off $T \sim r_h^{-z}$ and

$$C(r_h) = r_h^{\theta-2} \Rightarrow C(T) \sim T^{\frac{2-\theta}{z}}\,, \tag{4.12}$$

which is also the temperature scaling of the entropy density, $s \sim T^{\frac{2-\theta}{z}}$.

As in chapter 3, we take into account Gubser's criterion [42, 103] as well as the NEC to have a well defined geometry and a resolvable singularity. Depending on the location of the IR, these restrictions yield

$$\begin{aligned} &\text{IR } r \to \infty : \ [1 < z \leqslant 2, \theta < 2z - 2],\ [z > 2, \theta < 2]\,, \\ &\text{IR } r \to 0 : \ \ [z \leqslant 0, \theta > 2],\ [0 < z < 1, \theta > z + 2]\,. \end{aligned} \tag{4.13}$$

When the backreaction of the DBI action on the geometry is taken into account, exact $\{z, \theta\}$ solutions to our model can be found only for particular choices of scalar couplings $Z_1(\phi)$ and $Z_2(\phi)$ (typically single exponentials). In the probe limit where the backreaction of DBI sector can be neglected, there is a certain amount of freedom to choose the couplings Z_1, Z_2. For simplicity – and to eventually make contact with the fully backreacted case – we take them to be $Z_1 \sim e^{\gamma\phi}$ and $Z_2 \sim e^{\delta\phi}$, where γ, δ are free parameters. This ensures that they yield single powers of temperature when evaluated at the horizon. Indeed, combining this with the expression for the scalar field needed to support the scaling solutions, $\phi = -\frac{2}{\alpha}\ln(r)$, yields

$$Z_1 \sim T^{\frac{2\gamma}{z\alpha}} \quad \text{and} \quad Z_2 \sim T^{\frac{2\delta}{z\alpha}}\,. \tag{4.14}$$

Thus, for arbitrary couplings γ, δ one has

$$\frac{C}{Z_2} \sim T^{\frac{2-\theta}{z} - \frac{2\delta}{z\alpha}} \quad \text{and} \quad Z_1 Z_2^2 \sim T^{\frac{2\gamma+4\delta}{z\alpha}}\,, \tag{4.15}$$

and in turn

$$R_{xx} \sim T^{-\frac{2}{z}\left(\frac{\gamma}{\alpha}+2\frac{\delta}{\alpha}\right)}\,, \quad \cot\Theta_H \sim \frac{1}{h\rho} T^{\frac{2}{z}\left(2-\theta+\frac{\gamma}{\alpha}\right)}\,, \tag{4.16}$$

for the general scaling of the resistivity and Hall angle in the probe DBI limit. The condition required to realize the cuprates' scalings then becomes

$$\frac{\gamma}{\alpha} = z+\theta-2 \quad \text{and} \quad \frac{\delta}{\alpha} = 1-\frac{\theta}{2}-\frac{3}{4}z\,. \tag{4.17}$$

With this particular choice of Lagrangian parameters one obtains the celebrated cuprate behavior

$$R_{xx} \sim T\,, \qquad \cot\Theta_H \sim T^2\,. \tag{4.18}$$

In particular, one should demand that the contribution of the DBI terms should be subleading to the gravity background, and the geometry is seeded by the scalar ϕ and axions ψ^I. More precisely, we require the stress tensor of the DBI action to be much smaller than the Einstein tensor.

Using an analysis similar to that in [25], one obtains the constraint

$$Z_1^2 Z_2^2 r_h^{2\theta} L^2 \ll Z_2 r_h^2 \sqrt{\rho^2 + Z_1^2 Z_2^2 (C^2 + h^2 Z_2^2)} \ll Z_2^2/L^2\,, \tag{4.19}$$

evaluated at the horizon r_h. Recall that to reproduce the cuprate strange metal scalings, we need to fix the temperature dependence of (C, Z_1, Z_2). Using the dimensionless temperature and magnetic field, we then obtain

$$N_1\, \mathbf{T}^{\frac{z-4}{z}} \ll \mathbf{T}^{-\frac{2\theta+3z}{2z}} \sqrt{1+\mathbf{T}+\mathbf{h}^2/\mathbf{T}^2} \ll N_2\, \mathbf{T}^{\frac{4-2\theta-3z}{z}}\,, \tag{4.20}$$

where N_1 and N_2 are constants that are independent of $\mathbf{T}$ and $\mathbf{h}$.

Since we are interested in the high temperature limit $\mathbf{T} \gg 1 + \mathbf{h}^2/\mathbf{T}^2$, we find

$$\mathbf{T}^{\frac{4-\theta-2z}{z}} \gg 1 \quad \Rightarrow \quad \frac{4-\theta-2z}{z} > 0\,. \tag{4.21}$$

We point out that we neglected the last term in the DBI stress energy tensor (3.8) when deriving the constraint above. This is consistent with the probe approximation and indeed, as one can check, $V \gg Z_1$ in the regime we are interested in. To resolve the naked singularity which is present in the hyperscaling-violating ground state, we already considered Gubser's criterion and the null energy condition, which impose non-trivial constraints on (z, θ). The validity of the probe approximation then imposes further constraint (4.21) on the two scaling exponents. It is important to take into account all such constraints, in order to have a consistent parameter space for the holographic theory. Indeed, we find that there exists a large range of parameter space for (z, θ) satisfying all the above constraints. Finally, the magnetic field can not be too strong, with the upper bound given by $\mathbf{h} \ll \mathbf{T}^{3/2}$.

We stress that there is a wide range of values of z and θ (or equivalently of the theory parameters γ and δ) which satisfies all constraints and can be used to realize these two scaling laws. However, one still needs to identify a selection mechanism to explain why these scalings are robust and universal in the cuprates.

It is interesting to note that the $z = 4/3, \theta = 0$ case singled out by the purely field-theoretic analysis of [14] corresponds here to having $\delta = 0$, or equivalently a constant Z_2 (and $\gamma^2 = 4/3$). Thus, this corresponds to a minimal form of the Lagrangian, in which only the overall scalar coupling in the DBI term $Z_1(\phi)$ is turned on. This case is reminiscent of the standard dilaton coupling to the DBI action $\sim e^{-\Phi}$ in string theory. An interesting question is whether one could obtain the couplings needed to realize the cuprates within a top–down string theory construction. Indeed, with a UV completed theory all parameters would be entirely fixed. Note that

the scaling laws (4.18) would not be present if one turns off the DBI interaction. Our results provide further compelling evidence for the importance of non-linear interactions among the charge carriers for describing strange metals, as observed in other holographic models (see *e.g.* [54]).

4.3 The general backreacted case

As we have just seen, in the probe regime these DBI models admit the scaling laws (4.18) observed in the cuprates, and more generally cases in which R_{xx} and $\cot\Theta_H$ scale differently with temperature, as in (4.16). We expect to find the same behavior even when one moves away from the probe limit and takes into account the full backreaction of the DBI interactions on the geometry. However, finding exact analytical solutions that are fully backreacted is technically more challenging, and one does not expect them to be of the simple form of (4.12), especially in the presence of a magnetic field. Exact analytical solutions to the DBI theory are rare, and rely on making simplifying assumptions on theory parameters. One of the potential consequences then, is that they can lead to cases for which σ_{ij} is controlled by a single temperature dependent quantity – a single scale. In such instances one does not expect to have a clean separation between the behavior of the resistivity R_{xx} and the Hall angle $\cot\Theta_H$. Indeed, the two should have a similar T–structure. In this section we illustrate precisely this point with an analytical example.

Exact non-relativistic, hyperscaling-violating solutions to the full DBI theory (4.1) were put forth in [19]. In the presence of a background magnetic field $h \neq 0$, the scaling geometries of [19] had a fixed value of the hyperscaling-violating parameter, $\theta = 4$. Analytical solutions with arbitrary θ were also expected to exist, and to provide a more fruitful avenue to modeling possible scaling regimes. Indeed, when

the Lagrangian parameters are such that

$$\gamma = -2\delta, \quad \eta = \alpha - \delta\,,$$

we have identified another class of fully backreacted dyonic black branes of the form

$$\begin{aligned} ds^2 &= r^\theta \left(-f(r)\frac{dt^2}{r^{2z}} + \frac{L^2 dr^2}{r^2 f(r)} + \frac{dx^2+dy^2}{r^2}\right)\,, \\ \phi &= \kappa\,\ln(r)\,,\ \psi^1 = k\,x\,,\ \psi_2 = k\,y\,,\ A = A_t(r)dt + \frac{h}{2}(xdy - ydx)\,, \end{aligned} \tag{4.22}$$

with

$$\begin{aligned} f(r) &= 1 - \left(\frac{r}{r_h}\right)^{2+z-\theta} + \frac{2(z-1)(2+z-\theta)(h^2 z_1^2+\rho^2)}{k^2(z-2)(2z+\theta-6)\sqrt{(1+h^2)z_1^2+\rho^2}} r^{4-\theta}\left[1-\left(\frac{r}{r_h}\right)^{z-2}\right]\,, \\ \kappa &= -\frac{2}{\alpha}\,, \quad z = \frac{1+\alpha^2-\eta^2}{\alpha(\alpha-\eta)}\,, \quad \theta = 2\,\frac{\eta}{\alpha}\,, \quad k^2 = \frac{V_0}{1-\frac{(\eta-\alpha)^2-1}{(\eta^2-\alpha\eta-1)}\sqrt{(1+h^2)+\frac{\rho^2}{z_1^2}}}\,, \\ A_t'(r) &= \frac{L\rho}{z_1}\frac{r^{1-z}}{\sqrt{(1+h^2)+\frac{\rho^2}{z_1^2}}}\,, \quad L^2 = \frac{2(z-1)(2+z-\theta)}{k^2}\,. \end{aligned} \tag{4.23}$$

Here we have used $Z_1 = z_1 e^{\gamma\phi}$, $Z_2 = e^{\delta\phi}$, $Y = e^{\alpha\phi}$ and $V(\phi) = -V_0 e^{\eta\phi}$ with z_1 and V_0 two positive constants. The temperature of these black brane solutions is given by

$$T = \frac{1}{4\pi}\sqrt{\frac{2+z-\theta}{2(z-1)}}\left[k\,r_h^{-z} + \frac{2(z-1)}{k(\theta+2z-6)}\frac{h^2 z_1^2+\rho^2}{\sqrt{1+h^2 z_1^2+\rho^2}}\,r_h^{4-z-\theta}\right]\,. \tag{4.24}$$

We note that for these solutions the momentum dissipation parameter is not free, but is determined in terms of h, ρ and theory parameters. The main feature that distinguishes this solution from that in (4.12) is the complexity of the blackening function. As a result, the temperature of these black branes is related to the horizon

radius in a rather non-trivial way,

$$T \sim r_h^{-z} + \frac{c_0(z-2)}{(2+z-\theta)}\, r_h^{4-z-\theta}\,, \tag{4.25}$$

where c_0 is a constant that depends on theory parameters. As a result, (4.25) gives a much wider range of possible temperature dependence for the entropy density than the one (4.12) found in the probe limit. The general expression (4.24) is quite cumbersome, making it difficult to identify the existence of scaling regimes. However, in appropriate regions of parameter space only one of the two terms in (4.24) dominates, so that one can assume a clean scaling of the form $T \sim r_h^p$ for some parameter p.

These exact solutions are quite constrained (they require specific relationships between theory parameters), and in particular have the property that the metric component C and the couplings Z_1 and Z_2 are all related to each other,

$$C(r) = Z_2(r) = r^{\theta-2}\,, \quad Z_1 \sim r^{4-2\theta} = C^{-2}\,, \tag{4.26}$$

implying for example that the combination $Z_1 Z_2 C$ is simply a constant. As a consequence, evaluating the conductivities on the background solutions above, we find that the temperature dependence is controlled entirely by one single quantity, the combination CY. Thus, this quantity sets the *only* temperature scale available in the system (for early discussions of different timescales in holographic transport coefficients, see *e.g.* [18, 41]). Inspecting the expressions for the conductivities, we see that the resistivity and Hall angle have the schematic form

$$\begin{aligned} R_{xx} &= \frac{a_1 CY + a_2 (CY)^2 + a_3 (CY)^3 + a_4 (CY)^4}{a_5 + a_6 CY + a_7 (CY)^2 + a_8 (CY)^3 + a_9 (CY)^4}\,, \\ \cot\Theta_H &= \frac{b_1 CY + b_2 (CY)^2}{b_3 + b_4 CY + b_5 (CY)^2}\,, \end{aligned} \tag{4.27}$$

where the a_i, b_i are T-independent terms which depend on h, k, ρ. The expressions for the coefficients are quite complicated, but all share a similar structure. In particular, the coefficients of R_{xx} and $\cot\Theta_H$ in front of each power of CY are generically similar to each other (for instance, the pairs a_2 and b_2, or a_6 and b_4). What this implies is that, without *severe fine-tuning* of the parameters z_1, h and ρ, one can not generically decouple the temperature behavior of R_{xx} from that of $\cot\Theta_H$. The reason for this is that, unlike in the probe DBI case, the same quantity CY is responsible for giving rise to all T-dependence in this particular system. In closing, we note that by fine-tuning parameters so that some of these coefficients can be made to vanish, one can indeed force R_{xx} and $\cot\Theta_H$ to have a different scaling in terms of CY (and potentially obtain the cuprates' scalings). However, this would only hold in a very limited temperature region, and require unnatural choices of theory parameters. This procedure would give at best a very undesirable – highly fine-tuned – realization of the scalings of the cuprates.

In conclusion, the probe limit offers a window into the existence of clean scaling regimes, including those observed in the cuprate high temperature superconductors. We stress that in this class of DBI theories the cuprates' scaling laws would not be present if the DBI interaction was turned off – in that case the arguments developed for EMD theories would be relevant. Thus, our analysis provides evidence that to capture the complexity of the phase diagram of non-Fermi liquids it may be crucial to include the non-trivial dynamics between the (charged) degrees of freedom, in addition to the interplay between the various physical scales in the system.

Chapter 5

Generic Non-Linear Effects on Transport

Motivated by the results of chapters 3 and 4, we are interested in examining a generic non-linear gauge field sector and computing the associated DC conductivities. To this end, in this chapter we will study a model that describes a sector of probe charge carriers interacting amongst themselves and with a larger set of neutral quantum critical degrees of freedom. Indeed, there is evidence [56, 58, 20] that to reliably capture transport in these phases it may be crucial to take into account the non-trivial dynamics between the charge degrees of freedom. This is reasonable given that we are dealing with strongly correlated electron matter, and was already suggested in [54] and by the results of chapters 3 and 4. To examine to what extent the results of chapters 3 and 4 can be generalized, we will work with a completely generic gauge field sector and compute the corresponding holographic conductivities.

We will then choose to focus on a particularly simple non-linear model whose structure is natural from the point of view of the DBI. Remarkably, this simple, solvable model provides the first holographic realization of the temperature scalings of

the entropy $\sim T$, resistivity $\sim T$, Hall angle $\sim T^2$ and weak-field magnetoresistance $\sim T^{-4}$ observed in the cuprates [70, 71, 14] – with a minimal set of assumptions. Thus, this minimal model will allow us to to improve on the results of chapter 4, in which only the cuprate scalings of R and Θ_H were obtained. As we show below, the mechanism underlying our results relies on having a quantum critical IR fixed point and on the non-linear structure of the interactions between the charges. Our results also suggest that the strange metal behavior is intimately tied to the linear temperature dependence of the entropy.

5.1 Holographic Setup and Conductivities.

We are interested in describing a strongly coupled quantum theory containing a sector of dilute charge carriers that interact amongst themselves as well as with a quantum critical bath. The charge degrees of freedom should be thought of as a probe when compared to the larger set of neutral quantum critical degrees of freedom. What we have in mind are gravitational theories of the type

$$S = \int d^4x\sqrt{-g}\,\left[\mathcal{L}_{\rm Bath} + \mathcal{L}_{\rm U(1)}\right], \tag{5.1}$$

with a bath sector $\mathcal{L}_{\rm Bath}$ supported, for example, by a neutral scalar ϕ and axionic scalars, and a charge sector $\mathcal{L}_{\rm U(1)}$ describing the dynamics of a $U(1)$ gauge field A_μ. In particular, since we are interested in capturing generic non-linear electrodynamics effects, the latter will be encoded in the Lagrangian term $\mathcal{L}_{\rm U(1)} = \mathcal{L}(s, p, \phi)$, which is a generic function of the two combinations

$$s = -\frac{1}{4}F_{\mu\nu}F^{\mu\nu}\,, \qquad p = -\frac{1}{8}\epsilon_{\mu\nu\rho\sigma}F^{\mu\nu}F^{\rho\sigma}\,, \tag{5.2}$$

with $F_{\mu\nu}$ the field strength for A_μ and $\epsilon_{\mu\nu\rho\sigma}$ the covariant Levi-Civita tensor, and allows for couplings between the gauge field and the neutral scalar ϕ. Such theories includes as a special case the DBI model studied in [20, 25] and extend those studied in [73] by adding a scalar sector.

Assuming a background which is homogeneous and isotropic, the quantum critical bath can be described holographically using a black brane geometry supported by a nontrivial scalar $\phi = \phi(r)$ depending on the holographic radial coordinate r. The holographic DC conductivities associated with the conserved current J^μ dual to A_μ can be obtained following the prescription developed by [74] (see also [73]). In the probe limit the DC conductivity matrix σ_{ij} for the broad class of theories (5.1) is only sensitive to the structure of $\mathcal{L}(s, p, \phi)$ and in particular is given by

$$\sigma_{xx} = \mathcal{L}^{(1,0,0)}, \quad \sigma_{xy} = -\mathcal{L}^{(0,1,0)}, \tag{5.3}$$

where we have defined for convenience

$$\mathcal{L}^{(1,0,0)} \equiv \frac{\partial \mathcal{L}(s,p,\phi)}{\partial s}, \qquad \mathcal{L}^{(0,1,0)} \equiv \frac{\partial \mathcal{L}(s,p,\phi)}{\partial p}. \tag{5.4}$$

The corresponding resistivity and Hall angle are then

$$\begin{aligned} R_{xx} = \frac{\sigma_{xx}}{\sigma_{xx}^2 + \sigma_{xy}^2} &= \frac{\mathcal{L}^{(1,0,0)}}{\left(\mathcal{L}^{(1,0,0)}\right)^2 + \left(\mathcal{L}^{(0,1,0)}\right)^2}, \\ \cot\Theta_H = \frac{\sigma_{xx}}{\sigma_{xy}} &= -\frac{\mathcal{L}^{(1,0,0)}}{\mathcal{L}^{(0,1,0)}}, \end{aligned} \tag{5.5}$$

where it should be understood that all functions are evaluated at the horizon of the black brane.

Note that when $\mathcal{L}^{(0,1,0)} = 0$, $\sigma_{xy} = 0$ and hence $\tan\Theta_H = 0$. Thus, the presence of $p \sim F \wedge F$ in the theory leads to a distinctively different behavior for the con-

ductivities. As an example, in the standard linear EMD theory $\mathcal{L}(s,p,\phi) = Z(\phi)s$ thus far it has been difficult to realize the scaling behavior of the cuprates. In the probe limit this situation is not ameliorated, because although the associated resistivity $R_{xx} = 1/Z$ can in principle be engineered to be linear, the Hall conductivity is trivial. This compels us to study non-linear electrodynamics effects.

Finally, we stress that the result (5.5) is quite general, as it relies only on a minimal set of assumptions – a homogeneous and isotropic metric modeling the quantum critical bath, and the presence of a dilute set of charge carriers. The analysis of the DC conductivities away from the probe limit is discussed in the next section, where it can be seen that σ_{ij} in the backreacted case is sensitive not only to the gauge field sector, but also to the geometry and the structure of the model supporting the quantum critical bath. Interestingly, we find that the probe limit results can be obtained from the fully backreacted case when the scale of momentum dissipation dominates over the other physical scales in the system. Next, we turn to a more detailed discussion of our analysis.

5.2 Holographic Conductivity with Generic Gauge Sector

The holographic theory we examine describes gravity coupled to a neutral scalar field ϕ, two axions $\psi^I (I = 1, 2)$ and a $U(1)$ vector field A_μ,

$$S = \int d^4x\sqrt{-g}\left(\mathcal{R} - \frac{1}{2}(\partial\phi)^2 - V(\phi) - \frac{Y(\phi)}{2}\sum_{I=1}^{2}(\partial\psi^I)^2 - \mathcal{L}(s,p,\phi)\right), \qquad (5.6)$$

where $\mathcal{L}(s,p,\phi)$ is a generic function of the two combinations s and p defined in (5.2). A natural constraint is the requirement that in the weak flux limit $F \to 0$ one should recover the standard gauge field kinetic term, $\mathcal{L}(s,p,\phi) \sim s$.

The equations of motion associated with (5.6) are

$$\mathcal{R}_{\mu\nu} - \frac{1}{2}\mathcal{R}g_{\mu\nu} = \frac{Y(\phi)}{2}\sum_{I=1}^{2}\partial_\mu\psi^I\,\partial_\nu\psi^I + \frac{1}{2}\partial_\mu\phi\,\partial_\nu\phi - \frac{1}{2}\frac{\partial\mathcal{L}(s,p,\phi)}{\partial s}F_\mu{}^\sigma F_{\nu\sigma}$$
$$-\frac{g_{\mu\nu}}{2}\left(\frac{1}{2}(\partial\phi)^2 + \frac{Y(\phi)}{2}\sum_{I=1}^{2}(\partial\psi^I)^2 + V(\phi) + \mathcal{L}(s,p,\phi) - p\frac{\partial\mathcal{L}(s,p,\phi)}{\partial p}\right), \quad (5.7)$$

$$\nabla_\mu\nabla^\mu\phi - \partial_\phi V(\phi) - \frac{1}{2}\partial_\phi Y(\phi)\sum_{I=1}^{2}(\partial\psi^I)^2 - \partial_\phi\mathcal{L}(s,p,\phi) = 0\,, \quad (5.8)$$

$$\nabla_\mu(Y(\phi)\nabla^\mu\psi^I) = 0\,, \quad (5.9)$$

$$\nabla_\mu G^{\mu\nu} = 0\,, \quad (5.10)$$

where the tensor $G_{\mu\nu}$ is given by

$$G^{\mu\nu} = \frac{\partial\mathcal{L}(s,p,\phi)}{\partial s}F^{\mu\nu} + \frac{1}{2}\frac{\partial\mathcal{L}(s,p,\phi)}{\partial p}\epsilon^{\mu\nu\rho\sigma}F_{\rho\sigma}\,. \quad (5.11)$$

We are interested in finite temperature solutions to this theory which approach AdS at the boundary. Assuming homogeneity and isotropy, we consider the bulk metric and the matter fields of the background geometry to be of the following generic form,

$$\begin{aligned} ds^2 =& -U(r)\,dt^2 + \frac{dr^2}{U(r)} + C(r)(dx^2+dy^2)\,, \\ \phi =& \phi(r), \quad \psi^1 = k\,x, \quad \psi^2 = k\,y, \quad A = A_t(r)dt + \frac{h}{2}(x\,dy - y\,dx)\,, \end{aligned} \quad (5.12)$$

with h denoting the magnitude of the magnetic field. The temperature associated with these black branes is given by

$$T = \frac{U'(r_h)}{4\pi}\,, \quad (5.13)$$

with r_h denoting the horizon radius. The linear dependence of the axionic scalars

ψ^I on the spatial coordinates of the boundary field theory breaks translational invariance giving rise to momentum dissipation, whose strength is parametrized by k. Finally, from Maxwell's equation (5.10) we obtain a radially independent quantity,

$$\rho = C(r)G^{rt}\,, \quad \partial_r \rho = 0\,, \tag{5.14}$$

which describes the charge density of the dual boundary theory.

To construct the holographic DC conductivity matrix associated with the conserved current J^μ dual to the $U(1)$ gauge field A_μ we follow the prescription developed by [29]. In particular, we consider perturbations of the form in (3.17) to the background (5.12),

$$\begin{aligned} \delta g_{ti} = C(r)h_{ti}(r), \quad \delta g_{ri} = C(r)h_{ri}\,, \\ \delta A_i = -E_i t + a_i(r), \quad \delta\psi^1 = \chi_1(r), \quad \delta\psi^2 = \chi_2(r)\,, \end{aligned} \tag{5.15}$$

with $i = x, y$. Maxwell's equations (5.10) along the radial direction are then of the form $\partial_r J^i = 0$, with $J^i = \sqrt{-g}\, G^{ir}$ the spatial components of the conserved current in the dual theory,

$$J^x = -\mathcal{L}^{(1,0,0)}(s,p,\phi)\Big(hU(r)h_{ry}(r) + C(r)h_{tx}(r)A_t'(r) + U(r)a_x'(r)\Big) - E_y\,\mathcal{L}^{(0,1,0)}(s,p,\phi)\,, \tag{5.16}$$

$$J^y = \mathcal{L}^{(1,0,0)}(s,p,\phi)\Big(hU(r)h_{rx}(r) - C(r)h_{ty}(r)A_t'(r) - U(r)a_y'(r)\Big) + E_x\,\mathcal{L}^{(0,1,0)}(s,p,\phi)\,, \tag{5.17}$$

where we have defined

$$\mathcal{L}^{(1,0,0)} \equiv \frac{\partial \mathcal{L}(s,p,\phi)}{\partial s}\,, \qquad \mathcal{L}^{(0,1,0)} \equiv \frac{\partial \mathcal{L}(s,p,\phi)}{\partial p}\,. \tag{5.18}$$

Since the currents (J^x, J^y) are radially conserved, they may be calculated anywhere within the bulk. The horizon is a convenient choice.

Since the background geometry is regular near the horizon $r = r_h$, we impose the boundary conditions of (3.29)

$$\begin{aligned} A_t =& A_t'(r_h)(r-r_h) + \dots\,, \\ U =& U'(r_h)(r-r_h) + \dots = 4\pi\, T(r-r_h) + \dots\,. \end{aligned} \tag{5.19}$$

Then the constraint of regularity of the perturbation equations imposes the near-horizon expansions of (3.30)

$$\begin{aligned} a_i(r) =& -\frac{E_i}{4\pi T}\log(r-r_h) + \dots\,, \\ h_{ti}(r) =& U(r)h_{ri}(r) + \dots\,, \qquad \chi_i(r) = \chi_i(r_h) + \dots\,. \end{aligned} \tag{5.20}$$

The horizon data for h_{tx} and h_{ty} can be extracted from the perturbed Einstein's equations (5.7) using the regularity conditions, yielding

$$\begin{aligned} h_{tx}(r_h) &= \frac{\mathcal{L}^{(1,0,0)}(\mathrm{C}^2 A_t'\left(E_x k^2 Y - E_y h A_t' \mathcal{L}^{(1,0,0)}\right) - E_y h^3 \mathcal{L}^{(1,0,0)} + E_y h k^2 \mathrm{C} Y)}{\mathrm{C}^2\left(h^2 A_t'^2 \mathcal{L}^{(1,0,0)^2} + k^4 Y^2\right) - 2h^2 k^2 \mathrm{C} Y \mathcal{L}^{(1,0,0)} + h^4 \mathcal{L}^{(1,0,0)^2}}\,, \\ h_{ty}(r_h) &= \frac{\mathcal{L}^{(1,0,0)}(\mathrm{C}^2 A_t'(E_x h A_t' \mathcal{L}^{(1,0,0)} + E_y k^2 Y) + E_x h^3 \mathcal{L}^{(1,0,0)} - E_x h k^2 \mathrm{C} Y)}{\mathrm{C}^2\left(h^2 A_t'^2 \mathcal{L}^{(1,0,0)^2} + k^4 Y^2\right) - 2h^2 k^2 \mathrm{C} Y \mathcal{L}^{(1,0,0)} + h^4 \mathcal{L}^{(1,0,0)^2}}\,. \end{aligned} \tag{5.21}$$

From here on it should be understood that all functions are evaluated at the horizon $r = r_h$. Substituting the expressions (5.21) for the metric perturbations into (5.16)

and (5.17) finally yields Ohm's law in matrix form,

$$\begin{pmatrix} J^x \\ J^y \end{pmatrix} = \sigma \begin{pmatrix} E_x \\ E_y \end{pmatrix}, \tag{5.22}$$

with the components of the conductivity matrix σ_{ij} given by

$$\begin{aligned} \sigma_{xx} =& \sigma_{yy} = \frac{k^2 CY(k^2 CY - h^2 \mathcal{L}^{(1,0,0)} - C^2 (A_t')^2 \mathcal{L}^{(1,0,0)})}{h^2(-2k^2 CY + h^2 \mathcal{L}^{(1,0,0)} + C^2 A_t'^2 \mathcal{L}^{(1,0,0)}) + C^2 k^4 Y^2 \mathcal{L}^{(1,0,0)^{-1}}}\,, \\ \sigma_{xy} =& -\sigma_{yx} = \frac{hCA_t' \mathcal{L}^{(1,0,0)}(-2k^2 CY + h^2 \mathcal{L}^{(1,0,0)} + C^2 A_t'^2 \mathcal{L}^{(1,0,0)})}{h^2(-2k^2 CY + h^2 \mathcal{L}^{(1,0,0)} + C^2 A_t'^2 \mathcal{L}^{(1,0,0)}) + C^2 k^4 Y^2 \mathcal{L}^{(1,0,0)^{-1}}} - \mathcal{L}^{(0,1,0)}\,. \end{aligned} \tag{5.23}$$

These can be written in a slightly more compact form by defining the quantities

$$\xi \equiv k^2 CY - \left(h^2 + C^2 A_t'^2\right) \mathcal{L}^{(1,0,0)}\,, \quad \Omega \equiv -(k^2 CY + \xi)\,, \tag{5.24}$$

in terms of which we have the expressions included in the main body of the paper,

$$\begin{aligned} \sigma_{xx} =& \sigma_{yy} = \frac{k^2 CY\xi}{h^2\Omega + C^2 k^4 Y^2 \mathcal{L}^{(1,0,0)^{-1}}}\,, \\ \sigma_{xy} =& -\sigma_{yx} = \frac{hCA_t' \mathcal{L}^{(1,0,0)}\,\Omega}{h^2\Omega + C^2 k^4 Y^2 \mathcal{L}^{(1,0,0)^{-1}}} - \mathcal{L}^{(0,1,0)}\,. \end{aligned} \tag{5.25}$$

Notice that at this stage they depend on the gauge field term A_t' and not on the charge density ρ. Since the relationship between A_t' and ρ in these theories is generically non-linear, we will be able to express (5.25) explicitly in terms of the charge density only in special cases. Also, while both conductivities depend on the standard Maxwell term s through the dependence on $\mathcal{L}^{(1,0,0)}$, only σ_{xy} is sensitive to $\mathcal{L}^{(0,1,0)}$.

As a simple check of our analysis we consider the standard EMD theory described

by

$$\mathcal{L}(s,p,\phi) = Z(\phi)s\,, \tag{5.26}$$

for which $\mathcal{L}^{(1,0,0)} = Z$ and $\mathcal{L}^{(0,1,0)} = 0$. Expressed in terms of the charge density $\rho = CZA_t'$, the corresponding conductivities (5.25) are of the form

$$\begin{aligned}
\sigma_{xx} &= \sigma_{yy} = \frac{k^2 CY(k^2 CYZ - h^2 Z^2 - \rho^2)}{h^2(-2k^2 CYZ + h^2 Z^2 + \rho^2) + C^2 k^4 Y^2}\,, \\
\sigma_{xy} &= \sigma_{yx} = \frac{h\rho(-2k^2 CYZ + h^2 Z^2 + \rho^2)}{h^2(-2k^2 CYZ + h^2 Z^2 + \rho^2) + C^2 k^4 Y^2}\,,
\end{aligned} \tag{5.27}$$

in agreement with the results of [29], as expected. In addition, for the special case without a scalar sector, the quantities (5.25) agree with those computed in [93], a non-trivial check on our analysis.

Finally, from the conductivity matrix we can extract the inverse Hall angle as in (3.37),

$$\cot\Theta_H = \frac{\sigma_{xx}}{\sigma_{xy}}\,, \tag{5.28}$$

and the resistivity matrix as in (3.38),

$$R_{xx} = R_{yy} = \frac{\sigma_{xx}}{\sigma_{xx}^2 + \sigma_{xy}^2}\,, \qquad R_{xy} = -R_{yx} = -\frac{\sigma_{xy}}{\sigma_{xx}^2 + \sigma_{xy}^2}\,. \tag{5.29}$$

Written in terms of ξ and Ω we have

$$\begin{aligned}
\cot\Theta_H &= \frac{k^2\xi CY}{(h^2\Omega + k^4C^2Y^2\mathcal{L}^{(1,0,0)^{-1}})\mathcal{L}^{(0,1,0)} - hC\Omega A_t'\mathcal{L}^{(1,0,0)}}, \\
R_{xx} &= \frac{k^2\xi CY}{\left(h^2\Omega + k^4C^2Y^2\mathcal{L}^{(1,0,0)^{-1}}\right)\left[\frac{k^4\xi^2C^2Y^2}{(h^2\Omega+k^4C^2Y^2\mathcal{L}^{(1,0,0)^{-1}})^2} + \left(\mathcal{L}^{(0,1,0)} - \frac{hCA_t'\Omega\mathcal{L}^{(1,0,0)^2}}{(h^2\Omega\mathcal{L}^{(1,0,0)}+k^4C^2Y^2)}\right)^2\right]}, \\
R_{xy} &= \frac{\frac{hCA_t'\mathcal{L}^{(1,0,0)}\Omega}{h^2\Omega + C^2k^4Y^2\mathcal{L}^{(1,0,0)^{-1}}} - \mathcal{L}^{(0,1,0)}}{\left[\frac{k^4\xi^2C^2Y^2}{(h^2\Omega+k^4C^2Y^2\mathcal{L}^{(1,0,0)^{-1}})^2} + \left(\mathcal{L}^{(0,1,0)} - \frac{hCA_t'\Omega\mathcal{L}^{(1,0,0)^2}}{(h^2\Omega\mathcal{L}^{(1,0,0)}+k^4C^2Y^2)}\right)^2\right]}.
\end{aligned} \tag{5.30}$$

These expressions are entirely general and describe the conductivities resulting from theories of the form (5.6). Once the background solution (5.12) is known, $A_t'(r_h)$ and r_h can be expressed in terms of (T, ρ, h, k) by solving (5.13) and (5.14). Therefore, the resistivity and the Hall angle are general functions of the temperature T, the charge density ρ, the magnetic field h and the strength of momentum dissipation k.

We close by elaborating on the connection between the probe limit and the limit in which momentum dissipation is the dominant physical scale. Computing from scratch the conductivities under the assumption that the gauge field sector $\mathcal{L}_{\mathrm{U}(1)} = \mathcal{L}(s, p, \phi)$ is a probe and does not backreact on the geometry, which can be done by sending $\mathcal{L}_{\mathrm{U}(1)} \to \delta\mathcal{L}_{\mathrm{U}(1)}$ with δ a perturbatively small parameter, yields the expansions

$$\begin{aligned}
\sigma_{xx} &\approx \mathcal{L}^{(1,0,0)} + \delta\,\frac{(h^2 - C^2A_t'^2)\,\mathcal{L}^{(1,0,0)^2}}{CYk^2} + \mathcal{O}(\delta^2), \\
\sigma_{xy} &\approx -\mathcal{L}^{(0,1,0)} - \delta\,\frac{2hA_t'\,\mathcal{L}^{(1,0,0)^2}}{Yk^2} + \mathcal{O}(\delta^2)\,,
\end{aligned} \tag{5.31}$$

from which we extract the probe limit result we already mentioned in section 5.1,

$$R_{xx} \approx \frac{\mathcal{L}^{(1,0,0)}}{\mathcal{L}^{(0,1,0)^2} + \mathcal{L}^{(1,0,0)^2}}\,, \qquad \cot\Theta_H \approx -\frac{\mathcal{L}^{(1,0,0)}}{\mathcal{L}^{(0,1,0)}}\,. \tag{5.32}$$

On the other hand, if we expand the general expressions (5.27) in a large momentum dissipation expansion, by sending $k^2 \to \frac{k^2}{\delta}$ with $\delta \to 0$, we obtain the same result (5.31). Thus, from the point of view of the holographic conductivities, working under the assumption that the charge degrees of freedom are a probe is equivalent to assuming that the momentum dissipation scale k dominates over the other physical scales in the system, *i.e.* the charge density ρ and magnetic field h. We stress that this is not necessarily a large-k limit, but rather a statement about the hierarchy between k, ρ and h.

5.3 Quantum Critical Bath Geometry

Motivated by condensed matter studies of quantum criticality in strange metals [75, 76, 77], we will be specifically interested in solutions that are non-relativistic and violate hyperscaling in the IR of the geometry – thus, the dual system will be quantum critical in a generalized sense. To work with the standard holographic dictionary we consider geometries which asymptote to AdS at the boundary. The IR scaling behavior of such geometries will lead naturally to clean scaling regimes in the holographic transport coefficients and in particular in the DC conductivities, which are determined by horizon data.

One advantage of working in the probe limit is that we have a clean separation between the background geometry and the gauge field sector. In particular, the simple holographic model we introduced in (5.6),

$$\mathcal{L}_{\text{Bath}} = \mathcal{R} - \frac{(\partial\phi)^2}{2} - V(\phi) - \frac{Y(\phi)}{2}\sum_{I=1}^{2}(\partial\psi^I)^2\,, \tag{5.33}$$

supports analytical scaling geometries. When the scalar couplings are well approx-

imated by single exponentials in the IR of the geometry,

$$Y = e^{\alpha\phi}\,, \qquad V = -V_0 e^{-\beta\phi}\,, \tag{5.34}$$

with α, β and V_0 constants, the theory supports the following hyperscaling violating, Lifshitz-like black-branes,

$$\begin{aligned}
&ds^2 = -\left(\frac{r}{\ell}\right)^{2m} f(r)dt^2 + \left(\frac{r}{\ell}\right)^{-2m} f(r)^{-1}dr^2 + \left(\frac{r}{\ell}\right)^{2n} d\vec{x}^2,\\
&f(r) = 1 - \left(\frac{r_h}{r}\right)^{2m+2n-1}\,, \quad \phi(r) = \kappa \ln\left(\frac{r}{\ell}\right)\,,\\
&\kappa^2 = 4n(1-n), \;\; \alpha\kappa = 2(m+n-1), \;\; \beta\kappa = 2(1-m),\\
&\ell^2 V_0 = 2m(2m+2n-1)\,, \quad k^2 = \frac{(m-n)V_0}{m}\,,
\end{aligned} \tag{5.35}$$

where we have chosen the axion configuration

$$\psi^1 = k\,x, \quad \psi^2 = k\,y\,, \tag{5.36}$$

with the constant k denoting the strength of momentum dissipation. The temperature of these solutions scales with the horizon radius as $T \sim r_h^{2m-1}$ and the entropy as $S \sim T^{\frac{2n}{2m-1}}$. The scaling parameters n, m can be related to the standard dynamical critical exponent z and hyperscaling violating exponent θ by using

$$m = \frac{1}{2}\frac{\theta - 2z}{\theta - z}\,, \qquad n = \frac{1}{2}\frac{\theta - 2}{\theta - z}\,. \tag{5.37}$$

In terms of n, m the η-geometries discussed in [78], which arise from taking the limit $z \to \infty, \theta \to \infty$ with $\eta \equiv -\theta/z$ held fixed, correspond to taking $n + m = 1$ (with $\eta = \frac{2n}{1-2n}$). Finally, since these scaling geometries are generically singular, one needs to impose appropriate constraints on the parameter space in order to

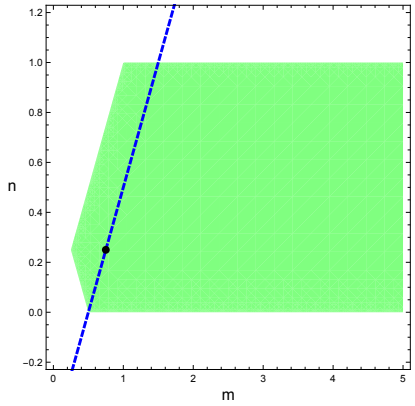

Figure 5.1: The green region denotes the values of (m, n) that satisfy the physical constraints which ensure a well defined ground state geometry. The dashed blue line shows the case which gives a linear entropy $S \sim T$. The black dot corresponds to the η-geometry with $m = 3/4, n = 1/4$ (or $\eta = 1$).

ensure a well-defined ground state solution, including Gubser's criterion [42] and the null energy condition (see *e.g.* the discussion in [103, 79]). The parameter space corresponding to physically acceptable ranges for the exponents (m, n) is shown in Fig. 5.1, with the dashed blue line denoting values for which the entropy is linear with temperature.

5.4 A Specific Non-Linear Model

Motivated in part by the DBI analysis of [54, 20], we choose to focus on a particularly simple non-linear model,

$$\mathcal{L}(s, p, \phi) = Z(\phi)s + \frac{1}{2}Z^2(\phi)p^2\,, \tag{5.38}$$

characterized by a single scalar coupling $Z(\phi)$. The combination (5.38) is natural from the viewpoint of the DBI action

$$\begin{aligned} S_{DBI} &= \sqrt{-g} - \sqrt{-\det(g + Z^{1/2}\, F)} \\ &= \sqrt{-g}\left[1 - \sqrt{1 - 2(Zs + Z^2 p^2/2)}\right] , \end{aligned} \tag{5.39}$$

and, despite its simplicity, will turn out to be sufficient to describe four of the scalings observed in the strange metal phase of the cuprates. Evaluating (5.3) for our non-linear model (5.38), we find that the resistivity and Hall angle are

$$\begin{aligned} R_{xx} &\sim \frac{Z}{Z^2 + Z^4\, p^2} = \frac{(C^2 + h^2 Z)^2}{Z\left[(C^2 + h^2 Z)^2 + h^2\rho^2\right]} , \\ \cot\Theta_H &\sim -\frac{1}{Z\, p} = \frac{C^2 + h^2 Z}{h\rho} , \end{aligned} \tag{5.40}$$

with the charge density

$$\rho = \frac{A_t'\, Z}{C}\left(C^2 + h^2 Z\right) , \tag{5.41}$$

and all functions evaluated at the horizon. The expressions (5.40) can be simplified further by taking a small h limit, which is consistent with our assumption of a dilute charge sector. This yields the simple expressions

$$R_{xx} \sim \frac{1}{Z} , \qquad \cot\Theta_H \sim \frac{C^2}{h\rho} , \tag{5.42}$$

each controlled by a different scale, the first by the scalar coupling Z and the second by the geometry through C. Finally, working with the small h expansion of the resistivity (5.40) we compute the magnetoresistance,

$$MR = \frac{R_{xx}(h) - R_{xx}(h=0)}{R_{xx}(h=0)} \sim -\frac{h^2\rho^2}{C^4} . \tag{5.43}$$

The results (5.42) agree with those obtained in the DBI construction of [20], for small values of the charge density and magnetic field. While this agreement is expected, since (5.38) is part of the low-energy expansion of the DBI model of [20], it also suggests that the much simpler non-linear model (5.42) may suffice to capture the key physics of more complex DBI-like theories. In addition, the particular DBI model of [20] predicts a weak-field magnetoresistance that goes as h^2/T^3, instead of the h^2/T^4 behavior of the cuprates, and therefore it may be more appropriate to describe other strange metal phases.

5.5 Physical Implications

We are now ready to comment on the implications of our results, and ask in particular whether the transport quantities we computed can describe the scaling behaviors observed in the cuprates. First of all, note that while R_{xx} depends on the scalar coupling Z, the Hall angle and magnetoresistance (at small h) are both controlled by the metric component C, which also determines the thermodynamic entropy S of the dual field theory, $S \sim C$. While the coupling Z can be chosen freely without affecting the geometry, the function C is fixed for a given background. Once the geometry is specified – and therefore the temperature dependence of the entropy – there is very little freedom in the system.

In our model a linear resistivity $R_{xx} \sim T$ can be realized by identifying a clean temperature scaling regime for the scalar coupling, of the form

$$Z \sim \frac{1}{T} \,. \tag{5.44}$$

Moreover, experimental data on the cuprates [80, 81] indicates that the entropy is

linear in temperature,

$$S \sim T\,, \tag{5.45}$$

which requires the spatial metric component to scale as

$$C \sim T\,, \tag{5.46}$$

and unambiguously fixes the temperature dependence of the Hall angle and magnetoresistance in our model to be

$$\cot\Theta_H \sim T^2\,, \;\; MR \sim -\frac{h^2}{T^4}\,. \tag{5.47}$$

In our setup (5.44) and (5.46) can indeed be realized quite naturally, making use of the quantum critical geometry. In particular, (5.44) can be obtained by making the simple single exponential choice $Z(\phi) \sim e^{\gamma\phi}$ with $\gamma = \frac{1-2m}{2-2m}\beta$. Moreover, the entropy associated with (5.35) is given by

$$S \sim C(r_h) \sim T^{\frac{2n}{2m-1}}\,. \tag{5.48}$$

Thus, we have a linear entropy $S \sim T$ when $2n = 2m - 1$. For z and θ finite this translates to the condition $z = 2 - \theta$ corresponding to a one-parameter family of black brane solutions, while for the case of η-geometries for which both exponents are infinite we have $m + n = 1$ and thus $n = 1/4$ and $m = 3/4$. The parameter choices that correspond to a linear entropy are represented by the dashed line in Fig. 5.1, with the dot denoting the special case corresponding to the $\eta = 1$ geometry.

It is intriguing and unexpected that the choice (5.44) and the experimental observation (5.45) are sufficient to reproduce the observed scaling properties of the cuprates. In particular, what we have seen is that the simple non-linear model (5.38)

supports the following behaviors,

$$S \sim T, \;\; R_{xx} \sim T \,, \; \cot\Theta_H \sim T^2 \,, \; MR \sim -\frac{h^2}{T^4} \,.$$

It is convenient to rescale the temperature and magnetic field and work with dimensionless quantities. In particular, if we introduce two positive constants z_0 and c_0 through $Z = z_0/T$ and $C = c_0 T$ (the values of the constants depend on the specific theory one examines), we can construct the dimensionless expressions

$$\mathbf{T} = \frac{c_0^2 z_0}{\rho^2} T, \quad \mathbf{h} = \frac{c_0^2 z_0^2}{\rho^3} h \,. \tag{5.49}$$

We then have

$$\begin{aligned} R_{xx} &= \zeta_0 \, \mathbf{T} \left[1 + \frac{\mathbf{T}^2 \mathbf{h}^2}{\left(\mathbf{T}^3 + \mathbf{h}^2\right)^2} \right]^{-1} \,, \;\; \zeta_0 \equiv \frac{\rho^2}{c_0^2 z_0^2} \,, \\ \cot\Theta_H &= \frac{\mathbf{T}^2}{\mathbf{h}} \left(1 + \frac{\mathbf{h}^2}{\mathbf{T}^3} \right) \,, \\ MR &= -\frac{\mathbf{T}^2 \mathbf{h}^2}{(\mathbf{T}^3 + \mathbf{h}^2)^2 + \mathbf{T}^2 \mathbf{h}^2} \,. \end{aligned} \tag{5.50}$$

We immediately observe that $R_{xx} \sim \mathbf{T}$ approaches zero as $\mathbf{T} \to 0$, and in particular $R_{xx} = \zeta_0 \mathbf{T}$ in the absence of a magnetic field. Thus, this system indeed describes a metal phase.

The temperature dependence of the quantities (5.50) is plotted in Fig. 5.2, from which it is clear that when the value of $\mathbf{T}$ is sufficiently bigger than $\mathbf{h}$ (more precisely, when $\mathbf{T}^3 >> \mathbf{h}^2$), one realizes the strange metal scalings

$$S \sim \mathbf{T}, \; R_{xx} \sim \zeta_0 \mathbf{T}, \; \cot\Theta_H \sim \frac{\mathbf{T}^2}{\mathbf{h}}, \; MR \sim -\frac{\mathbf{h}^2}{\mathbf{T}^4}. \tag{5.51}$$

Our discussion is based on the rescaled temperature $\mathbf{T}$ which is defined with respect

to the scale $\rho^2/(c_0^2 z_0^2)$, as seen from (5.54). Therefore, note that the regime we are considering is not necessarily a high$-T$ limit. It could indeed describe low temperature physics provided that this scale is sufficiently higher than the temperature the experiment is probing.

In closing, we would like to mention a few additional features that are visible in our analysis. First, note that in the absence of a magnetic field the linear temperature dependence of the resistivity is exact. Moreover, as long as we are away from the transition regime in which **T** and **h** are comparable, the in-plane resistivity (5.50) is not very sensitive to the magnetic field. As a result, in the temperature range in which one can realize (5.51), the magnetoresistance is small (and negative), suggesting that the effect of a magnetic field does not alter the underlying normal state. This is consistent with the observation in the experiment of [82]. Finally, we note that the increase in the Hall angle at very small temperatures (visible in Fig. 5.2) is similar to the behavior observed in [83, 84].

5.6 Magnetotransport in the DBI Theory

In this section we include the magneto-transport results for a theory whose gauge field sector is described by the non-linear DBI model,

$$S_{DBI} = \sqrt{-g} - \sqrt{-\det(g + Z^{1/2} F)} = \sqrt{-g}\left[1 - \sqrt{1 - 2(Zs + Z^2 p^2/2)}\right] , \quad (5.52)$$

and which can be used to describe an ensemble of probe charge carriers interacting with a larger neutral quantum critical bath. Note that (5.52) corresponds to the special case $Z_1(\phi) = 1$, $Z_2(\phi) = \sqrt{Z(\phi)}$ of the theory studied in [19, 20, 25].

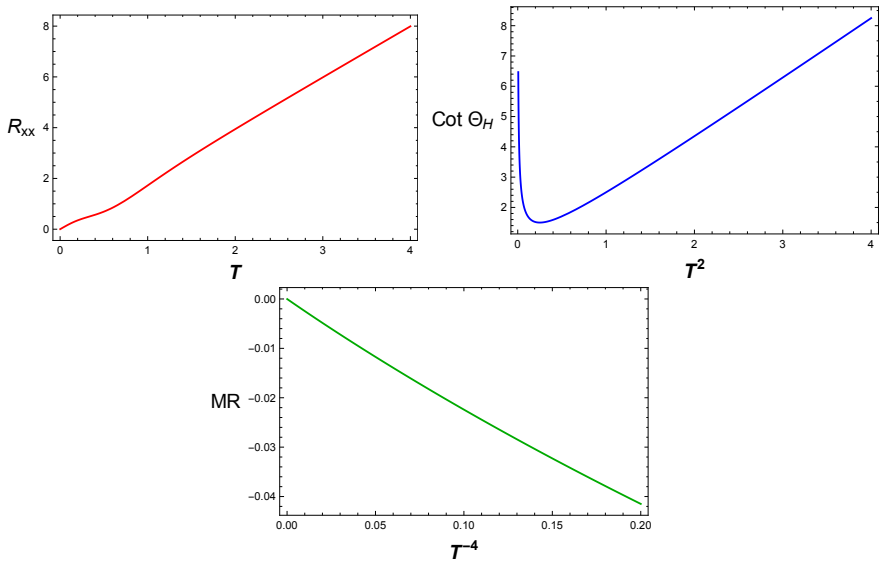

Figure 5.2: Dependence of the resistivity, Hall angle and magnetoresistance in the expressions (5.50) on the dimensionless temperature $\mathbf{T}$. We fix $\mathbf{h} = 0.5$ and find good scaling behaviors when $\mathbf{T} \gtrsim 3\mathbf{h} = 1.5$. We have chosen $\zeta_0 = 2$.

The associated in-plane resistivity and Hall angle are given by

$$R_{xx} = \frac{C}{\sqrt{Z}} \frac{\sqrt{\rho^2 + Z(C^2 + h^2 Z)}}{\rho^2 + C^2 Z}, \qquad \cot\Theta = \frac{C}{h\rho\sqrt{Z}} \sqrt{\rho^2 + Z(C^2 + h^2 Z)}\,, \quad (5.53)$$

with ρ denoting the charge density. We introduce two constants z_0 and c_0 through $Z = z_0/T$ and $C = c_0 T$, and construct the dimensionless expressions

$$\mathbf{T} = \frac{c_0^2 z_0}{\rho^2} T, \qquad \mathbf{h} = \frac{c_0^2 z_0^2}{\rho^3} h\,. \quad (5.54)$$

We then have

$$
\begin{aligned}
R_{xx} &= \zeta_0 \frac{\mathbf{T}^{3/2}}{1+\mathbf{T}} \sqrt{1+\mathbf{T}+\mathbf{h}^2/\mathbf{T}^2}, \\
\cot\Theta_H &= \frac{\mathbf{T}^{3/2}}{\mathbf{h}} \sqrt{1+\mathbf{T}+\mathbf{h}^2/\mathbf{T}^2}\,, \\
MR &= \sqrt{1+\frac{\mathbf{h}^2}{\mathbf{T}^2(1+\mathbf{T})}} - 1\,.
\end{aligned}
\tag{5.55}
$$

In the "high-temperature" limit $\mathbf{T} \gg 1+\mathbf{h}^2/\mathbf{T}^2$, one obtains [20] the simple scalings

$$
R_{xx} \sim \zeta_0 \mathbf{T}, \;\; \cot\Theta_H \sim \frac{\mathbf{T}^2}{\mathbf{h}}\,,
\tag{5.56}
$$

while the magneto-resistance reads

$$
MR \sim \frac{\mathbf{h}^2}{\mathbf{T}^3}\,.
\tag{5.57}
$$

It is now obvious that the DBI theory (5.52) gives a weak-field magneto-resistance that goes as h^2/T^3, instead of the observed h^2/T^4 for the cuprates, and therefore it could be a contender to describe strange metals other than the cuprates. Finally, when $\mathbf{h}$ dominates over the temperature we obtain the strong-field magneto-transport results,

$$
R_{xx} \sim \zeta_0 \frac{\mathbf{T}^{1/2}}{1+\mathbf{T}}\,\mathbf{h}, \;\; \cot\Theta_H \sim \mathbf{T}^{1/2}, \;\; MR \sim \frac{\mathbf{h}}{\mathbf{T}\sqrt{1+\mathbf{T}}}\,.
\tag{5.58}
$$

We find that both R_{xx} and MR scale linearly with magnetic field, while the Hall angle $\cot\Theta_H$ is almost $\mathbf{h}$ independent.

5.7 Final Remarks

Our analysis has provided the first holographic realization of the temperature scalings (5.51) through a simple and rather minimal non-linear model. In particular, our results relied crucially on the presence of non-linear interactions among the charge carriers, which appear to be a necessary ingredient for a bulk description of strongly correlated electron matter. Working in the dilute charge limit allowed us to construct a neutral quantum critical bath, key to identifying clean scaling regimes in the transport coefficients.

In the model (5.38) the scaling of the Hall angle and of the magnetoresistance, T^2 and T^{-4} respectively, were entirely fixed by the observation that the entropy in the cuprates should be linear in temperature [80, 81], $S \sim T$. Note that the linear resistivity $R_{xx} \sim T$ would then follow immediately by requiring R_{xx} to scale like the entropy, making the choice (5.44) natural. Although [85, 86] argues that the resistivity should indeed be proportional to the entropy, their arguments are not applicable in our model – the inclusion of axions leads to a temperature dependent shear viscosity to entropy ratio [87]. Nonetheless, our study lends evidence to the idea that the cuprates' strange metal behavior depends crucially on the linear entropy as well as on the existence of a strongly coupled quantum critical IR sector.

Note that the magnetoresistance associated with (5.38) is negative. Possible mechanisms for a negative magnetoresistance have been proposed for example in [88, 89, 90]. We should stress, however, that both the sign and scaling properties of quantities such as the magnetoresistance depend entirely on the specific model one works with as we saw in Section 5.6. Indeed, the minimal model (5.38) is only one among a large class of non-linear theories one could construct, which generically lead to a highly non-trivial transport structure, as shown in (5.5) (and in (5.30) away from the probe limit). Understanding this rich structure in more detail is

especially important given the additional scaling regimes that have been recently observed in different high-T_c superconductors, including the cuprates [91] and also iron pnictides [92].

Chapter 6

Summary and Outlook

String theory provides a powerful framework in which to describe quantum gravitational effects. By replacing point-like particles with string-like excitations, string theory overcomes the challenges faced by other theories attempting to quantize gravity. One of the most remarkable developments that has emerged from string theory is the holographic AdS/CFT correspondence. In its original formulation, holography relates a certain string theory in $AdS_5 \times S^5$ to $\mathcal{N} = 4$ SU(N) SYM, a conformal field theory in four dimensions. The duality has by now been extended in a number of ways, as we have discussed in the early chapters of the thesis. Due to the strong/weak coupling relationship between the gravitational side of the correspondence and its quantum field theory counterpart, quantum theories with a large coupling constant correspond to gravitational systems with a small coupling. Thus, we see that by working in the perturbative gravity regime, one can probe the strong coupling sector of the dual field theory, which is notoriously difficult to understand. As a result, holography provides novel techniques for probing the dynamical behavior of these strongly coupled systems by mapping them to gravitational theories. A prime example is the application of these techniques to the celebrated high T_C

superconductors.

Traditional BCS theory describes conventional superconducting materials through the formation of Cooper pairs. As we have seen, these pairs are an energetically favorable solution to Schrödinger's equation describing a second order phase transition as the material enters a superconducting state. However, high temperature superconductors differ from BCS superconductors in fundamental ways, with their pairing mechanism still unknown. More generally, strongly correlated electron systems are challenging to model due to the complexity of their phase diagram and the presence of strong correlations between the charge carriers. Standard Fermi liquid theory breaks down for systems of this kind.

In this thesis, we have explored the role of non-linear electromagnetic interactions – well motivated by non-perturbative effects in string theory – on the transport properties of strongly correlated quantum phases. The inclusion of such non-linear terms is motivated by the strongly interacting nature of the charged degrees of freedom in these systems. In particular, we have focused on applications to the physics of the cuprate high T_C superconductors, whose anomalous scaling behavior could not be reproduced within holographic models with standard Maxwell terms. The non-linear effects that we have examined arise from the DBI action for D-branes in string theory. We have found fully backreacted solutions to this theory from which it has become clear that DBI terms lead to a rich and complex structure for the magnetotransport properties of the dual system.

We have extended this analysis by including a generic non-linear gauge sector, which includes the DBI action as a special case. In addition to computing the associated magnetotransport properties, we have focused on understanding the origin of possible scaling behaviors in these theories. In particular, one can ask under which conditions the resistivity will scale linearly with temperature, a crucial feature of the

strange metal phase. Moreover, in the cuprates, the entropy, the Hall angle and the magnetoresistance have also been shown to exhibit specific scalings not explained by Fermi liquid theory. Working in the dilute charge limit (in which the backreaction on the geometry can be ignored) we were able to realize several of the scalings seen in the cuprates, for the first time in the holographic literature. This provides a proof of principle that holographic model building can capture non-trivial properties of these systems. In particular, in order for these scalings to be realized, it was crucial to take into account nonlinear interactions among the charged degrees of freedom. This model not only reproduces the scaling of the Hall angle and resistivity, but also the entropy and magnetoresistance of the cuprates.

While our results provide the first holographic realization of these anomalous scalings, we still lack a deeper understanding of their origin. In particular, reproducing them required us to tune two of the parameters of our model. The origin of this choice is still not clear. Additionally, we would like a deeper physical motivation for the simple model of chapter 5, which led to the successful realization of the cuprate scalings. More broadly, it would be valuable to identify any universal features that are predicted by holographic models that account for interactions between the charge carriers. Such generic properties would provide additional insight into the driving force of strongly interacting systems. Moreover, for holography to have a bigger impact on the broader physics community, it is crucial that it leads to testable predictions. We hope that our results can provide guidance towards the construction of more realistic theories and help build intuition for the mechanisms underlying the unconventional behavior of strongly correlated systems such as the cuprates.

Bibliography

[1] S. Hawking, "Particle creation by black holes", Commun.Math.Phys. 43 (1975) 199

[2] J. D. Bekenstein, "Black Holes and Entropy", Phys. Rev. D 7, 2333 (1973)

[3] A. Strominger and C. Vafa, "Microscopic Origin of the Bekenstein-Hawking Entropy", arXiv:hep-th/9601029 (1996)

[4] J. Maldacena, "The Large N Limit of Superconformal Field Theories and Supergravity", arXiv:hep-th/9711200 (1997)

[5] E. Witten, "Anti De Sitter Space And Holography", arXiv:hep-th/9802150 (1998)

[6] S. Gubser, I. Klebanov, A. Polyakov, "Gauge Theory Correlators from Non-Critical String Theory", arXiv:hep-th/9802109 (1998)

[7] G. Horowitz, "Introduction to Holographic Superconductors," arxiv:1002.1722 [hep-th]

[8] V. L. Ginzburg and L. D. Landau, "On the Theory of superconductivity," Zh. Eksp. Teor. Fiz. 20, 1064 (1950).

[9] J. Bardeen, L. N. Cooper and J. R. Schrieffer, "Theory Of Superconductivity," Phys. Rev. 108, 1175 (1957).

[10] D. Musso, "Introductory notes on holographic superconductors", PoS Modave2013 (2013) 004, [arXiv:1401.1504].

[11] T. Timusk, B.W. Statt "The pseudogap in high-temperature superconductors: an experimental survey," [arXiv:9905219 [cond-mat]].

[12] B. Keimer, S. A .Kivelson, M. R. Norman, S. Uchida, J. Zaanen, "High Temperature Superconductivity in the Cuprates," Nature **518**, 179 (2015) [arXiv:1409.4673 [cond-mat.supr-con]].

[13] D. v. d. Marel, H. J. A. Molegraaf, J. Zaanen, Z. Nussinov, F. Carbone, A. Damascelli, H. Eisaki, M. Greven, P. H. Kes, and M. Li, Nature 425 (2003) 271, [cond-mat/0309172].

[14] S. A. Hartnoll and A. Karch, "Scaling theory of the cuprate strange metals," Phys. Rev. B **91**, no. 15, 155126 (2015) [arXiv:1501.03165 [cond-mat.str-el]].

[15] S. Cremonini "The Shear Viscosity to Entropy Ratio: A Status Report" arXiv:hep-th/1108.0677 (2011)

[16] S. Gubser "Breaking an Abelian gauge symmetry near a black hole horizon" arXiv:hep-th/0801.2977 (2008)

[17] S. Hartnoll, C. Herzog, G. Horowitz "Holographic Superconductors" arXiv:hep-th/0810.1563 (2008)

[18] A. Donos and J. P. Gauntlett, "Novel metals and insulators from holography," JHEP **1406**, 007 (2014) doi:10.1007/JHEP06(2014)007 [arXiv:1401.5077 [hep-th]].

[19] S. Cremonini, A. Hoover and L. Li, "Backreacted DBI Magnetotransport with Momentum Dissipation," JHEP **1710**, 133 (2017) [arXiv:1707.01505 [hep-th]].

[20] E. Blauvelt, S. Cremonini, A. Hoover, L. Li and S. Waskie, "A Holographic Model for the Anomalous Scalings of the Cuprates," arXiv:1710.01326 [hep-th].

[21] S. Cremonini, A. Hoover, L. Li, S. Waskie, "Anomalous scalings of the cuprate strange metals from nonlinear electrodynamics," Phys. Rev. D **99**, no. 061901(R) (2019) [arXiv:1812.01040 [hep-th]].

[22] S. A. Hartnoll, A. Lucas and S. Sachdev, "Holographic quantum matter," arXiv:1612.07324 [hep-th].

[23] X. Wang, E. Berg, "Scattering mechanisms and electrical transport near an Ising nematic quantum critical point," [arXiv:1902.04590v1 [hep-th]].

[24] I. M. Hayes, N. P. Breznay, T. Helm, P. Moll, M. Wartenbe, R. D. McDonald, A. Shekhter, J. G. Analytis, "Magnetoresistance near a quantum critical point," [arXiv:1412.6484 [cond-mat.str-el]];

I. M. Hayes, R. D. McDonald, N. P. Breznay, T. Helm, P. J. W. Moll, M. Wartenbe, A. Shekhter, J. G. Analytis, "Scaling between magnetic field and temperature in the high-temperature superconductor $BaFe_2(As_{1-x}P_x)_2$," Nature Phys. **12**, 916-919 (2016) doi:10.1038/nphys3773.

[25] E. Kiritsis and L. Li, "Quantum Criticality and DBI Magneto-resistance," J. Phys. A **50**, no. 11, 115402 (2017) doi:10.1088/1751-8121/aa59c6 [arXiv:1608.02598 [cond-mat.str-el]].

[26] A. Karch and A. O'Bannon, "Metallic AdS/CFT," JHEP **0709**, 024 (2007) doi:10.1088/1126-6708/2007/09/024 [arXiv:0705.3870 [hep-th]].

[27] A. O'Bannon, "Hall Conductivity of Flavor Fields from AdS/CFT," Phys. Rev. D **76**, 086007 (2007) doi:10.1103/PhysRevD.76.086007 [arXiv:0708.1994 [hep-th]].

[28] T. Andrade and B. Withers, "A simple holographic model of momentum relaxation," JHEP **1405**, 101 (2014) doi:10.1007/JHEP05(2014)101 [arXiv:1311.5157 [hep-th]].

[29] M. Blake and A. Donos, "Quantum Critical Transport and the Hall Angle," Phys. Rev. Lett. **114**, no. 2, 021601 (2015) doi:10.1103/PhysRevLett.114.021601 [arXiv:1406.1659 [hep-th]].

[30] M. Blake, A. Donos and N. Lohitsiri, "Magnetothermoelectric Response from Holography," JHEP **1508**, 124 (2015) doi:10.1007/JHEP08(2015)124 [arXiv:1502.03789 [hep-th]].

[31] A. Amoretti and D. Musso, "Magneto-transport from momentum dissipating holography," JHEP **1509**, 094 (2015) doi:10.1007/JHEP09(2015)094 [arXiv:1502.02631 [hep-th]].

[32] M. Blake, "Magnetotransport from the fluid/gravity correspondence," JHEP **1510**, 078 (2015) doi:10.1007/JHEP10(2015)078 [arXiv:1507.04870 [hep-th]].

[33] K. Y. Kim, K. K. Kim, Y. Seo and S. J. Sin, "Thermoelectric Conductivities at Finite Magnetic Field and the Nernst Effect," JHEP **1507**, 027 (2015) doi:10.1007/JHEP07(2015)027 [arXiv:1502.05386 [hep-th]].

[34] Z. Zhou, J. P. Wu and Y. Ling, "DC and Hall conductivity in holographic massive Einstein-Maxwell-Dilaton gravity," JHEP **1508**, 067 (2015) doi:10.1007/JHEP08(2015)067 [arXiv:1504.00535 [hep-th]].

[35] A. Donos, J. P. Gauntlett, T. Griffin and L. Melgar, "DC Conductivity of Magnetised Holographic Matter," JHEP **1601**, 113 (2016) doi:10.1007/JHEP01(2016)113 [arXiv:1511.00713 [hep-th]].

[36] A. Amoretti, M. Baggioli, N. Magnoli and D. Musso, "Chasing the cuprates with dilatonic dyons," JHEP **1606**, 113 (2016) doi:10.1007/JHEP06(2016)113 [arXiv:1603.03029 [hep-th]].

[37] X. H. Ge, Y. Tian, S. Y. Wu and S. F. Wu, "Hyperscaling violating black hole solutions and Magneto-thermoelectric DC conductivities in holography," Phys. Rev. D **96**, no. 4, 046015 (2017) doi:10.1103/PhysRevD.96.046015 [arXiv:1606.05959 [hep-th]].

[38] M. Blake, R. A. Davison and S. Sachdev, "Thermal diffusivity and chaos in metals without quasiparticles," arXiv:1705.07896 [hep-th].

[39] S. A. Hartnoll and P. Kovtun, "Hall conductivity from dyonic black holes," Phys. Rev. D **76**, 066001 (2007) doi:10.1103/PhysRevD.76.066001 [arXiv:0704.1160 [hep-th]].

[40] R. A. Davison and B. Gouteraux, "Dissecting holographic conductivities," JHEP **1509**, 090 (2015) doi:10.1007/JHEP09(2015)090 [arXiv:1505.05092 [hep-th]].

[41] B. Gouteraux, "Charge transport in holography with momentum dissipation," JHEP **1404**, 181 (2014) doi:10.1007/JHEP04(2014)181 [arXiv:1401.5436 [hep-th]].

[42] S. S. Gubser, "Curvature singularities: The Good, the bad, and the naked," Adv. Theor. Math. Phys. **4**, 679 (2000) [hep-th/0002160].

[43] C. Charmousis, B. Gouteraux, B. S. Kim, E. Kiritsis and R. Meyer, "Effective Holographic Theories for low-temperature condensed matter systems," JHEP **1011**, 151 (2010) doi:10.1007/JHEP11(2010)151 [arXiv:1005.4690 [hep-th]].

[44] A. Kundu and N. Kundu, "Fundamental Flavours, Fields and Fixed Points: A Brief Account," JHEP **1703**, 071 (2017) doi:10.1007/JHEP03(2017)071 [arXiv:1612.08624 [hep-th]].

[45] A. Donos and S. A. Hartnoll, "Interaction-driven localization in holography," Nature Phys. **9**, 649 (2013) doi:10.1038/nphys2701 [arXiv:1212.2998 [hep-th]].

[46] Y. Ling, P. Liu, C. Niu and J. P. Wu, "Building a doped Mott system by holography," Phys. Rev. D **92**, no. 8, 086003 (2015) doi:10.1103/PhysRevD.92.086003 [arXiv:1507.02514 [hep-th]].

[47] R. G. Cai and R. Q. Yang, "Insulator/metal phase transition and colossal magnetoresistance in holographic model," Phys. Rev. D **92**, no. 10, 106002 (2015) doi:10.1103/PhysRevD.92.106002 [arXiv:1507.03105 [hep-th]].

[48] M. Baggioli and O. Pujolas, "On holographic disorder-driven metal-insulator transitions," JHEP **1701**, 040 (2017) doi:10.1007/JHEP01(2017)040 [arXiv:1601.07897 [hep-th]].

[49] Y. Ling, P. Liu, J. P. Wu and Z. Zhou, "Holographic Metal-Insulator Transition in Higher Derivative Gravity," Phys. Lett. B **766**, 41 (2017) doi:10.1016/j.physletb.2016.12.051 [arXiv:1606.07866 [hep-th]].

[50] S. Cremonini, H. S. Liu, H. Lu and C. N. Pope, "DC Conductivities from Non-Relativistic Scaling Geometries with Momentum Dissipation," JHEP **1704**, 009 (2017) doi:10.1007/JHEP04(2017)009 [arXiv:1608.04394 [hep-th]].

[51] S. S. Pal, "Fermi-like Liquid From Einstein-DBI-Dilaton System," JHEP **1304**, 007 (2013) doi:10.1007/JHEP04(2013)007 [arXiv:1209.3559 [hep-th]].

[52] J. Tarrio, "Transport properties of spacetime-filling branes," JHEP **1404**, 042 (2014) doi:10.1007/JHEP04(2014)042 [arXiv:1312.2902 [hep-th]].

[53] E. Kiritsis and J. Ren, "On Holographic Insulators and Supersolids," JHEP **1509**, 168 (2015) doi:10.1007/JHEP09(2015)168 [arXiv:1503.03481 [hep-th]].

[54] S. A. Hartnoll, J. Polchinski, E. Silverstein and D. Tong, "Towards strange metallic holography," JHEP **1004**, 120 (2010) doi:10.1007/JHEP04(2010)120 [arXiv:0912.1061 [hep-th]].

[55] B. H. Lee, D. W. Pang and C. Park, "Strange Metallic Behavior in Anisotropic Background," JHEP **1007**, 057 (2010) doi:10.1007/JHEP07(2010)057 [arXiv:1006.1719 [hep-th]].

[56] B. S. Kim, E. Kiritsis and C. Panagopoulos, "Holographic quantum criticality and strange metal transport," New J. Phys. **14**, 043045 (2012) doi:10.1088/1367-2630/14/4/043045 [arXiv:1012.3464 [cond-mat.str-el]].

[57] S. S. Pal, "Model building in AdS/CMT: DC Conductivity and Hall angle," Phys. Rev. D **84**, 126009 (2011) doi:10.1103/PhysRevD.84.126009 [arXiv:1011.3117 [hep-th]].

[58] A. Karch, "Conductivities for Hyperscaling Violating Geometries," JHEP **1406**, 140 (2014) doi:10.1007/JHEP06(2014)140 [arXiv:1405.2926 [hep-th]].

[59] J. F. Woods and C. Y. Chen, "Negative Magnetoresistance in Impurity Conduction," Phys. Rev. 135, A1462.

[60] H. Negishi, H. Yamada, K. Yuri, M. Sasaki and M. Inoue "Negative magnetoresistance in crystals of the paramagnetic intercalation compound Mn_xTiS_2," Phys. Rev. B **56**, 11144 (1997).

[61] Y. B. Zhou, B. H. Han, Z. M. Liao1, H. C. Wu and D. P. Yu, "From positive to negative magnetoresistance in graphene with increasing disorder," Appl. Phys. Lett. **98**, 222502 (2011).

[62] X. C. Huang *et al*, "Observation of the Chiral-Anomaly-Induced Negative Magnetoresistance in 3D Weyl Semimetal TaAs," Phys. Rev. X **5**, 031023 (2015).

[63] C. Z. Li *et al*, "Giant negative magnetoresistance induced by the chiral anomaly in individual Cd3As2 nanowires," Nature Communications 6, 10137 (2015), [arXiv:1504.07398 [cond-mat.str-el]].

[64] H. Li *et al*, "Negative Magnetoresistance in Dirac Semimetal Cd3As2," Nat. Commun. 7:10301 (2016), [arXiv:1507.06470 [cond-mat.str-el]].

[65] M. Culo *et al* "Magnetotransport properties of $La_{1-x}Ca_xMnO_3(0.52 \leqslant x \leqslant 0.75)$: Signature of phase coexistence ," Thin Solid Films, **631**, 205-212, [arXiv:1704.07315 [cond-mat.str-el]].

[66] N. Jiang, Y. Nii, R. Ishii, Z. Hiroi, Y. Onose, "Magnetotransport properties in a noncentrosymmetric itinerant magnet $Cr_{11}Ge_{19}$," arXiv:1705.06026 [cond-mat.str-el].

[67] P. Goswami, J. H. Pixley and S. Das Sarma, "Axial anomaly and longitudinal magnetoresistance of a generic three dimensional metal," Phys. Rev. B **92**, no. 7, 075205 (2015) doi:10.1103/PhysRevB.92.075205 [arXiv:1503.02069 [cond-mat.mes-hall]].

[68] A. Baumgartner, A. Karch and A. Lucas, "Magnetoresistance in relativistic hydrodynamics without anomalies," JHEP **1706**, 054 (2017) doi:10.1007/JHEP06(2017)054 [arXiv:1704.01592 [hep-th]].

[69] M. Baggioli and O. Pujolas, "On Effective Holographic Mott Insulators," JHEP **1612**, 107 (2016) doi:10.1007/JHEP12(2016)107 [arXiv:1604.08915 [hep-th]].

[70] J. M. Harris *et al.*, "Violation of Kohler's Rule in the Normal-State Magnetoresistance of $YBa_2Cu_3O_{7-\delta}$ and $La_2Sr_xCuO_4$," Phys. Rev. Lett. **75**, 1391(1995).

[71] N. E. Hussey, "Phenomenology of the normal state in-plane transport properties of high-Tc cuprates," J. Phys. Cond. Matt. **20** 123201 (2008) [arXiv:0804.2984 [cond-mat.supr-con]].

[72] J. Zaanen, Y. W. Sun, Y. Liu and S. Schalm, "Holographic duality in condensed matter physics," Cambridge Univ. Press, 2015.

[73] X. Guo, P. Wang and H. Yang, "Membrane Paradigm and Holographic DC Conductivity for Nonlinear Electrodynamics," Phys. Rev. D **98**, no. 2, 026021 (2018) [arXiv:1711.03298 [hep-th]].

[74] N. Iqbal and H. Liu, "Universality of the hydrodynamic limit in AdS/CFT and the membrane paradigm," Phys. Rev. D **79**, 025023 (2009) [arXiv:0809.3808 [hep-th]].

[75] A. L. Fitzpatrick, S. Kachru, J. Kaplan and S. Raghu, "Non-Fermi liquid fixed point in a Wilsonian theory of quantum critical metals," Phys. Rev. B **88**, 125116 (2013) [arXiv:1307.0004 [cond-mat.str-el]].

[76] A. L. Fitzpatrick, S. Kachru, J. Kaplan and S. Raghu, "Non-Fermi-liquid behavior of large-N_B quantum critical metals," Phys. Rev. B **89**, no. 16, 165114 (2014) [arXiv:1312.3321 [cond-mat.str-el]].

[77] S. A. Hartnoll, R. Mahajan, M. Punk and S. Sachdev, "Transport near the Ising-nematic quantum critical point of metals in two dimensions," Phys. Rev. B **89**, no. 15, 155130 (2014) [arXiv:1401.7012 [cond-mat.str-el]].

[78] S. A. Hartnoll and E. Shaghoulian, "Spectral weight in holographic scaling geometries," JHEP **1207**, 078 (2012) [arXiv:1203.4236 [hep-th]].

[79] S. Cremonini and L. Li, "Criteria For Superfluid Instabilities of Geometries with Hyperscaling Violation," JHEP **1611**, 137 (2016) [arXiv:1606.02745 [hep-th]].

[80] J. W. Loram, K. A. Mirza, J. R. Cooper and W. Y. Liang, "Electronic specific heat of $YBa_2Cu_3O_{6+x}$ from 1.8 to 300 K," Phys. Rev. Lett. **71**, 1740 (1993).

[81] J. W. Loram, J. Luo, J. R. Cooper, W .Y. Liang and J. L. Tallon, "Evidence on the pseudogap and condensate from the electronic specific heat," J. Phys. Chem. Sol. **62** (2001) 59-64.

[82] R. Daou *et al.* "Linear-T resistivity and change in Fermi surface at the pseudogap critical point of a high-Tc superconductor," Nature Phys. **5**, 31 (2009) [arXiv:0806.2881 [cond-mat.supr-con]].

[83] T. F. Rosenbaum, A. Husmann, S. A. Carter and J. M. Honig, "Temperature dependence of the Hall angle in a correlated three-dimensional metal," Phys. Rev. B. **57**, 22 (1998).

[84] Z. Konstantinovic, Z. Z. Li and H. Raffy, "Temperature dependence of the Hall angle in single-layer and bilayer $Bi_2Sr_2Ca_{n-1}Cu_nO_y$ thin films at various oxygen contents," Phys. Rev. B. **42**, 18 (2000).

[85] R. A. Davison, K. Schalm and J. Zaanen, "Holographic duality and the resistivity of strange metals," Phys. Rev. B **89**, no. 24, 245116 (2014) [arXiv:1311.2451 [hep-th]].

[86] J. Zaanen, "Planckian dissipation, minimal viscosity and the transport in cuprate strange metals," arXiv:1807.10951 [cond-mat.str-el].

[87] S. A. Hartnoll, D. M. Ramirez and J. E. Santos, "Entropy production, viscosity bounds and bumpy black holes," JHEP **1603**, 170 (2016) [arXiv:1601.02757 [hep-th]].

[88] P. Fournier *et al.*, "Anomalous saturation of the phase coherence length in underdoped $Pr_{2-x}Ce_xCuO_4$ thin films," Phys. Rev. B **62**, R11993(R) (2000).

[89] T. Sekitani, M. Naito and N. Miura, "Kondo effect in underdoped n-type superconductors," Phys. Rev. B **67**, 174503 (2003).

[90] I. M. Hayes *at al.*, "Magnetoresistance Scaling Reveals Symmetries of the Strongly Correlated Dynamics in $BaFe_2(As_{1-x}P_x)_2$," Phys. Rev. Lett. **121**, 197002 (2018).

[91] P. G-. Gallo *et al.*, "Scale-invariant magnetoresistance in a cuprate superconductor," Science **361**, 479 (2018) [arXiv:1705.05806 [cond-mat.str-el]].

[92] I. M. Hayes *at al.*, "Scaling between magnetic field and temperature in the high-temperature superconductor $BaFe_2(As_{1-x}P_x)_2$," Nature Phys. **12**, 916-919 (2016).

[93] P. Wang, H. Wu and H. Yang, "Holographic DC Conductivity for Backreacted Nonlinear Electrodynamics with Momentum Dissipation," arXiv:1805.07913 [hep-th].

[94] O. Aharony, S.S. Gubser, J. Maldacena, H. Ooguri, and Y. Oz, "Large N Field Theories, String Theory and Gravity," arxiv:9905111v3 [hep-th]

[95] F. London, and H. London, "The electromagnetic equations of the supraconductor," Proc. Roy. Soc. (London) A149, 71 (1935)

[96] Y. Ando, S. Komiya, K. Segawa, S. Ono, and Y. Kurita, "Electronic Phase Diagram of High-Tc Cuprate Superconductors from a Mapping of the In-Plane Resistivity Curvature," Phys. Rev. Lett. **93**, 267001 (2004).

[97] R. A. Cooper *et al.* "Anomalous Criticality in the Electrical Resistivity of $La2_xSr_xCuO_4$," 2009. Science **323**,603 (2009).

[98] T. R. Chien, Z. Z. Wang, and N. P. Ong, "Effect of Zn impurities on the normal-state Hall angle in single-crystal $YBa_2Cu_{3-x}Zn_xO_{7-\delta}$," Phys. Rev. Lett. **67**, 2088 (1991).

[99] A. W. Tyler and A. P. Mackenzie, "Hall effect of single layer, tetragonal $Tl_2Ba_2CuO_{6+\delta}$ near optimal doping," Physica C: Superconductivity **282-287**, 1185 (1997).

[100] Z. N. Chen, X. H. Ge, S. Y. Wu, G. H. Yang and H. S. Zhang, "Magnetothermoelectric DC conductivities from holography models with hyperscaling factor in Lifshitz spacetime," Nucl. Phys. B **924**, 387 (2017) [arXiv:1709.08428 [hep-th]].

[101] J. Lindgren, I. Papadimitriou, A. Taliotis and J. Vanhoof, "Holographic Hall conductivities from dyonic backgrounds," JHEP **1507** (2015) 094 [arXiv:1505.04131 [hep-th]].

[102] Y. Seo, G. Song, C. Park and S. J. Sin, "Small Fermi Surfaces and Strong Correlation Effects in Dirac Materials with Holography," JHEP **1710**, 204 (2017) [arXiv:1708.02257 [hep-th]].

[103] C. Charmousis, B. Gouteraux, B. S. Kim, E. Kiritsis and R. Meyer, "Effective Holographic Theories for low-temperature condensed matter systems," JHEP **1011**, 151 (2010) [arXiv:1005.4690 [hep-th]].

Biography

Anthony grew up in Lancaster, Pennsylvania where he attended Manheim Township High School. Due to a number of fun and entertaining teachers, Anthony learned he had a passion for both science and mathematics. Since he was unable to decide which he liked more, Anthony graduated in 2011 with over 30 credits of AP coursework in math and science classes. That same year, Anthony enrolled at Lebanon Valley College (LVC) in Annville, Pennsylvania where he had enough preliminary credits to be considered a sophomore. While at LVC, Anthony met and fell in love with his now wife, Liz. In 2014, Anthony graduated from LVC with his B.S in both physics and mathematics. Later that year, Anthony began attending Lehigh University in Bethlehem, PA as a graduate student in the physics program. In 2016 Anthony began research with Professor Sera Cremonini in the field of string theory, where he could put to use his interests in both physics and mathematics. Anthony will graduate from Lehigh with both his M.S. and Ph.D.